Metabolic Analysis of a CHO Cell Line in Batch and Fed-batch Culture

by

Saeideh Naderi

A thesis
presented to the University of Waterloo
in fulfillment of the
thesis requirement for the degree of
Doctor of Philosophy
in
Chemical Engineering

Waterloo, Ontario, Canada, 2011

AUTHOR'S DECLARATION

I hereby declare that I am the sole author of this thesis. This is a true copy of the thesis, including any required final revisions, as accepted by my examiners.

I understand that my thesis may be made electronically available to the public.

Saeideh Naderi

Abstract

Animal cell culture is widely used as a platform for the production of a variety of biopharmaceuticals. The development of an efficient and productive cell culture requires a deep understanding of intra-cellular mechanisms as well as extra-cellular conditions for optimal synthesis. Mathematical modeling can be an effective strategy to predict, control, and optimize cell performance under different culture conditions. This research presents the evaluation of Chinese hamster ovary (CHO) cell culture secreting recombinant anti-RhD monoclonal antibody (MAb) through different processing modes, namely batch, fed-batch and perfusion operations.

The ultimate objective of this study was to establish a comprehensive dynamic model which may be used for model-based optimization of the cell culture for MAb production in both batch, fed-batch or perfusion systems. In analyzing process performance, the key potential cause of cell growth inhibition was attributed to lowering of pH in the culture possibly due to the accumulation of dissolved carbon dioxide. The most important finding in this regard was the significantly different observed maximum total viable cell density in two identical cultures differing in culture volume only (250mL and 500mL). However, the other byproduct metabolites such as lactate and ammonia and glucose depletion were also capable affecting growth adversely causing growth arrest, viability reduction, apoptosis initiation and progress.

Employing the experimental results of nutrient consumption, metabolite and biomass production, a metabolic flux based methodology was developed for modeling the metabolism of a CHO cell line. The elimination of insignificant fluxes resulted in a simplified metabolic network which was the basis for modeling the significant extracellular metabolites. Using kinetic rate expressions for growing and non-growing subpopulations, a logistic model was first developed for cell growth and dynamic models were formulated to describe culture composition and monoclonal antibody (MAb) secretion. The viable cell population was assumed to consist of normal growing, normal non-growing and apoptotic cell subpopulations. The rate of apoptotic cell formation was assumed to have a second order

dependence on the normal cell concentration. The proposed mathematical model for metabolites included distinct terms that reflected the metabolic rates of growing and non-growing cell populations. The model was validated for a range of glutamine and glucose concentrations. Good agreement was obtained between model predictions and experimental data. In subsequent steps the attempt was to correlate the growth kinetics to significant variables of the culture. The regulatory effects identified through each culture condition were combined for a rational design of a dynamic model constructed for the viable cell subpopulation. A Tessier-based model was applied for defining the fraction of growing cells as a function of a growth inhibitor, presumably dissolved carbon dioxide. Although only few variables appeared in the biomass model, all equations were solved simultaneously. The parameters were estimated using the Metropolis-Hastings algorithm and the *fmincon* function in MATLAB. The final model adequately predicted the effect of significant variables on the metabolic behavior of CHO cells in batch, fed-batch and perfusion systems.

Acknowledgements

I am heartily thankful to my supervisors, Dr. Jeno Scharer and Dr. Hector Budman, whose encouragement, guidance and support from the initial to the final level enabled me to develop an understanding of the subject.

Lastly, I offer my regards and blessings to all of those who supported me in any respect during the completion of the project.

Saeideh Naderi

Dedication

I would like to dedicate this thesis with love and gratitude to my mentor Professor Jeno Scharer, an outstanding scholar and an exceptional human being with a heart of gold.

Table of Contents

List of Figures

List of Tables

Chapter 1
Introduction

With the development of recombinant DNA-technology, animal cell culture has gained a pivotal role in biomedical research, diagnosis and therapeutics production. Over the past two decades, the emergence of variety of recombinant-proteins produced by animal cells and the high demand for these biopharmaceuticals have proven the importance of this technology (Walsh 2010). Biopharmaceuticals comprise a class of therapeutic agents that improved significantly the treatment options for variety of disease (Sekhon 2010). These R-proteins consist of hormones, growth factors, vaccines and monoclonal antibodies (MAbs) that are extensively used as therapeutic tools for the treatment of cancer, chronic and autoimmune diseases or as diagnostic kits in biomedical research and disease testing (Sekhon 2010).

The annual global market value for all recombinant therapeutic proteins has been reported to be over $99 billion in 2009, whereas $38 billion is allocated to MAb-based products (Walsh 2010). Around 60 to 70% of all approved and successfully commercialized recombinant protein pharmaceuticals are produced in mammalian cells and more than a hundred of these bioproducts are undergoing clinical trials at various stages (Wurm 2004; Matasci et al. 2008). This high percentage use as host platforms is largely due to possessing complex metabolic systems for authentic protein production and post-translational modification (such as glycosylation and sialylation) making them superior to other host platforms such as bacteria or yeasts (Sunley and Butler 2010). Chinese Hamster Ovary (CHO) cells have been routinely employed as host for a range of recombinant glycosylated protein production, including monoclonal antibodies (Hacker et al. 2009).

Although the productivity of animal cell cultures in bioreactors has been raised to the gram per liter range resulting from intracellular and extracellular modifications of cell culture, the projected annual consumption rate exceeds the current production capacity to produce these therapeutics (Butler 2005). In this regard optimizing cell culture systems and host cell

engineering are essential in order to increase the performance of the process. Significant progress has been made in cell culture technology through genetic engineering (Dorai et al. 2009; Majors et al. 2009), which led to improvement of the strains in terms of robustness and high specific protein expression. However, often low productivity and cell death are still major obstacles for efficient and economical production on an industrial scale.

In batch culture, which is still a common cell culture method for the majority of industrial bioprocesses, cells are prone to programmed cell death or apoptosis (Laken and Leonard 2001; Arden and Betenbaugh 2004). Programmed cell death is a key event which restricts cell growth and viability; hence the product yield in bioreactors ultimately decreases. Reduction in viability, which is a result of apoptosis, is followed by increasing amounts of non-viable cells and results in an increase in the amount of harmful cell-released metabolites. The release of these metabolites, such as proteases, can lead to damaging the rest of the viable cells or may inactivate proteins of interest (Chong et al. 2011). Since it has been observed that apoptosis is a common mode of cell death, especially in the late exponential phase, research focused on the mechanism and main pathways of apoptosis as well as identifying the key factors that trigger apoptosis. This knowledge will help to find ways to delay apoptosis, thus enhancing the performance of the cell culture. This is a critical point especially for some cell lines such as Hybridoma and CHO in which the production of recombinant proteins may not be growth-associated and synthesis continues during the stationary phase (Mercille and Massie 1994).

Apoptosis can be triggered by environmental causes, such as essential nutrient depletion, metabolic byproduct accumulation such as ammonia, lactate or carbon dioxide, changes in pH, oxygen limitation, hyperosmolality (Laken and Leonard 2001; Han et al. 2010). Besides apoptosis, another type of programmed cell death called autophagy has been attributed to nutrient exhaustion (Hwang and Lee 2008). It is important to assess the extent of apoptosis and autophagy since they affect not only productivity, but also correct glycosylation, thus impacting the quality of the MAbs (Wong et al. 2005).

Fed-batch and perfusion systems are two efficient strategies that are applied to mitigate the stressful conditions during the course of batch culture. In both systems, controlled nutrient feeding, either continuously or at regular intervals, is performed, while spent medium is partially removed in the perfusion mode (Rodrigues et al. 2010). This results in longer cell viability and higher R-protein production (Zhang et al. 2004; Burky et al. 2007). However, formulating an optimal nutrient feeding strategy (i.e. feeding component, frequency and volume of feeding) requires a detailed understanding of cell metabolism and physiology. Due to the complexity of cell metabolism and the many unknown intracellular factors involved in regulating cellular mechanisms, most applied strategies have been based on trial-and-error approach (Altamirano et al. 2004).

Mathematical modeling has been recognized as a rational approach to systematize the experimental observations with the aim of identifying and quantifying fundamental correlation between process parameters, metabolic variables and production rates. These models can then be used for the optimization and effective control of bioprocess performance (Sidoli et al. 2004). In order to achieve this goal, a model must provide an accurate explanation of intracellular reactions involving all key metabolites. This requires a better understanding of cell behavior throughout culture condition variation, in terms of essential nutrient availability and production of some byproducts affecting cell metabolism (Nolan and Lee 2011).

The main purpose of the present study was to develop a comprehensive dynamic model for Chinese hamster ovary (CHO) cells producing anti-RhD monoclonal antibody (MAb) to describe cell metabolic behavior over time for both batch and fed-batch culture modes. This required an evaluation of the culture process as the basis for identifying the underlying parameters that play key roles in cellular metabolism. This could provide insight into the internal mechanism of cells and lead to acquiring information regarding intracellular metabolism and their interactions with the metabolites in the extracellular environment. In addition, the effect of the significant parameters in the cellular mechanism will be added in the model. Nutritional factor assessment was the first priority due to their important role regarding cell growth, maximum population density, programmed cell death, and longevity

of the culture. As a first step, cellular response to various initial concentrations of the key nutrients, i.e. glucose, glutamine and asparagine, was assessed. In each set of the experiments, the attempt was to identify the correlation between cell growth, apoptosis, and metabolic activity with these external metabolites. Subsequently, further studies were performed on culture supplementation via a periodic feeding strategy in order to improve the culture conditions by compensating for the possible exhaustion of any significant nutrient in the culture. Due to uncertainty about the particular nutrient that becomes depleted, complete medium or supplement was used. In our study, the cell density effect seemed a significant parameter and hence it was assessed by changing either inoculation density or through diluting the culture after the cell density peak. However, during the examination of culture under different conditions, the contribution of inhibitory factors affecting cell growth and metabolic behavior directed us to recover the culture environment via partial or complete replacement of the spent media to mitigate the harsh cells' environmental conditions.

All experiments were performed in 500 mL stirred (rpm=100) spinner flasks in a suspended growth inside a humidified CO_2 incubator with 5% CO_2 at 37^{o}C. Different analysis of the biomass and supernatant containing key metabolites were performed on-line and off-line by daily sampling throughout the culture process.

To construct the dynamic model for significant metabolites, metabolic flux analysis was applied as a tool to investigate the flux distribution and to establish the significance of intracellular fluxes through measured extracellular metabolites. Considering this rational assumption, the metabolic network was simplified by ignoring any insignificant flux. The dynamic model for each metabolite was developed based on the macro-reactions attained from the resulting simplified metabolic network. Development of a dynamic model for each subpopulation of cells, i.e. normal and apoptotic cells was based on the observation of cell behavior in terms of growth, initiation of apoptosis, cell death/viability in diverse culture conditions imposed in each experiment. It was attempted to include all significant factors evaluated in this study in the final model. The dynamic models for extracellular metabolites and biomass were solved simultaneously and the model parameters were obtained using Metropolis-Hastings algorithm and optimization using the fmincon function in MATLAB.

The novelty of the present work is the partitioning and dynamic modeling of the heterogeneous populations of CHO cells into three main sub-populations, i.e. normal growing, normal resting and apoptotic cells. Depending on the level of environmental stress in terms of nutrient starvation, high level of inhibitors, each subpopulation may react in different ways and have different stress-resistance. This partitioning provides a means for a detailed evaluation of each subpopulation in terms of metabolic activity and MAb secretion under various culture conditions. Perfusion studies were performed to elucidate the effect of cell population density and the inhibitory effect of metabolites on cell growth. It was also found that cells may undergo replicative senescence rather than direct transition to apoptosis. While the majority of cells were normal non-growing cells in stationary phase, there was a low chance of successful revival of cells in each periodic perfusion of the culture. The comprehensive model included the combination of metabolism and growth kinetics. The Metropolis-Hastings algorithm was applied in this study to estimate the value and the confidence interval of each parameter. A MATLAB program was written to interpret cell morphology the fluorescent images and identify apoptotic cells by changes in their contour (blebbing).

This thesis is comprised of 9 chapters and is organized as follows:

Chapter 1 contains the introduction, research objectives, and research methods.

Chapter 2 provides a comprehensive literature review including monoclonal antibody production, Chinese Hamster Ovary Cells, cell culture medium, cell culture process development, programmed cell death, and mathematical modeling.

Chapter 3 presents the materials and methods applied in this research, including cell line, culture medium development, culture preparation, and analytical procedures performed for the analysis of different metabolites in the CHO cell culture.

Chapter 4 describes the evaluation of cellular behavior under essential nutrient starvation (glucose, glutamine and asparagine).This identifies the importance of the most significant nutrients effect on cell growth, viability, and MAb production.

Chapter 5 evaluates the culture supplementation approach. The experiments were based on single or multiple feeding of normal and concentrated medium at various time intervals.

Chapter 6 represents the examination of cell density influence on cell growth arrest. The experiments are based on examining different seeding density and diluting the culture.

Chapter 7 explores the importance of the culture environment in terms of inhibitory levels of significant variables such as dissolved oxygen, dissolved carbon dioxide, and pH. The experiments of this part of study comprise fed-batch and perfusion cultures that were conducted to alleviate the inhibitory effect and examine cell revival at each semi- or full perfusion.

Chapter 8 describes the development of a mathematical model for all significant external metabolites and cell density of subpopulations. The model development was based on observations and experimental data analysis in each of the above chapters. Metabolic flux analysis was the basis of proposed model for significant extracellular metabolites.

Chapter 9 reviews the significant findings of this research and presents some recommendations for future research.

Chapter 2
Literature Review

2.1 Monoclonal Antibody Production

Monoclonal antibodies (MAb), as highly specific reagents, have rapidly developed an extensive role in the treatment of diseases such as viral infections and cancer, for both *in-vitro or in-vivo* diagnostic purposes, for blocking the natural rejection mechanism after organ transplantation, for efficient in-vivo transfection (which is also called antifection method) and as carriers in drug delivery systems (Sanna and Burton 2000; Houdebine 2002; Farid 2007). In fact, their high binding specificity and affinity to various antigens make these an important tool for fundamental biomedical research and for therapeutic applications. At present they account for more than 30% of all biopharmaceuticals under clinical trials (Hudson and Souriau 2003). In the past most monoclonal antibodies were murine in origin and were produced by immunizing the animal and by taking the naturally produced immune cells from its spleen and then fusing them with cancerous cells such as a myeloma to obtain hybridoma cells with a capability of MAb secretion (NRC 1999). The hybrid cells can be subsequently proliferated by injecting them into the peritoneal cavity of a mouse (transgenic animal) or in vitro (cell culture technique). However, there are some critical considerations for applying murine monoclonal antibody for therapeutic purposes such as the possibility of adverse immunological reactions in the recipient that will limit successful antibody therapy. The use of fully human monoclonal antibody can eliminate this side effect significantly, although preparing a stable hybridoma cell line is currently the major obstacle in the production of human monoclonal antibodies (Wong et al. 1989).

Engineered monoclonal antibodies occurring in two distinct forms, chimeric and humanized, exhibit particular advantages in terms of low immunogenicity, high stability, optimized specificity and effective functionality (Dinnis and James 2005; Birch and Racher 2006). Antibody expression systems can be achieved by cloning the target gene via recombinant DNA methodology in either animal cell culture or in transgenic plants and

animals. *In-vitro* production of monoclonal antibody provides a high degree of control, safety, consistency and more importantly, it eliminates animal usage and animal welfare concerns. Despite conflicting viewpoints on the respective advantages and disadvantages of in vitro and in vivo production modes, cell culture based manufacturing, particularly employing CHO cells, has become an economically viable and cost-effective approach (Chadd and Chamow 2001).

2.2 Chinese Hamster Ovary Cells

Continuous cell lines that have the ability to grow indefinitely are desirable hosts in recombinant protein production. Choosing a suitable animal cell line is essential at the initial stages of bioprocess development. In selecting a host, both high specific productivity and high specific growth rate should be considered, since focusing on maximizing cell density does not necessarily results in high recombinant protein titer. For instance, it has been observed that some sub-clones of a cell line with high specific productivity grow very slowly (Browne and Al-Rubeai 2007). A key consideration when selecting a cell line as host is the achievement of post translational modification of R-protein which ultimately affects the final product properties such as biological function, stability, solubility and safety (Jayapal et al. 2007). Thus, many parameters should be considered when choosing a cell line for scale-up and commercial production.

The most common cell lines for recombinant protein production are CHO (Chinese Hamster Ovary), NS0 (Mouse Myeloma-Derived), BHK (Baby Hamster Kidney), HEK (Human Embryo Kidney) and PER-C6 (Human-Retina-Derived) cells. Although all these cell lines have been found to adapt well for growth in suspension cell culture, CHO and NS0 cell lines are superior candidates since they have been well-characterized through decades of research regarding efficient transfection, amplification and screening for high producer clones. Also, their capability for relatively high recombinant protein production and their adaptability to several medium formulations are additional advantages that make them suitable for use in different applications (Invitrogen 2006).

In summary, CHO cells as hosts dominate the production of recombinant protein products because of their high capacity for suspension growth, good quality and product safety in therapeutic applications. Some highly successful therapeutic CHO-based proteins are tissue plasminogen activator (r-tPA), interferon β-1a, coagulation factor and MAbs such as Herceptin, Rituxan, Avastin, Xolair and Vectibix. Currently about 70% of all recombinant therapeutics are produced via CHO cell lines with an approximate annual sales of more than US$30 billion (Jayapal et al. 2007) .

Theodore. T. Puck first derived the original Chinese hamster ovary (CHO) cell line in 1957 and then, in 1980, Urlaub and Chasin obtained a CHO cell line lacking in DHFR enzyme activity by using mutagenesis and by selectively isolating thymidine auxotrophic cell mutants (Jayapal et al. 2007). Chinese Hamster Ovary "$DHFR^-$ "cells are routinely used to create a cell line with capability for expressing a recombinant protein (Lucas et al. 1996; Wurm 2004). The marker, "DHFR-", indicates the cell's deficiency in terms of an essential metabolic enzyme, dihydrofolate reductase that is involved in biosynthesis of nucleotide components. These DHFR- cells are generated through mutagenesis and have particular nutritional needs for growth and proliferation. These needs are the basis for isolation and selection of stable clones containing the exogenous plasmid. This is accomplished by introducing a plasmid containing the heterologous genes along with co-transfection of the DHFR gene into the cell line and subsequent growth in a medium lacking glycine, hypoxanthine and thymidine. Thus, only clones containing the active plasmid will survive. The DHFR system also paves the way for an efficient amplification of the target gene during exposure to different concentration of methotrexate (MTX) that inhibits DHFR enzyme activity resulting in great increase in the number of copies of both the DHFR gene and the target protein gene. The final step is selecting a cell clone with high specific productivity, high specific growth rate and best product quality i.e. with the correct glycoforms. Despite their widespread application, the genomic and proteomic information of CHO cells are not fully understood and further research is required. Nevertheless, CHO cells are viewed as the mammalian cell equivalent of the bacterial workhorse, *E. coli* in biotechnology research.

2.3 Cell Culture Medium

Cell culture medium development is a very challenging aspect in mammalian cell technology. This is due to incomplete knowledge about cell metabolism and essential nutritional requirements. Currently used cell culture medium is mostly originated from Basal Medium Eagle (BME) developed by Harry Eagle in 1955 (Even et al. 2006). BME consisted of carbohydrates, inorganic salts, amino acids, vitamins and co-factors. However, in order to support and promote cell growth, the medium is often supplemented with animal sera, mostly fetal bovine serum (FBS). While serum is a rich source of complex hormones, growth factors (impact cell attachment), proliferation factors (such as insulin) and trace elements (Johnston and Siegel 1990); undesirable effects of serum include lot-to-lot inconsistency in composition due to the presence of undefined components, high cost and risk of contaminants (Even et al. 2006). Due to these technical and safety concerns, there is a concerted effort to eliminate serum and animal-derived components and to achieve higher consistency by using biochemically defined medium, especially for therapeutic purposes. Following these considerations, there is currently a variety of cell culture media available for production such as basal, serum free, animal-derived component free, protein-free and biochemically defined media as well (Hodge 2005). Although significant progress has been made in the development of serum-free media, cell culture processes are still frequently employ serum supplementation.

In this study serum-free SFX-CHO medium has been used as a basal medium. Despite an attempt to eliminate serum during culture adaptation, it was found that cell growth was not satisfactory in completely serum-free culture. Hence, a minimal level of 1% serum was found to be necessary during subculturing and part of the experiments.

2.4 Cell Culture Process Development

Although, due to its simplicity, batch culture operation is the most common mode in biotech industry, because of limitations in cell growth and productivity, other more productive systems have been used (Rodrigues et al. 2010). The limits of batch cultures are related to

depletion of essential nutrients such as glucose or glutamine or accumulation of metabolic by-products such as ammonia, lactate and CO_2 which changes the culture condition to a deteriorating environment that inhibits cell growth. This ultimately leads to reduction in viability, product titer and quality as well. To mitigate these limitations, both fed-batch and perfusion systems have been developed extensively at industrial scale (Chu and Robinson 2001). Fed-batch culture, considered to be a flexible and simple method of operation, is performed by controlled feeding concentrated nutrients based upon the identified requirements of cells, or slow feeding of low concentrations of essential nutrients which leads to lower detrimental byproduct production. The feeding rate is either set to a pre-specified constant value or it may be adjusted based on measurements of the critical parameters such as cell concentration, essential nutrient concentration and oxygen consumption rate. Thus, fed-batch operation often results in a significant retention of high viability, high cell density and product yield (Zhang et al. 2004). However, accumulation of waste by-products to an inhibitory concentration is still inevitable. Regarding this, perfusion system can be applied to alleviate the accumulation effect. In this mode of operation, the used medium is partially substituted by fresh medium, without removing cells. This provides high cell density and relatively mild culture condition resulted in higher volumetric productivity. In this method, reduction in residence time of the product in the culture improves quality which is particularly appropriate for very sensitive products (Huang et al. 2010).

By applying the optimized feeding strategy, production of monoclonal antibody by Hybridoma cell culture with total cell concentration of up to 5×10^{10} cells/l and MAb concentration of up to 2.4g/l has been reported which is about 10 fold higher than the amount that can be typically obtained by a simple batch system (Xie et al. 2003). The selection of culture operation mode is dependent on various parameters including product secretion (growth or non-growth associated), quality and stability of product in the culture, manufacturing capacity and costs (Meuwly et al. 2006).

2.5 Programmed Cell Death

Cell death of mammalian cells occurs by three distinct processes: necrosis, autophagy and apoptosis. Necrosis is a passive, uncontrolled death caused by sudden and harsh cellular damage occurring upon severe culture conditions. These include high shear stresses on the cell membrane, exposure to high level of toxic metabolites or any environmental insult which ultimately leads to swelling of the cell, rupturing of the plasma membrane and the release of cytoplasmic contents to the extracellular environment (Knight 2006). During necrotic death, neither specific signaling nor particular degradation of DNA has been observed (Mercille and Massie 1994). Autophagy is programmed cell death resulting from essential nutrient depletion. The cell begins to lyse internal proteins to satisfy some metabolic needs (Hwang and Lee 2008). In contrast, apoptosis that refers to an active intrinsically controlled form of cell death, which is a regulated response to specific shifts in the culture environment. This non-optimal change, which in some cases is inevitable, is associated with many causes including: (1) serum withdrawal (Even et al. 2006), (2) depletion of some essential nutrients (Kim et al. 2009) such as glutamine, glucose, growth factors and oxygen (hypoxia) or (3) accumulation of toxic by-products such as ammonia and/or lactate (Hwang and Lee 2008), (4) hyperosmolality (Han et al. 2010) and (5) excess oxygen (hyperoxia), (Laken and Leonard 2001).

Apoptosis follows a successive set of events whereby a death signal stimulates the activation of a cellular cascade of reactions leading to high level of transglutaminase activity, exposure of phosphatidylserine on the cell membrane and nuclear condensation accompanied by endonuclease DNA fragmentation (DNA fragments contain 180-200 base pairs). In fact, the earliest morphological changes occur in the cell nucleus. Simultaneously, the cytoplasm increasingly excludes water and the cellular cytoskeleton breaks down and causes cell deformation and shrinkage. Apoptotic blebbing of plasma membrane and finally cytoplasmic membrane degradation and formation of apoptotic bodies are significant characteristics of late stages of apoptosis.

2.5.1 Mechanism of Apoptosis

Apoptosis involves the cascaded activation of a family of proteases, called caspases, that contain cysteine at their active site and can recognize a sequence of four amino acids. These caspases cleave target proteins at the aspartic acid residue of the known sequence. Splitting causes the activation of other proteases or disruption of key cellular components (Goswami et al. 1999; Laken and Leonard 2001; Kaufmann and Fussenegger 2004).

At present, around 14 different caspases have been identified in animal cells (Yun et al. 2007). Caspases are synthesized as inactive enzyme precursors (zymogen) which are proteolytically activated through either autocatalytic reactions such as for initiator caspases- 8, 9 or by initiator caspases which cleave and activate other caspases such as executioner caspases- 3, 6. In such a way, the caspase cascade irreversibly extends and amplifies proteolitic activation or results in cleavage of some key proteins which provide structural function or transcriptional regulation inside the cell. This ultimately results in dismantling and destruction of the cell.

Despite of the complexity of the apoptotic process which depends on the type of cell and different internal or external death signals, three main apoptotic pathways have been identified as shown schematically in Figure 2.1. The pathways are explained in the following subsections.

2.5.1.1 The Death Receptor-Mediated Signal Transduction Pathway (Extrinsic Pathway)

In this pathway the induction of apoptosis is triggered by the binding of some extracellular protein ligands to the specific death receptor proteins on the surface of the membrane of the target cell. These receptors such as Fas/CD95, DR4, DR5 and Apo2L/TRAIL are members of the tumor necrosis factor (TNF) superfamily (Arden and Betenbaugh 2004; Huerta et al. 2007). Ligand binding causes the death domains of receptors to cluster and recruit the adaptor proteins called Fas associated death domain (FADD) or Tumor associated death domain (TRADD). Following the binding of procaspase-8 to the death-effector domain

(DED) of the attached FADD, dimerization and activation of the initiator caspases by bilateral proteolytic cleavage results. The activated procaspase-8 activates the downstream executioner caspases such as caspase-3 and the death signal cascades throughout the cell.

2.5.1.2 Mitochondrial (Intrinsic) Pathway

The programmed cell death signals can be triggered from within the cell in the mitochondrion in which the accumulation and activation of some apoptosis-stimuli proteins such as electron carrier protein cytochrome-c, second mitochondrial activator of caspases (SMAC)/DIABLO and apoptosis inducing factor (AIF) occur (Arden and Betenbaugh 2004). For example, following its release from the mitochondrial inter-membrane into the cytosol, cytochrome-c binds to an adaptor protein called apoptosis activating factor-1(Apaf-1), to ATP and also to pro-caspase-9 to form an apoptosome complex. This complex in turn facilitates the cleavage and activation of pro-caspase-9. Similar to caspase-8, activated caspase-9 can cleave and activate executioner caspases 3, 6 and 7 and thereby complete the apoptotic caspases' cascade.

Two main groups of proteins that are involved in the intracellular regulation of the apoptotic cascade are: the Inhibitor of apoptosis (IAP) and the bcl-2 family. The IAP family proteins are synthesized by the nuclear factor kappa B (NFκB). This transcriptional factor contains two subunits called p50 and p65 and it is found in the cytoplasm in an inactive form coupled with the IκB molecule. The activation of this complex is made possible by phosphorylation of IκB and degradation of this factor leads to the release and translocation of the two subunits (p50 and p65) into the nucleus to start the transcription of IAP molecules. IAP regulators act on pro and executioner caspases directly to prevent their activation or inhibit their activity.

The bcl-2 family comprises both anti-apoptotic and pro-apoptotic proteins which are categorized as follows:

1. Pro-apoptotic bcl-2 member such as Bax and Bak with 3 Bcl-2 homology (BH) domains (BH1, BH2 and BH3).This group can alter the permeability of the mitochondrial membrane

either by forming new channels or by creating a conformational change in the voltage-dependent anion channel (VDAC) causing cytochrome-c or pro-apoptotic molecules to permeate the membrane. Additionally, this group can bind to the anti-apoptotic bcl2-family and neutralize its function. In fact, the relative ratio of pro and anti-apoptotic proteins determines the permeability of mitochondrial membrane and the amount of cytochrome-c leakage. This ratio is controlled by protein P53, a transcription factor that regulates the cell cycle. Upon stress condition, P53 induces proapoptotic proteins and represses the anti-apoptotic group of the Bcl-2 family and relays stress-induced apoptosis (Fussenegger et al. 2000). It has also been reported that at high anti-apoptotic Bcl-2 level , replicative senescence might occur by the oncogene p53 activation (Rincheval et al. 2002).

2. Anti-apoptotic bcl-2 member such as Bcl-2 and Bcl-X_L with 4 BH domains (BH1, BH2, BH3and BH4). This group of proteins has a key role in apoptosis by blocking the release of cytochrome C and other pro-apoptotic proteins from the mitochondria (Wong et al. 2006). The inhibition mechanism is assumed to protect the entire mitochondrial membrane by binding to the pro-apoptotic member of the Bcl-2 family. It also competes with procaspase-9 to bind Apaf-1, thus preventing activation of procaspase-9.

3. The pro-apoptotic bcl-2 subfamily includes BH3, Bid, Bad and Bik. Some of these apoptosis promoters such as Bad can bind to anti-apoptotic molecules and make them inactive. Bid is cleaved and activated by caspase-8, which in turn activates pro-apoptotic proteins, BAX and BAK. Moreover, Bid initiates cytochrome C release from the mitochondrion (Laken and Leonard 2001).

2.5.1.3 The Endoplasmic Reticulum (ER) Stress-Induced Pathway

The Endoplasmic Reticulum (ER) also participates in the apoptotic cell death pathway. Various conditions such as dysfunction in protein glycosylation, depletion of calcium from the lumen of the endoplasmic reticulum, deficiency in synthesis, folding, disulfide bond formation and indiscriminate transport of proteins from the ER to the Golgi can initiate the ER-stress induced apoptotic pathway.

Similar to the mitochondrion, the members of all three groups of the bcl-2 family are involved in the ER-apoptotic pathway. For example, upon ER malfunction, ER-stress transducer proteins are activated and cause the pro-apoptotic proteins, Bax and Bak to translocate to the ER membrane thus affecting membrane permeability and leading to calcium release from the ER and activation of caspase-12. In addition to stimulating cell death signals on its own, the ER can influence mitochondrial extrinsic and intrinsic death signals. Moreover, the contribution of the ER pathway to Fas-mediated apoptosis pathway and to the p53-related pathway has been reported (Breckenridge et al. 2003).

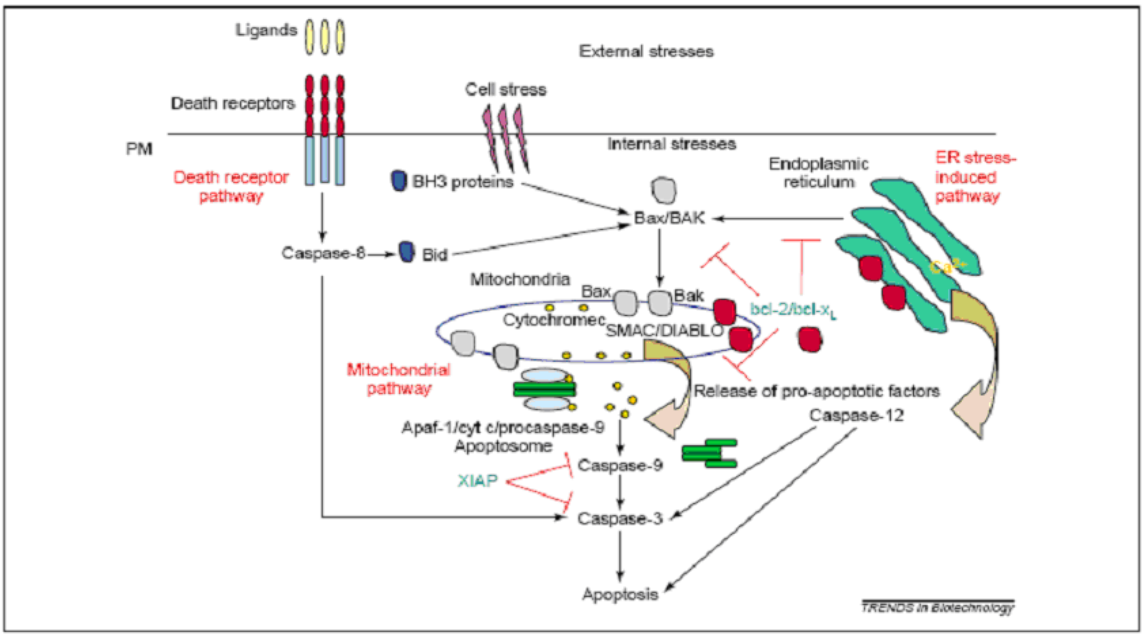

Figure 2.1: Three main apoptotic cell death pathways (Arden and Betenbaugh 2004), copyright granted by Elsevier.

2.5.2 Detection of Apoptosis

Several methods can be applied to detect whether cells are undergoing programmed cell death in cell culture. This section discusses some general detection techniques. Microscopic observation of morphological changes in the cells is a common standard technique to discriminate between normal viable, apoptotic, and necrotic cells. The morphological

difference between apoptosis and necrosis was first observed by electron microscopy. Due to its high resolution, EM has the capability of detecting the specific morphological changes during early and late apoptosis. Moreover, EM can be accompanied by TUNEL assay to improve the detection of DNA fragmentation. This technique is costly, it requires special technical training and it takes much time which limits its wide application (Huerta et al. 2007) .

Light microscopy (LM), cannot detect apoptosis clearly. However, it is possible to enhance the observation of apoptotic bodies and also distinguish necrosis by staining the cells with fluorescent dyes, hematoxylin and eosin (H&E) and propidium iodide (PI). This microscopic technique can be improved by fluorescent microscopy. Different fluorescent dyes such as Hoechst stains and Annexin V are available for labeling the cells to visualize nuclear and morphological changes by fluorescence microscopy (FM). This technique has also been used to differentiate and quantify apoptotic versus normal cells as well as for determining cell viability (Mercille and Massie 1994). This method involves two nuclear-fluorescent dyes, acridine orange (AO) in conjunction with ethidium bromide (EB). These dies are mixed in a fixed ratio with the cell suspension and analyzed by fluorescence microscopy. The microscope has a filter combination suited for detecting fluorescein. The nucleic acid selective cationic fluorescent dye AO can penetrate both viable and nonviable cells, interact with DNA and RNA by intercalation or electrostatic attraction and make the cells appear green. In contrast, EB which is another nucleic acid intercalating agent can only diffuse into nonviable cells and as a predominant dye makes them appear red-orange. So both normal or apoptotic viable cells are exhibited green, whereas non-viable cells look red-orange. This technique was used in the current research for estimating the quantity of apoptotic cells during culturing. By applying a special image processing program called ImageJ, a number of images of cells in various states can be obtained, analyzed and displayed. Figure 2.2 is a typical fluorescent photomicrograph of CHO cells stained with AO and EB. The lack of capability to detect early stages of the apoptotic process and the limitation in testing a large number of samples are significant shortcomings of these microscopic techniques.

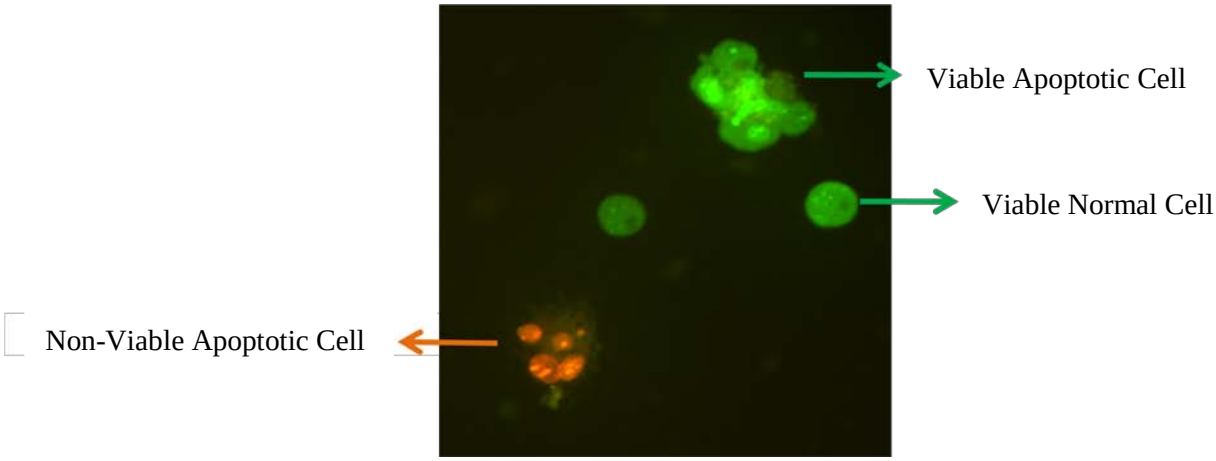

Figure 2.2: Fluorescent photomicrograph of CHO cells stained with Acridine Orange and Ethidum Bromide.

Flow cytometry is a powerful technique that provides simultaneous multi-parametric analysis of the heterogeneous cell population based on light scattering and light emission fluorescence allowing the identification of a homogeneous subpopulation within the total cell population. According to this method, the cells pass through a beam of laser light individually and they are differentiated and quantified according to a specific characteristic and phenotype data such as size, granularity or fluorescent molecular binding to the cell. The fluorescent agent may be coupled with a dye or conjugated to a MAb specific for molecules either on the cell surface or within specific intracellular components. The instrument consists of five functional units: (i) a fluidic system where cells flow through a sensing system inside a chamber one at a time. (ii) Laser as a light source for scatter and fluorescent emission (iii) Optics that collect and direct the light to the detectors; one set for forward light scatter which is a criterion for cell size, and one set for side scatter that is correlated with the complexity and granularity inside the cell. In addition, fluorescence emitted from fluorescently labeled cells are focused in the same direction as the side scatter through a combination of beam splitters, filters and mirrors to the particular color detectors (iv) Detectors which collect and process the light and finally (v) Electronics and computer system which translate the signal received from the detector to digital data for further analysis using various plots. This

technique is able to rapidly screen large numbers of samples (Harding et al. 2000; Macey 2007).

Gel electrophoresis is also a useful tool to detect DNA laddering which is a hallmark of early event in apoptosis (Huerta et al. 2007). Moreover, the enzyme-linked immunosorbent assay (ELISA) has been applied for detection of DNA fragmentation using specific monoclonal antibody (Huerta et al. 2007).

Since in most current methods, the detection of apoptosis in vitro involves fixing and staining the cells to explore morphological or biochemical characteristic of apoptosis, the challenge is to eliminate the time-consuming preparation of samples and make the assay faster and possibly in real time without damaging the cells. Elastic Scattering spectroscopy (ESS) is an optical technique which is based on changes in light scattering properties of cells that are related to morphological changes during the progress of apoptosis (Mulvey et al. 2007).

The type of method used to detect apoptosis depends on the individual study, type of cells and the number of samples. Since each technique has some disadvantages and due to the highly variable and dynamic nature of apoptotic phenomena, it is best to perform two methods simultaneously for mutual verification of the findings. Accordingly, in the current research, apoptotic cells were assessed by staining and fluorescence as explained above and the results were corroborated by comparisons to flow-cytometry measurements obtained by another member of our research group.

2.6 Prevention or Delay in Apoptosis

In order to achieve prolonged and high cell culture viability and increase antibody production, two main strategies have been evaluated to inhibit or at least delay apoptosis: optimizing the extracellular environment through medium supplementation (Altamirano et al. 2004), adding chemical inhibitors of caspases (Sauerwald et al. 2003) and manipulation of the intracellular environment using genetic engineering (Wong et al. 2006). However this study addresses the optimization of the extracellular environment.

In most cell lines, glutamine exhaustion was found to be the most effective inducer of apoptotic cell death (Singh et al. 1994; Fuchs and Bode 2006). The mechanism of apoptosis, i.e. intrinsic or extrinsic pathway, occurring at a given moment depends on the cell type. Although glutamine is a non-essential amino acid it contributes to cellular metabolism, physiological regulation, synthesis of some amino acids, nucleotides, proteins and fatty acids. It also has a key role in growth, survival and normal functioning of cells. Glutamine acts as a growth promoter as well as apoptosis suppressor and stress modulator. The time of onset of apoptosis by glutamine deprivation depends on the type of cell line and culture condition. Despite the reported crucial role of glutamine in cell survival for some cell lines, it has been found that glutamine is not a limiting nutrient for CHO cell lines (Sun and Zhang 2004). On the other hand, it was found that cell death occurs in the absence of both glutamine and glutamate. This can be attributed to endogenous glutamine synthetase activity which catalyses the conversion of glutamic acid to glutamine. Unlike Hybridoma, CHO cell growth seems to be glucose-dependent and it cannot be substituted by glutamine (Sun and Zhang 2004). Induction of apoptosis in Hybridoma and Myeloma cell lines is much faster than in CHO cells which may be related to relatively lower levels of glutamine synthetase (GS) activity, anti-apoptotic bcl-2 expression or deregulation of the c-myc proto-oncogene which can stimulate cell division indefinitely regardless of the absence of essential growth factors and nutrients (Sanfeliu and Stephanopoulos 1999). In addition to glutamine and glucose as two main energy sources, lack of other amino acids (essential and non-essential) in Hybridoma cell cultures has been examined individually. The results showed that cells undergo apoptosis in the absence of a key amino acid especially EAA. Although some of the essential amino acids are involved in cellular energy supplementation, both EAAs and NEAAs are the basic component of proteins and nucleotides. Due to the latter, both EAAs and NEAAs seem to play significant roles in cell death by starvation (Simpson et al. 1998).

In addition to apoptosis, autophagy is also a type of programmed cell death which similarly to apoptosis can be triggered through different signaling pathways, but without caspase involvement. Although more studies have been performed on apoptotic cell death, any culture insult might effect autophagy induction as well (Hwang and Lee 2008).

2.7 Mathematical Modeling

Our increasing knowledge of biological systems in which many known and unknown genes influence bioreactions, biological behavior and cellular control and regulation needs to be integrated to achieve optimum efficiency. Mathematical modeling can be a convenient means to reach the goal in this domain. The importance of mathematical models is to describe different experimental data in a coherent and systematic manner; elucidate interactions in complex biological phenomena; identify the main components, mechanisms and their relationship, and furthermore capture the essential quantitative and qualitative phenomena that characterize the biological system under study. Models can also be used as useful tools to direct experimental design with the aim of improving and optimizing the culture performance and to discover novel approaches for production of biopharmaceuticals (Bailey 1998; Sandadi et al. 2005). Hence, a mathematical model provides a cost-effective and time saving strategy to optimize bioprocesses by reducing the number of experiments significantly and facilitate the predictability of the biological process.

Unlike chemical systems, biological organisms such as mammalian cells behave as highly complex networks with appropriate control mechanisms which make them capable of adapting to slight changes in the environment. This property, along with the fact that the intracellular metabolism is often not accurately known, reflects the difficulty to set-up dynamic models which thoroughly describe and predict cell behavior during the cultivation process.

In general, mathematical models for biological organisms are constructed based on two mechanisms: structured modeling which integrates intracellular knowledge by considering cellular compartments individually and unstructured modeling which neglects internal structure and it consists of empirical models derived solely from extracellular metabolites analysis. Although the former provides a more comprehensive description of the inner structure of cell which makes it applicable to a wide variety of growth conditions, it is often difficult to calibrate such models since they require intracellular measurements for model

validation. Also, their high computational demand limits their practical application for real time control or optimization (Nyberg et al. 1999; Sidoli et al. 2004).

On the other hand, unstructured models are simpler to obtain but are limited to the conditions and data used for calibration and they ignore the internal structure of the cells. In spite of this, they are valuable tools for control and optimization purposes and to model the behavior of biological organisms with limited mechanistic information (Sidoli et al. 2004). In this regard, a new prevailing modeling approach has been to place the emphasis on what happens within the cell through "Metabolic Flux Analysis" (Boghigian et al. 2010). This analysis, which is the basis of mathematical modeling in the present work, refers to the calculation of intracellular fluxes from measured extracellular fluxes using material balances of associated metabolic network (Bonarius et al. 1996; Xie and Wang 1996; Nyberg et al. 1999) and it is further described in the following subsection.

2.7.1 Metabolic Flux Analysis

A metabolic network of a cell line is a graphical representation of the metabolism occurring inside the cell. The network includes all main metabolic reaction pathways where the inputs and outputs of the network are the substrates and products respectively. The structure of a metabolic network is set up via experimental observations and a variety of techniques are used to identify the intracellular fluxes directly to determine the main interconnections and pathways in the network (Zupke and Stephanopoulos 1995; Bonarius et al. 1996; Bonarius et al. 2001).

Usually a specific metabolic network for animal cells is applicable for similar cell lines with slight modifications. In metabolic flux analysis, based on the identified network and experimental data of some extracellular fluxes, the flux distribution inside the cell is computed using stoichiometric balances. It should be noticed that the quasi-steady state condition is often the main assumption in this analysis whereby it is assumed that there is no accumulation of intracellular metabolites inside the cell during the culture process (Quek et al. 2010). Since the number of unknown fluxes is usually larger than the number of mass-

balance equations, the system of equations is generally underdetermined and needs to be solved by a specific optimization method (Stephanopoulos 1998).

The intracellular fluxes estimated from measured extracellular fluxes by applying least square programming and by imposing constraints, have been found to be in good agreement with the results obtained experimentally by nuclear magnetic resonance (NMR) or other methods (Paredes et al. 1998; Goudar et al. 2010).

2.7.2 Dynamic Model

A large variety of dynamical models for animal cells, particularly Hybridoma cells, have been proposed (Portner and Schafer 1996) for which only cell biomass and some extracellular chemical species in the culture medium are the only available data. Most of these models are very simplistic since they include only a few substrates, e.g. glucose and glutamine that are the typical growth-limiting nutrients (Portner and Schafer 1996). These models may also include reaction rate terms containing activation and inhibition constants and Monod-type constants (Xing et al. 2010). The considerable deviation between experimental and theoretical results may arise from analytical error and most probably from ignoring the intracellular metabolism. Logistic models have also been used successfully (Tsoularis and Wallace 2002) in cases when there was no obvious correlation between the measured metabolites and cell growth kinetics. These models also provide feasible estimation of cell-specific rates that are comparable with Monod-type kinetic models (Goudar et al. 2005).

Most of the derived macroscopic models proposed for animal cell lines are only suitable for the exponential growth phase or steady state continuous culture, since the parameters of the model are often obtained from experimental data collected during the growth phase (Goudar et al. 2005). However, in order to achieve an appropriate and reliable model design that will be applicable to an entire batch, more comprehensive models are needed. In this regard, Provost (Provost and Bastin 2006; Provost et al. 2006) has developed a dynamic model which is a combination of three separate models derived based on the condition of

each three phases in batch system, namely exponential growth phase, transition phase and death phase. A comprehensive dynamic model of CHO cell metabolism in fed-batch culture was published recently by Nolan and Lee (Nolan and Lee 2011). It considers nutrient uptake and intracellular reactions in the cytosol and the mitochondria. This model is based on Flux Balance Analysis and accounts for metabolic shift in fed-batch culture by incorporating temperature and redox-dependent (NAD^+/NADH) variables in the kinetic rate expression.

Amino acids play a key role in the synthesis of building blocks for biomass and recombinant protein production in mammalian cells. Only few studies (Sanderson et al. 1999; Gao et al. 2007; Kontoravdi et al. 2007) have included these nutritional factors in mathematical models.

From an industrial point of view, maintaining cell viability at a high level to achieve prolonged recombinant protein production is a main goal. One of the promising strategies to achieve this goal is preventing essential nutrient depletion by applying a fed-batch feeding strategy. However cell growth repression or induction of apoptosis might occur due to hyperosmolality during feeding or pH control in fed-batch culture (Han et al. 2010). A comprehensive dynamic model has been developed for both batch and fed-batch systems for a Hybridoma cell line based on metabolic flux analysis (Dorka et al. 2009). A similar set of significant fluxes was achieved for both culture modes which ultimately resulted in a unique model structure. However, some parameter values for reaction rates were different in the post-exponential phase which was attributed to differences in energy metabolism during batch and fed-batch operations. Energy needs for cell maintenance were higher in the fed-batch operation. An integrated model was proposed by combining the dynamic metabolite model with the cell concentration model in order to predict all significant metabolites as well as cell concentration over time by using only initial conditions of these variables. The cell concentration model was based on Monod-type kinetics employing significant metabolites such as glutamine and lactate as independent variables. The significance of these particular nutrients and products was identified by correlation analysis. This model predicted that as nutrients were depleted the MAb stopped to increase whereas in the experiments the MAb continued to increase beyond the point of complete exhaustion of nutrient (glutamine). A

possible explanation for this disagreement between experiment and the model is that an increasing amount of apoptotic cells appearing after the depletion of nutrient continue to produce MAb. A way to correct for this effect was to add a constant production term to the nutrient related kinetic term in the MAb dynamic balance.

The occurrence of apoptosis is an important constraint that limits the productivity and efficiency of the bioprocess. Starvation-induced programmed cell death could arise as explained in previous sections by the exhaustion of some key nutrients during cell culture. This also happens in fed-batch systems with feeding strategies based on low levels of nutrients, particularly in large-scale bioreactors in which the lack of complete mixing leads to insufficient nutrient availability under heterogeneous nutritional conditions. Studies with Hybridoma cells have revealed that the exhaustion of any amino acid can trigger apoptosis; however the apoptotic effect of some amino acids is not significant (Simpson et al. 1998). In order to detect apoptosis and investigate which pathway of programmed cell death is dominant under nutrient starvation conditions, specifically glutamine starvation, different methods have been examined (Fuchs and Bode 2006). For example, peptide inhibitors such as Z-VAD-FMK, Z-YVAD-CMK, which are widely used in controlling apoptosis via binding and neutralizing specific caspases, were employed to determine which particular caspase participated in the apoptosis mechanism. Based on the results of Anexin V staining and DNA-laddering assay along with the observed cytochrome-c release it was suggested that the intrinsic pathway is the main mechanism of apoptotic cell death in Hybridoma cell line under glutamine deprivation (Fuchs and Bode 2006). However, in another study of glutamine or glucose starvation in Hybridoma culture, the transcriptional profile of some specific genes seem to indicate that both the intrinsic and extrinsic mechanisms could be involved in programmed cell death (Yeo et al. 2006).

It has also been shown that two amino acids, glutamine and asparagine, may play a key role in the suppression of apoptosis in CHO cells and, based on experimental observations, a dynamic equation has been proposed which expresses the apoptotic cell density as a function of viable cells, glutamine and asparagine concentrations (Simon and Karim 2002). Because of the importance of this phenomenon, it is expected that finding connections between

apoptosis and specific extracellular components concentrations may be helpful for estimating the apoptotic cell death progress and for finding the mechanism for controlling it by means of supplying the culture medium with the required nutrients.

The goal of the present work is to develop a comprehensive dynamic model of anti-RhD MAb-secreting CHO cell culture describing cell metabolism, cell sub-population kinetics of normal and apoptotic cells and MAb production. Metabolic Flux Analysis will be the basic approach to identify significant fluxes and to simplify the metabolic network. A dynamic mass-balance model will be constructed for each significant metabolite in the network. The purpose is to describe the culture system in sufficient detail in order to achieve a dynamic model for predicting the changes of each significant metabolite in the process over time and its applicability for model-based optimization in both batch and fed-batch culture.

Chapter 3
Materials and Methods

3.1 Cell Line

A dihydrofolate reductase-deficient CHO cell line (dhfr- CHO) transfected with a fully human IgG-Variant gene for anti-RhD MAb was provided by the industrial partner, Cangene Corporation, Mississauga, Ontario. This recombinant MAb (IgG1-r9B8) has shown a relatively high affinity for the human RhD antigen making it suitable for therapeutic application (Wiersma 2000).

3.2 Culture Medium Development

Three different CHO-specific media have been examined for suspension cell culture:

1- SFX-CHO, a liquid serum-free medium provided by Hyclone for suspension growth. This medium has only 10μg/mL total proteins (animal-derived). It also contains no glutamine, glycine, hypoxanthine or thymidine.

2- HYQ-CDM4CHO is a protein-free medium with no animal-derived components. It contains Pluronic F-68 to protect cells from shear forces.

3- EX-CELL CD-CHO which is another liquid, chemically defined, animal-component free and serum free medium developed by Sigma for growth of CHO cells in suspension culture. Similar to SFX-CHO, EX-CELL CD CHO is formulated without hypoxanthine, thymidine or L-glutamine, making it an appropriate medium for DHFR- and GS- (glutamine synthetase) cell systems.

These three basal media do not contain glutamine and consequently they are supplemented with L-glutamine (Sigma) to a final concentration between 1 to 4mM and are also supplemented by 1-4% serum during adaptation to serum-free suspension culture. Although all three medium resulted in confluent attached cell growth with high cell viability in

stationary T-flasks, appreciable cell suspension growth was achieved only using SFX-CHO medium. Amino acid analysis was performed to assay and compare differences in the main components of the three media. Most amino acids assayed higher in the SFX-CHO medium.

In addition, in experiments using nutrient feeding, two types of supplements were used: CHO Feed Bioreactor Supplement (from Sigma) and SFX-CHO medium. The former medium is an animal component-free concentrated supplement developed specifically for fed-batch CHO cultures. This product is glutamine and glucose free feed, designed to replenish utilized nutrients such as amino acids and vitamins without significantly affecting the pH and osmolality of the culture. The second feed was the current SFX-CHO medium at three different concentrations (1X, 2X and 5X).

3.3 Culture Preparation

3.3.1 Initiation of Cell Culture

Cell culture preserved in liquid nitrogen was recovered by rapid thawing lasting approximately 2 minutes of a frozen vial of cells in a 37 water bath with gentle swirling while keeping the o-ring and cap out of the water. To avoid any microbial contamination the water bath was disinfected with the anti-microbial reagent (Acryl AquaClean, WAK–Chemie). The vial was removed as soon as the contents were thawed and decontaminated with 70% ethanol.

All operations, i.e. seeding and sub-culturing, from this point on were accomplished under aseptic conditions in a biological safety cabinet. The contents of the vial were then transferred to a 25-cm^2 T-flask containing approximately 4-5mL fresh medium supplemented with 2-4% serum. Prior to the addition of the cell content, the flask containing the medium was placed in a CO_2 incubator (Sanyo IR Sensor, 37 °C) for at least 15 minutes to provide optimal temperature and pH conditions. The prepared (seed) culture was incubated in a humidified atmosphere of 5% CO_2 at 37˚C.

3.3.2 Sub-Culturing Procedures

Depending on the rate of cell growth and initial concentration, cells from the mid-exponential phase were harvested and passaged to a fresh medium every two or three days as follows:

First, all supernatant was removed and 1mL (for 75cm^2 T-flask) TryplE (Invitrogen) as dissociating agent was added to the flask and incubated at 37 °C for approximately 5 minutes. This incubation generally facilitates cell dispersal and so reduces the enzyme exposure period. Cell detachment was checked by an inverted phase-contrast microscope and after complete detachment was observed, approximately 5mL of fresh medium was added and the cells were aspirated by gently pipetting. Since the TryplE is gentle on the cells and the concentration was negligible after dilution, there was no need to inactivate or remove it by centrifugation. Cells were counted by a hemocytometer and based on this count a new subculture was prepared with a cell concentration of 0.2×10^6 cells/mL. The original serum concentration in the flask (2%) was gradually reduced to 1% or less during the subculturing procedure.

3.3.3 Cryogenic Preservation of CHO Cells

In order to maintain a cell bank reserve, cryogenic preservation of CHO cells was carried out. Cells were harvested in mid-exponential phase of growth with viability higher than 90%, centrifuged and resuspended in a cryopreservation medium to a concentration of approximately 1×10^6cells per mL. The cryopreservation medium contained 45% fresh medium, 45% conditioned medium and 10% of a cryoprotective agent, DMSO (dimethyl sulphoxide). Serum with a concentration of 2% by volume was also added to the fresh medium to improve post-freezing survival and recovery of the cells. The prepared cell suspension was aliquoted into labeled 1mL cryovials, placed overnight in a -80˚C freezer and then immediately transferred to a liquid nitrogen container for long term storage.

3.3.4 Adaptation to Suspension Culture

Prior to the commencement of the experiments in spinner flask, the cells were adapted to suspension culture. The cell suspension obtained from a trypsinized monolayer culture was used to establish a suspension culture in a 250mL spinner flask containing serum-supplemented SFX-CHO medium at a density of (0.1-0.3) $\times 10^6$ cells/mL. The agitation was provided by a 4-position magnetic stirrer inside the CO_2 incubator which was set up under similar conditions of temperature, humidity and CO_2 atmosphere for T-flask cultures. The stir rate was adjusted to 100rpm. Every 2-3 days, the viable cell concentration and viability were determined and the culture diluted to (0.1- 0.3) $\times 10^6$ cells/mL by adding fresh medium. In case of insufficient growth during the initial passages, the cells were centrifuged and re-suspended in fresh medium with higher serum and higher initial cell density. The serum concentration was adjusted to 2-4 %, depending on the cell growth performance, at the beginning and then it was gradually reduced to 1% after the growth rate of the suspension culture stabilized at suitable levels (Sinacore et al. 1999).

3.4 Analytical Procedure

3.4.1 Viable Cell Concentration

Trypan Blue is the most common stain used to distinguish between viable and dead cells. Only nonviable cells can absorb the dye and appear blue. 100 μL of cell suspension sample was taken and diluted in 1:1 or 1:2 ratios (depend on the cell concentration) in 0.5% Trypan Blue dye. The optimal concentration of cells for counting was found to be 5-10$\times 10^5$cells/mL (50-100 cells per large square) after dilution with the Trypan Blue solution. The stained cells were counted using a hemocytometer under the light microscope within 3 minutes upon mixing with Trypan Blue. After this time period the viable cells will begin to take up the dye and consequently the result of the test will be misleading. The viability of cells was also quantified by the ratio of viable cell to total cell density.

3.4.2 Glucose and Lactate Assay

The glucose content of cell culture samples was measured enzymatically using a glucose kit (Megazyme Glucose Test Kit). The assay is based on the glucose oxidase/peroxidase reactions. The intensity of the produced dye is proportional to glucose concentration. The absorbance of the assay mixture was read at 510 nm against the reagent blank after 20 minutes incubation at 40°C. In addition, Ascensia Contour Glucose meter from Bayer Healthcare was used for instant assay of glucose immediately after sampling. Lactate assay was performed by a Lactate Plus meter from Nova Biomedical that contains a lactate oxidase biosensor with a measurement range between 0.3-25 mmol/L.

3.4.3 Ammonia and Dissolved Oxygen Assay

The dissolved ammonia concentration of the samples was estimated using a pH/ISE meter model 710A equipped with an Ammonia Ion-Selective electrode (VWR). The electrode contains a hydrophobic gas-permeable membrane to separate the sample solution from an electrode internal standard solution of ammonium chloride. The measurement of the ammonium ion was made by increasing the pH above 11 with a 10M NaOH solution just before the measurement is taken. This converts the dissolved ammonium to the gaseous form (NH3), which then diffuses through a membrane and changes the internal solution's pH that is measured by a pH electrode. Standard ammonia solutions (NH4CL) with known concentrations were used to calibrate the measurements within the required ammonia concentration range. Dissolved oxygen (DO) was also measured by VWR symphony Dissolved Oxygen probes designed for use with VWR symphony series Dissolved Oxygen Meters. The electrode calibration was performed in water-saturated air in a special calibration chamber.

3.4.4 Amino Acid Analysis

The pre-column derivatization technique with a high-performance reverse-phase column using phenylisothiocyanate (PITC) was applied to analyze the free amino acids in culture. The method is based on the formation of phenylthiocarbamyl (PTC) derivatives of amino acids (Bidlingmeyer et al. 1984). According to this method, a 10μL sample and a standard amino acid solution (Sigma) at a concentration of 2.5 μmol/mL were dried under vacuum. Then, 20μL of ethanol: water: triethylamine (TEA) (2:2:1) was added to each tube and dried again under vacuum. A fresh derivatization reagent was obtained that consisted of ethanol: TEA: water: PITC (7:1:1:1). Since PITC is unstable in air, it was added to the mixture in a nitrogen environment. The PTC-amino acids derivatives were formed by adding 20μL of the reagent to the dried samples under a nitrogen atmosphere and kept sealed for 20min in room temperature. After completion of the reaction occurring after a 20 min period, the samples were then dried under vacuum to remove the un-reacted reagent. The derivatized samples could be stored dry and frozen with no significant degradation. Dried samples and amino acid standards at various dilutions were then dissolved in 500 μL of solvent A (50mM sodium acetate) for constructing the calibration curve. Exactly 10 μL of each sample was subsequently injected into the column using an autosampler. The chromatography system was a Varian ProStar reverse phase HPLC (Varian analytical Instruments, USA) and the separation was performed using an Eclipse Plus C18 column (150×4.6mm, I.D.). The temperature of the column was maintained at 40˚C and the UV detector was set at 250nm. The solvent system consisted of two eluents at a flow rate of 1.0mL/min: Solvent A, an aqueous buffer, was 50mM sodium acetate containing 0.4 mL/L TEA which titrated to pH 6.35 using glacial acetic acid. Solvent B was a 60% solution of acetonitrile in water. The optimum gradient profile for a good separation of amino acids consisted of starting with a 10% B/90% A solution and subsequently gradually changing the concentration to 51% B/49% A in a period of 20 min, followed by the injection of a 100% B solution that was used to wash out any residual sample component from the column (Gheshlaghi et al. 2008). A typical separation of amino acids standards is shown in Figure 3.1. A calibration curve was plotted for each amino acid standard at different dilutions (Appendix D). The correlation

coefficient of the calibration curves for all amino acids was over 0.99 corresponding to an almost linear correlation in the range of 30-500 pmoL.

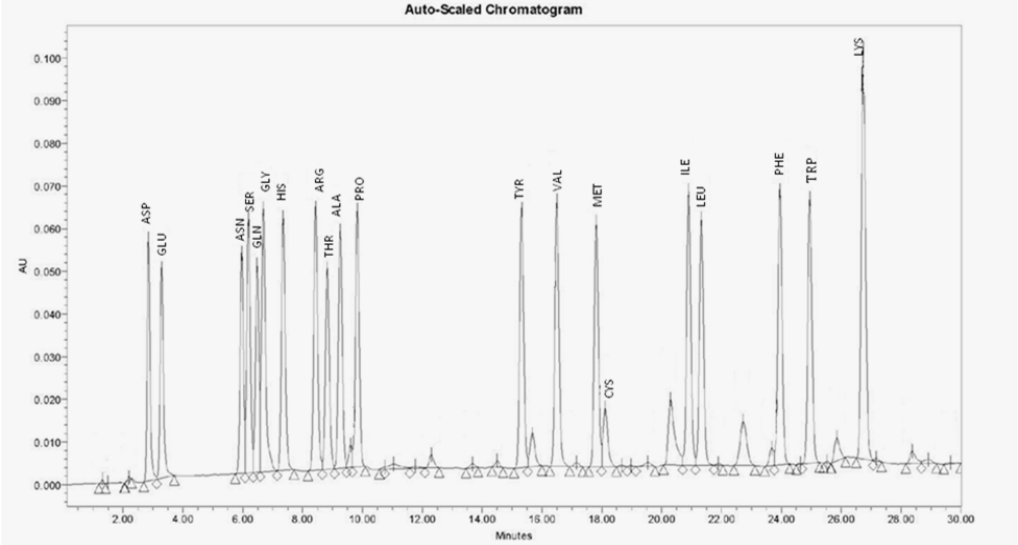

Figure 3.1: Separation of amino acid standards by HPLC (Eluent A: 50mM sodium acetate, 0.4 mL TEA, pH 6.35; Eluent B: 60% acetonitrile in water. Flow rate 1.0 ml/ min).

3.4.5 Monoclonal Antibody Assay

Total human IgG1 antibody concentration was estimated using the Enzyme-Linked Immunosorbent Assay (ELISA) method developed for this IgG_1 by Cangene. The assay was performed in 96-well flat-bottom microtiter plates, Immulon® 2HB. The primary and secondary antibodies used in this assay were goat anti-human IgG and alkaline-phosphatase conjugated goat-anti-human IgG (Jackson ImmunoResearch Laboratories, Inc.) respectively along with p-nitro-phenyl (Sigma Aldrich Ltd.) as substrate for alkaline-phosphatase. The absorbance was measured in a DU 520 UV/Vis spectrophotometer (Beckman Coulter) at 405nm. To quantify the amount of IgG_1 present in the sample, a dilution series (standard curve) of the standard human IgG_1 myeloma (Calbiochem) was used to compare the absorbance of the samples with the standard.

3.4.6 Fluorescence Imaging

During daily sampling of batch cultivation, images of stained cells were taken and processed by the software Image J (Burger and Burge 2008). For this purpose, 250 μL samples were mixed with 10 μL of fluorescent dye mixtures (Acridine Orange and Ethidium Bromide in equal ratio) and examined with a 40X objective under a florescence microscope. The average number of total cells counted for each prepared sample was between 200-400 cells. Cells were categorized and counted based on three different states: normal viable, apoptotic viable and necrotic cells.

3.4.7 An Automated Quantification of the Cells' Physiological State

Fluorescent microscopy and image processing have been applied to recognize three physiological states of CHO cells: i) normal viable state, ii) apoptotic viable state and iii) necrotic state. The CHO cells are stained using a conventional ethidium bromide and acridine orange fluorescent dye staining protocol. In order to facilitate identification and obtain accurate quantification of cells, a MATLAB-based computer program using the image processing toolbox has been written to classify the fluorescent microscope images based on color and shape (Lewis 2008).

First, the cell images are captured and stored into an "ImageJ" image stack as an ordered set image sequence. Each image is then interpreted by the MATLAB code that creates a binary (logical) image by setting a specified level or higher color intensity as "on" (white pixels), while less than the specified intensity is set to "zero" (black pixels). These logical images are processed by the image processing toolbox functions for black/white boundaries, area, eccentricity (a criterion of circularity) and solidity to analyze and determine the cell's characteristics individually. It should be noted that the object in the image was considered to be a cell if it contained more than 350 white pixels. The calculation of the total number of "on" pixels (white pixels) and the recognition of an object as a "cell" is done by employing the proprietary MATLAB functions "*regionprops*" and "*bwboundaries*" functions. Whenever more than one object appears in an image, these functions consider separate array containing

information for each object in the image. The methodology related to the identification and classification of cells in clusters is incomplete and requires further research. For instance cells within large clumps are sometimes counted as one single cell.

Once the cell boundaries including cells in cluster were delineated, the cell outlines are superimposed on the corresponding colored images. The color of the stained cells is the main criterion to discriminate between necrotic (dead) and viable cells. Measuring the average intensity of each color by the MATLAB code was the main principle used to assess this differentiation. Since the necrotic cells fluoresce with an orange-red color, any cell with higher than the preselected baseline red intensity was classified as necrotic cell, while cells fluorescing green are further differentiated as being either viable normal or apoptotic. This classification is based on the solidity of the image boundary.

Shrinkage and blebbing of the cytoplasmic membrane was found to be a significant characteristics of the apoptotic cells which cause them to lose their normal, smooth and circular shape (Arden and Betenbaugh 2004). Accordingly, in order to discern normal cells from apoptotic viable cells, the solidity parameter in "regionprops" function has been used. First a polygon surrounding each viable (green) cell is constructed. Solidity of the image is defined as the ratio of the entire area of the binary image to the polygon's area. The difference between these two areas is a significant feature of apoptotic cells that serves as an indicator that the membrane integrity has been compromised. Thus, it is expected that the high solidity, i.e. small area difference, corresponds to a non-apoptotic cell, whereas apoptotic cells will exhibit lower levels of solidity. The discriminating level of solidity is somewhat arbitrary and need to be chosen based on experience. In this work, a solidity of 0.96 was selected as the discriminant level between apoptotic and non-apoptotic cells, due to good agreement with visual observations. Cells with solidity greater than 0.96 were classified as normal, while those with less than this prescribed value of solidity were categorized as apoptotic.

The MATLAB program also calculates and reports the degree of apoptosis in a normalized form according to the relation $\left(\frac{1-Solidity}{0.1}\right)$. The results of the classification based on the

method outlined above are summarized and presented in Excel table that includes average cell area, average circularity, average degree of apoptosis, total number of viable apoptotic, non-apoptotic and necrotic cells along with the percentage of each cell type. In addition, the information for each cell regarding cell area, circularity, color and degree of apoptosis is presented separately.

Chapter 4
Essential Nutrient Starvation

4.1 Introduction

Essential nutrient depletion is considered a major environmental stress which can result in cell death, through either apoptosis or autophagy (Yeo et al. 2006; Mendonca et al. 2009). To further understand the phenomenon of apoptosis, a first objective of this research involves the assessment of the relative contribution of essential nutrient deprivation and inhibitory byproduct accumulation on cell culture conditions through the induction of apoptosis in CHO cells during batch cultivation. These sets of experiments are based on starvation involving the most significant nutrients, namely glucose, glutamine and asparagine that were identified as main energy sources or as precursors for biomass production. Selection of these three substrates as the key substrates is based on a preliminary correlation analysis of experimental data of previous batch cultures. The importance of this study is that starvation may trigger apoptosis leading to cell growth arrest thus affecting MAb production.

4.2 Materials and Methods

4.2.1 Medium Composition

SFX-CHO as a basal medium was used along with 1% serum for all experiments. Depending on the specific nutrient under examination, different concentrations of the nutrients in the main culture medium were prepared. Since the basal medium was glutamine-free, the culture was supplemented with L-glutamine to a final concentration between 0 to 4mM. In case of glucose, glucose-free SFX-CHO medium was ordered and different concentrations were prepared by mixing the original medium with glucose- free medium. The asparagine content (0.3 mM) in the basal medium (SFX-CHO) was considered as the lowest level. Due to complete exhaustion (near zero) of it in the post exponential phase of the batch culture,

higher concentration was achieved by adding more asparagine solution (Sigma) as well as by using concentrated medium (Sigma) containing amino acids in higher concentrations.

4.2.2 Experimental Design

Each set of batch culture was carried out in 500mL spinner flasks in the humidified incubator at 37°C with 5% CO_2 and 100 rpm. Each spinner flask was inoculated with a common seed culture. Continuous daily sampling was performed to assess cell growth, viability and metabolite analysis.

The experimental design consists of three distinct sets. In each set, the significant effect of a designated nutrient depletion at different initial concentration in the culture was assessed. Accordingly, these 3 sets were designed to test glutamine, glucose and asparagine depletions respectively. The results of these are discussed in detail below.

The effect of different concentrations of glutamine and glucose was analyzed by ANOVA method. The results are shown in Appendix E. Using the F test as criterion, the observed values were 0.2753 for glutamine and 1.6662 for glucose. These were compared with the critical values of $F_{0.05,2,20} = 3.49$ for glutamine and $F_{0.05,3,30} = 2.92$ for the glucose experiments, respectively. Consequently, it was concluded that neither the initial glutamine nor the initial glucose concentrations had significant effect on cell growth and the maximum population density within the ranges tested.

4.3 Results and Discussion

4.3.1 Glutamine Effect

Glutamine, as one of the main nutritive requirements of mammalian cells, was evaluated in the first set of batch experiments. The concentrations ranged from 0.2 mM upwards to 4 mM. The low concentrations resulted when no glutamine was added to the culture but it existed in the seed culture. Some experiments at concentrations of 1 and 4mM were performed in

duplicate. For the set of experiments with replicates, the paired comparison *t*-Test was applied for examining the reproducibility of the data. The average difference between the data pairs taken at the same time for the various variables such as total viable cell, glucose, glutamine, and lactate and ammonia concentrations were assessed using the null hypothesis of zero as the expected difference. The results are shown in Appendix F. The analysis found no significant differences occurred between data pairs of any two individual experiments at the 95% confidence level. This confirmed the reproducibility of the experimental observations.

All the other nutrients and culture condition were kept unchanged. Figure 4.1 shows the time course of the total viable cell density at different glutamine concentration. In all four cultures, same trends and growth rates were observed, except that the maximum cell density in glutamine-free culture reached an average of 0.9×10^6 cells/mL which was lower than in the other three cultures (approximately 1.2×10^6 cells/mL). Although glutamine deprivation can be an impediment in reaching maximum cell density, viability for the duration of the culture show similar trend in all four cultures. Sanfeliu and Stephanopoulos also reported that growth of CHO cells in the absence of glutamine is feasible (Sanfeliu and Stephanopoulos 1999). This could be related to the endogenous glutamine synthetase (GS) enzyme activated to compensate for glutamine exhaustion by converting glutamic acid to glutamine. On the other hand, the current experiments show that higher concentration of glutamine (4mM) did not improve the culture, but rather increased the concentration of ammonia which is known as a toxic by-product. Significant differences in glutamine utilization between the experiments conducted with 1mM and 4 mM initial glutamine concentrations were observed (see Figure 4.2).

An important finding was the apparent switch in the rate of metabolism as the culture ages and non-growing cells become predominant. Although high levels of glutamine are not essential, there is an apparent switch from the dominance of glycolysis to transamination with pyruvate to form alanine and oxidative deamination of glutamine in case of resting cells if excess glutamine is present. This results in higher ammonia levels when using 4 mM glutamine (shown in Figure 4.4). The accumulation of toxic ammonia in the medium by

either mechanism adversely affects viability. In case of lower glutamine concentration the long term accumulation of ammonia was less significant. One possibility to avoid the detrimental accumulation of ammonia while providing for the glutamine requirements is to feed glutamine in a fed-batch mode or alternatively to operate at low glutamine levels in view that its impact on viability is small.

Glutamine seems to have an effect on the rate of apoptosis as shown in Figure 4.3 where for the higher glutamine concentrations the level of apoptotic cells is slightly lower as compared to cultures with low initial glutamine concentration. In general, for all four initial concentrations of glutamine, the trends in the evolution of apoptotic cells are similar. The number of apoptotic cells began to increase significantly during the late exponential phase reaching a maximum level in the post-exponential phase (Figure 4.3). Apoptotic cells are expected to die eventually. In the late post-exponential phase the population of apoptotic cells started to decrease with increasing concentrations of necrotic cells. This trend is expected since apoptosis involves a progressive loss in cell membrane integrity also occurring in necrosis (Arden and Betenbaugh 2004) thus, the number of apoptotic cells is expected to decline as the number of necrotic cells increases. The total population also decreases as the necrotic cells undergo lysis.

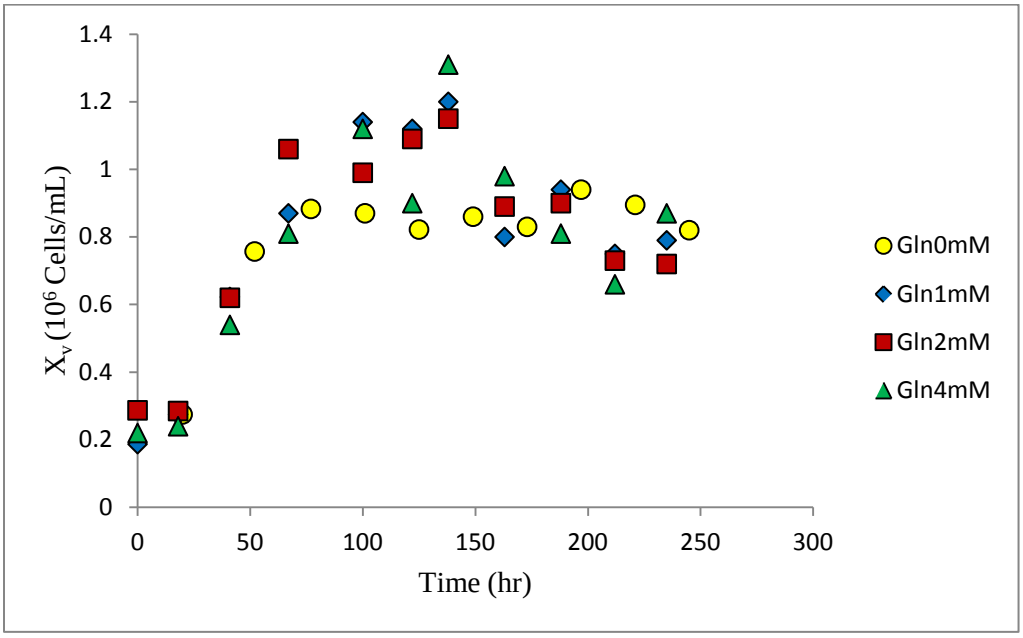

Figure 4.1: Time profile of total viable cell density of CHO cells cultured at different glutamine concentrations.

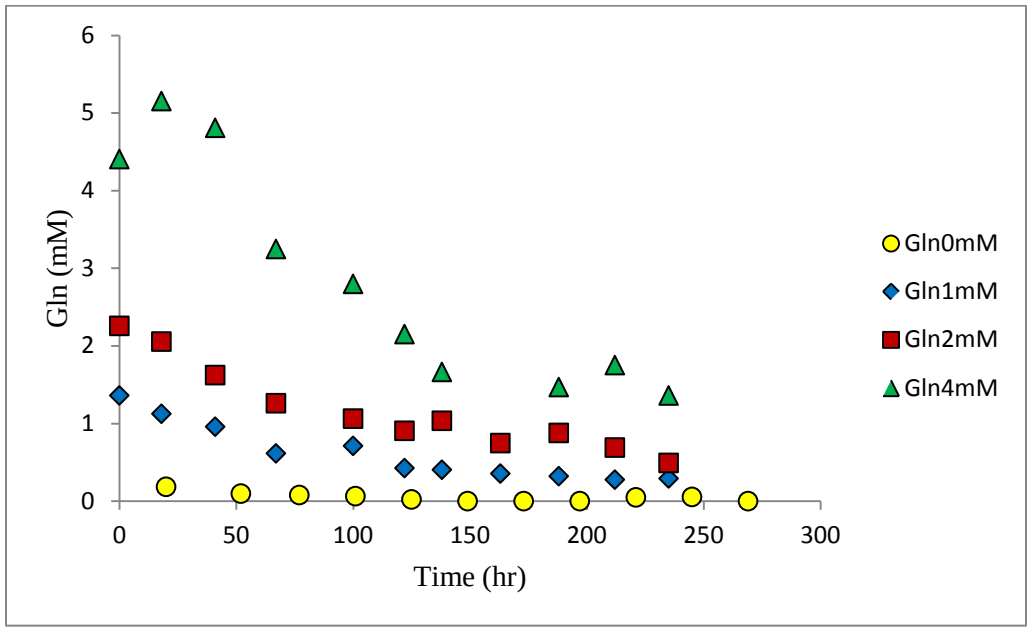

4.2: Time profile of glutamine concentration of CHO cells cultured at different glutamine concentrations.

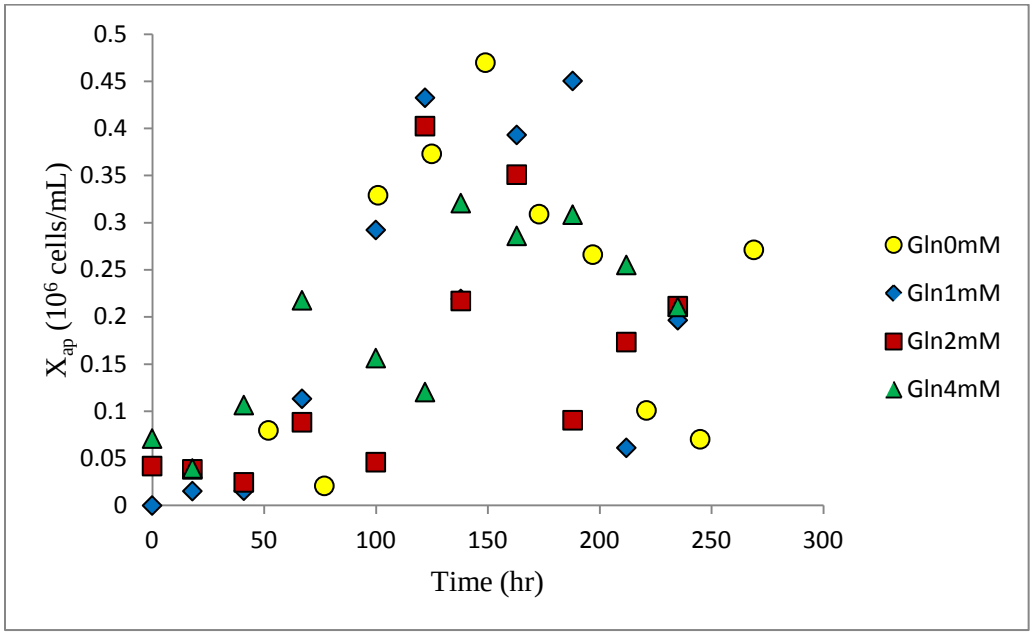

4.3: Time profile of total viable apoptotic cell density of CHO cells cultured at different glutamine concentrations.

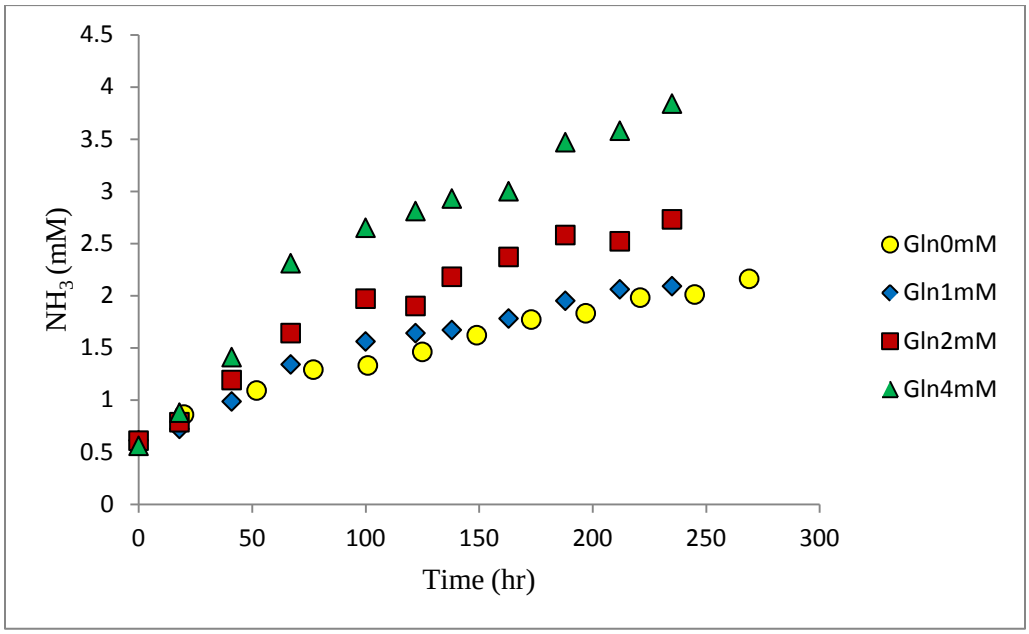

Figure 4.4: Time profile of NH_3 concentration of CHO cells cultured at different glutamine concentrations.

4.3.2 Glucose Effect

To determine the effect of glucose as a main energy source for cell growth, different initial concentrations were examined in a set of batch experiments. Figure 4.5 shows the growth curve of CHO cell culture provided with 4mM, 8mM, 10mM, 12mM and 14mM of glucose. As in case of glutamine studies, experiments using 4mM, 8mM and 14 mM initial glucose levels were performed in duplicate. Almost identical cell growth rates and corresponding peak cell concentrations were observed in all batches, even when employing the lowest glucose concentration (4mM). In addition, the maximum cell density did not increase by increasing the initial glucose level (14mM). The effect of glucose exhaustion obtained after this concentration approach zero at t=70 hrs (Figure 4.6) in the low concentration (4mM) was quite drastic. It is seen in Figure 4.5 that glucose depletion resulted in faster cell death rate as the viability declined dramatically after the stationary state.

Similarly, the rate of apoptosis was higher at low initial level of glucose, implying the clear role of glucose depletion, in cell death (Figure 4.7); however, this does not imply that glucose depletion is the only factor leading to apoptosis. There are likely other, yet unknown, nutrients involved. This was confirmed by culturing at higher initial glucose concentrations where cells underwent apoptosis even in the absence of glucose limitation.

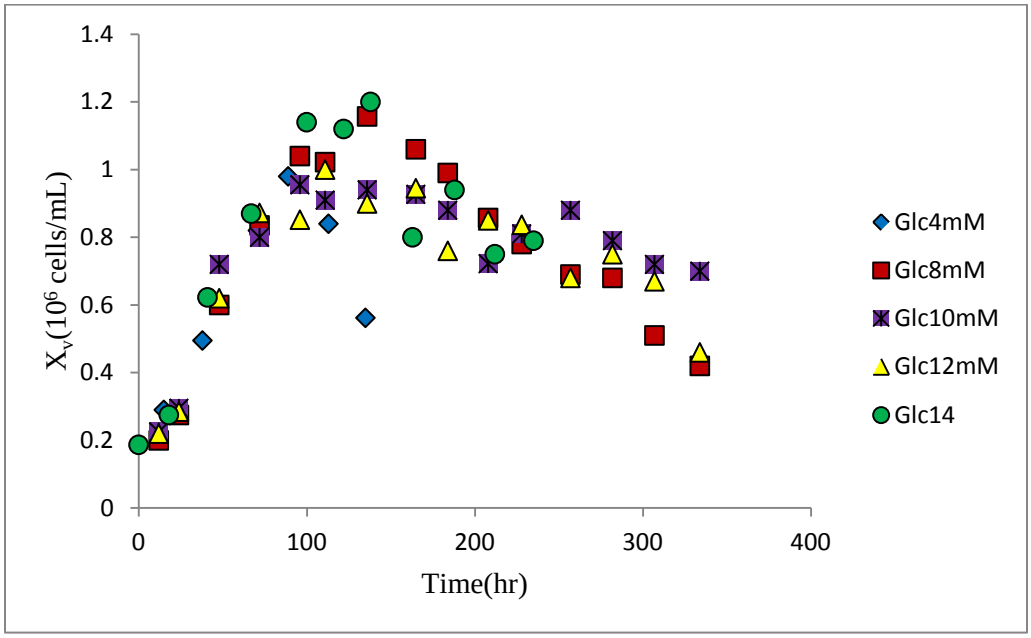

Figure 4.5: Time profile of total viable cell density of CHO cells cultured at different glucose concentrations.

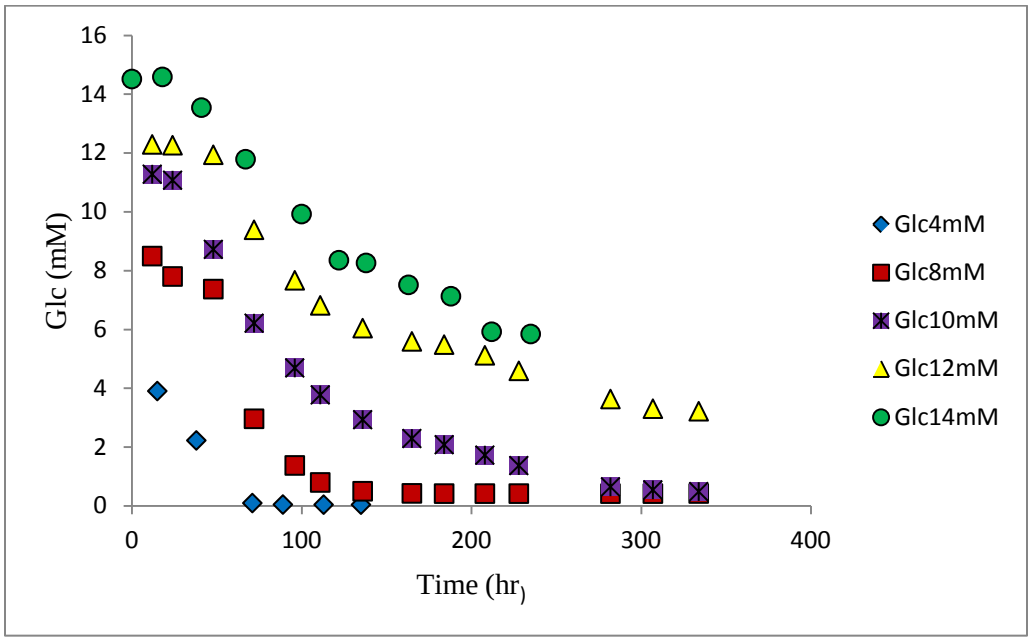

Figure 4.6: Time profile of glucose concentration of CHO cells cultured at different glucose concentrations.

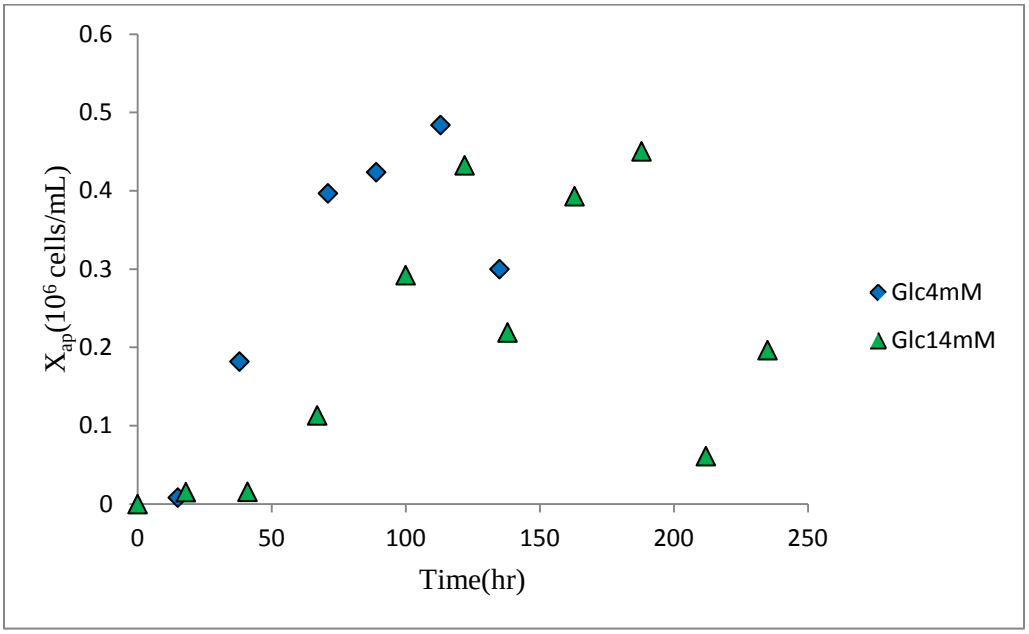

Figure 4.7: Time profile of total viable apoptotic cell density of CHO cells cultured at different glucose concentrations.

4.3.3 Asparagine Effect

Similarly to glutamine metabolism, asparagine has been found to possess a significant consumption rate in CHO cell culture. Based on previous studies (Simon and Karim 2002), asparagine has been reported to be a key amino acid that could potentially suppress apoptosis. Hence, in the following set of batch experiments, different concentrations of asparagine (0.3mM, 0.5mM, 1.5mM and 4mM) were employed (Figure 4.8). Experiments employing 0.3 mM of asparagine were performed in duplicate. Figure 4.9 shows similar trend for cell growth curve in all four batches. Neither the specific growth rate nor the peak concentrations could be correlated with the asparagine concentration. This implies that increasing the level of asparagine does not improve the culture in terms of growth rate, maximum cell density and viability.

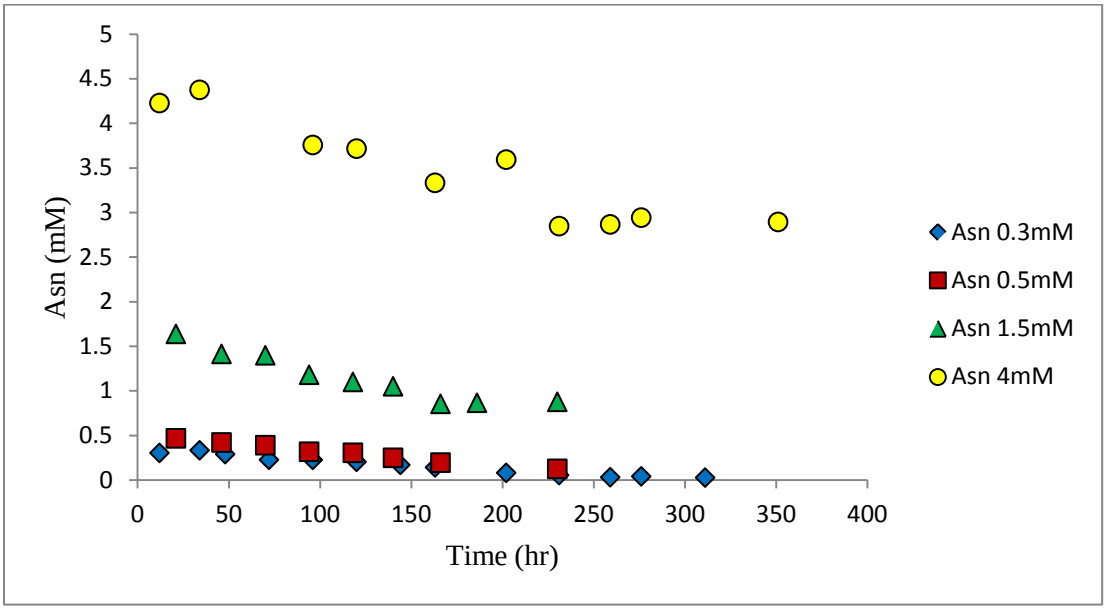

Figure 4.8: Time profile of asparagine concentration of CHO cells cultured at different asparagine concentrations.

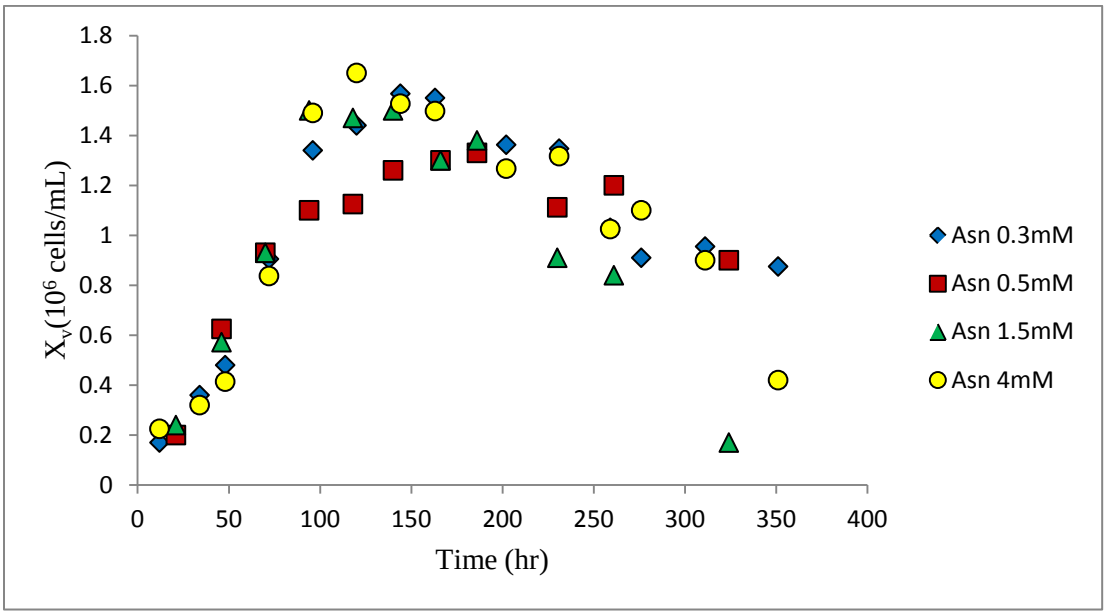

Figure 4.9: Time profile of total viable cell density of CHO cells cultured at different asparagine concentrations.

Chapter 5
Cell Culture Media Supplement

5.1 Introduction

Although glutamine, glucose and asparagine are basic multi-functional nutrients that are essential in nucleotide biosynthesis, energy production and recombinant protein synthesis, it is assumed that there are other essential components which restrict cell growth and survival upon depletion. It was found in this work that cell growth was arrested in spite of low level of by-product (i.e. lactate and ammonia) accumulation and surplus of glucose and glutamine exhaustion. This implies that the influence of these toxic byproducts might not be significant. Hence, the approach at this stage was enriching the cell culture environment to avoid exhaustion of any essential component.

Due to the complexity of the culture's requirements and lack of knowledge of the exact composition of the basal and feed medium, it is impossible to characterize and quantify the depleting ingredient, particularly in the presence of serum in the culture which is a specific source of variability. Therefore, because of the aforementioned considerations, supplementation of the culture was limited to employ the current regular medium SFX-CHO at different concentrations (1X, 2X and 5X enrichment) and animal-derived component free concentrated CHO medium (Sigma). Culture supplementation was examined at three modes of operation: simple batch, single-pulse feeding and fed-batch culture using identical feeding intervals. In the pulse experiments a single amount of feed was added whereas in the fed-batch experiments smaller amounts were added periodically at different instances during the post-exponential phase. The single pulse feeding was attempted in order to elucidate effects with a larger sensitivity. On the other hand fed-batch operation was done since a final objective of the work was to assess the possibility of improving growth and productivity by a suitable fed-batch strategy. In case of batch operations the concentrated medium was added at the beginning (t=0).

5.2 Materials and Methods

5.2.1 Medium Composition

Previously (Chapter 4) SFX-CHO medium was the basal medium to perform sub-culturing and to perform the experiments. In the present studies initial glutamine and serum supplementation in the culture was maintained at 1-2 mM and 1-2 % respectively. Feed medium contained the SFX-CHO medium at either normal or concentrated levels by approximately two fold (2X) and five fold (5X). Following our communications with the manufacturer, the concentrated medium was prepared with higher amino acid and growth factor concentrations in comparison to the normal one. Glucose and salt concentrations were kept identical in order to prevent more lactate formation and osmolality effect. The additional feed medium used in experiments was animal derived component free CHO feed supplement (Sigma-C1615) formulated to optimize CHO cell growth and recombinant protein production in fed-batch cultures.

5.2.2 Experimental Design

The first set of experiments involved 3 sets of spinners (500mL) and performed as preliminary un-optimized fed-batch cultures. The initial volume of the spinner culture was 300mL with seeding density of around 0.3×10^6 cells/mL prepared from the same inoculum in each spinner flask. Then, regular SFX-CHO was used as a feed medium together with 2% serum, 30mM glucose and 2mM glutamine. This feeding consisted in adding 25 mL aliquots starting after 52 hours at 3 different feeding times: 12 hr, 24 hr and 48 hr for each spinner.

Subsequently, a second set of experiments was conducted to test the feeding of single pulses. Four 500mL spinners were run and one pulse feed of concentrated medium C1615 at different quantity, with/without serum was added at two different time points as follows. To serve as control, the first spinner was conducted with 5mL/L of concentrated feed at t=0, i.e. simple batch culture. In the second and third spinners pulse feeding of 5mL/L of concentrated medium was performed after the cells concentration passed the peak at t=118hr,

except that in the second spinner the feeding solution also contained 1% serum. The fourth spinner was run similarly to the first one as batch culture, but contained a higher amount of concentrated feed (30mL/L). The CHO cell seeding density was between 0.2-0.3×10^6 cells/mL in all spinner cultures.

Based on the results obtained from the aforementioned experiments, a third set of experiments was carried out by applying higher amount of concentrated feed. This third set of experiments also involved four 500mL spinners. The first spinner consisted of a batch culture with regular medium as a control. A second spinner involved a batch culture of 460mL regular medium with 40mL of concentrated CHO feed supplement (Sigma-C1615). The third spinner was started with 460 mL of regular medium and pulse fed with 40 mL concentrated medium (Sigma-C1615) at t=48 hrs, and the last spinner was a fed-batch culture initiated with 360 mL regular medium and daily feeding started at t=48hrs. The feeding medium of 25 mL at each occasion was obtained from a mixture containing 100/40 ratio between regular medium and concentrated medium (Sigma-C1615). The seeding density was almost identical in all 4 spinners (approximately 0.2×10^6 cells/mL) and serum (1%) and glutamine (1mM) were added only at the beginning of the culture.

The fourth set of experiments involving 3 batch cultures was conducted to test the effect of 1X, 2X and 5X concentrations of medium that were especially ordered from the manufacturer. The basal medium used was SFX-CHO at different concentrations, i.e. 1X, 2X and 5X respectively. The working volume was 500mL with seeding density of 0.2×10^6 cells/mL, 1% serum and 1mM glutamine. The goal of this experiment was to evaluate the influence of the current medium with higher concentrations of amino acids, vitamins and growth factors, but identical glucose, glutamine, salt and serum values.

The incubator set point was kept unchanged as described in Chapter 3. The culture time for each experiment was nearly 2 weeks. Samples of 3mL were taken aseptically each day for further off-line and at-line analysis.

5.3 Results and Discussion

Figure 5.1 is the comparison of the total viable cell concentration of the un-optimized fed-batch runs using different feeding time intervals. No consistent improvement in the concentration of viable cell was observed and the peak of viable cell for the shorter feeding time (every 12 hrs) is lower. This can be attributed to the dilution effect of the culture, in which cell growth could not compensate for the dilution effect of feeding. In addition, almost identical volumetric cell-hour (VCH) was computed for the 3 runs as shown in Figure 5.2. This implies that change in feeding time has no significant effect on the maximum viable cell density or culture time extension. The corresponding glucose and glutamine data (Figure 5.3 and 5.4) obtained during these experiments also show that the concentration is almost constant during feeding and no exhaustion occurred, even at the longer feeding time (48 hrs) when the consumption rate was slightly higher. As expected, similar lactate and ammonia concentration results (Figure 5.5 and 5.6) were obtained for the 3 fed-batch runs and their maximum concentrations reached to less than 20 mM and up to 3 mM, respectively which are considered to be low in terms of toxic effects. For instance, several studies have reported that CHO cells can survive at these concentrations of ammonia and lactate (SUN and ZHANG 2002; Xing et al. 2008).

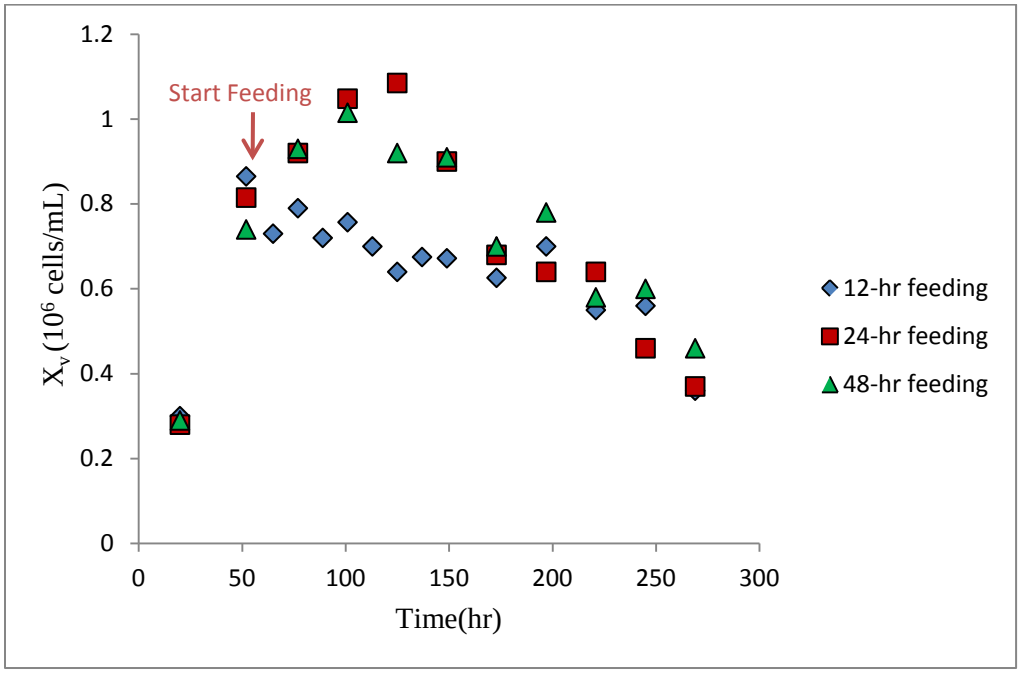

Figure 5.1: Time profile of total viable cell density of CHO cells in fed-batch culture at different time feeding intervals.

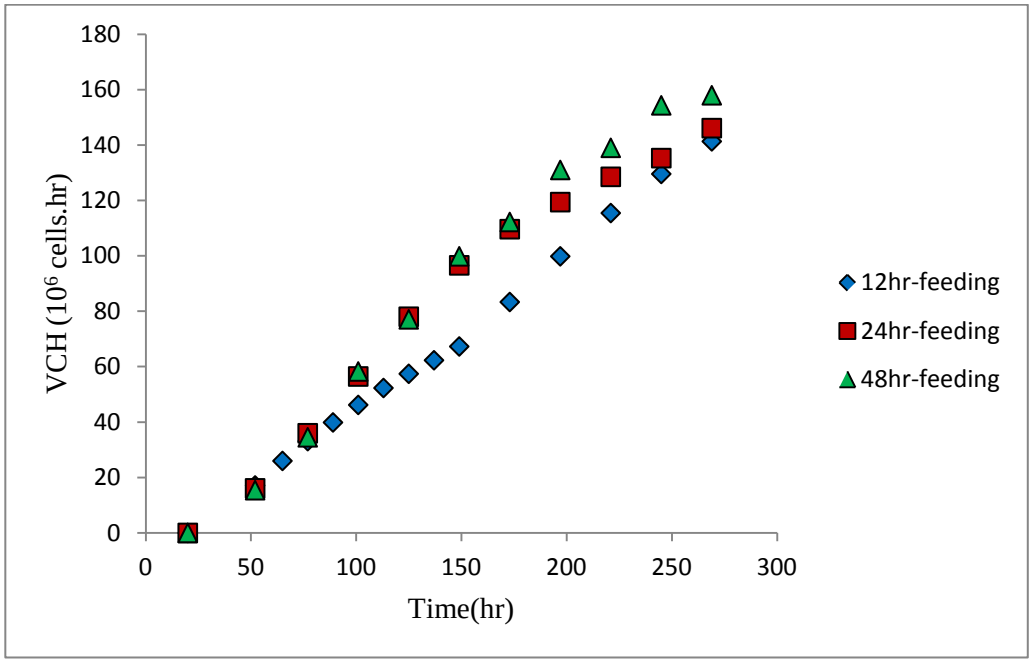

Figure 5.2: Time profile of volumetric cell hour of CHO cells in fed-batch culture at different time feeding intervals.

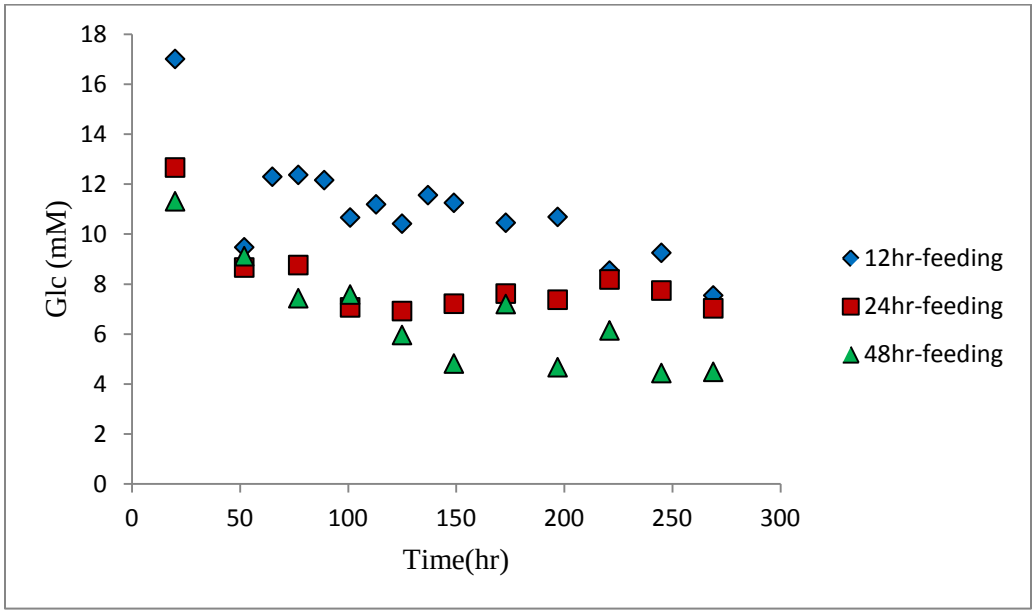

Figure 5.3: Time profile of glucose concentration of CHO cells in fed-batch culture at different time feeding intervals.

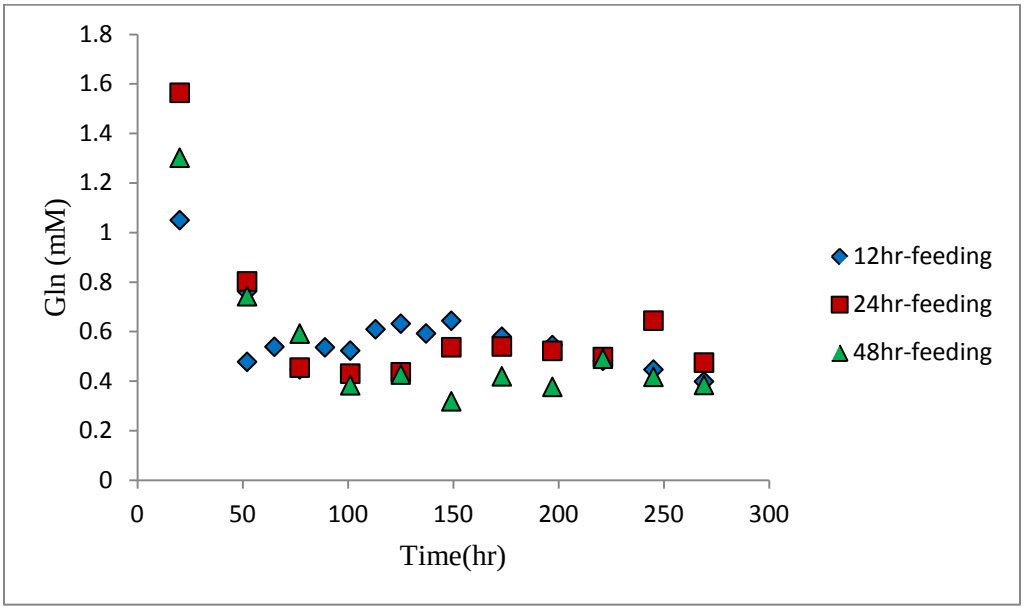

Figure 5.4: Time profile of glutamine concentration of CHO cells in fed-batch culture at different time feeding intervals.

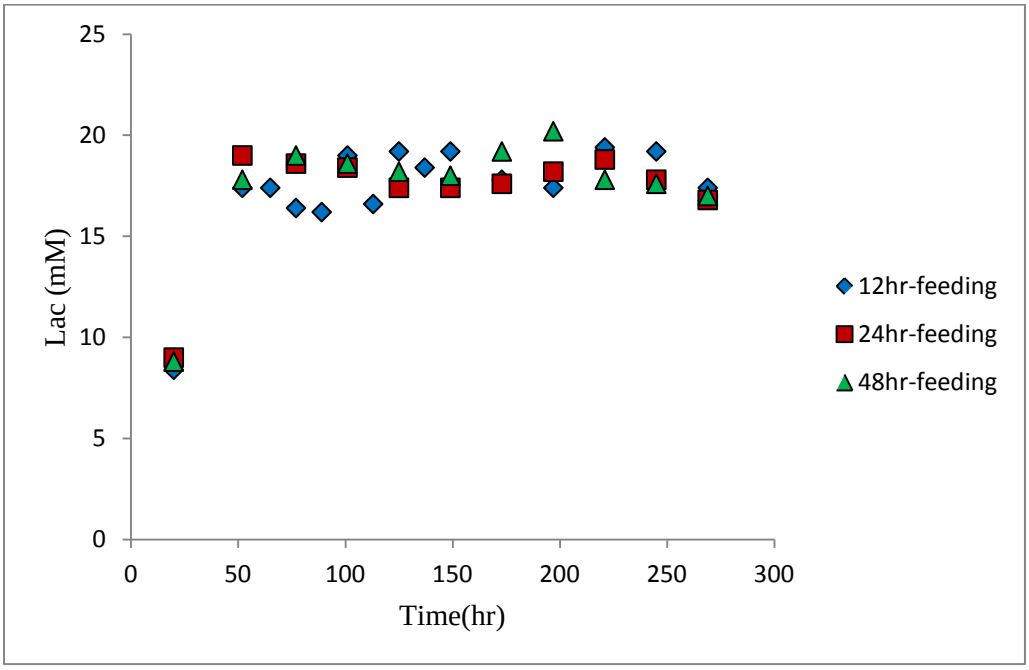

Figure 5.5: Time profile of lactate concentration of CHO cells in fed-batch culture at different time feeding intervals.

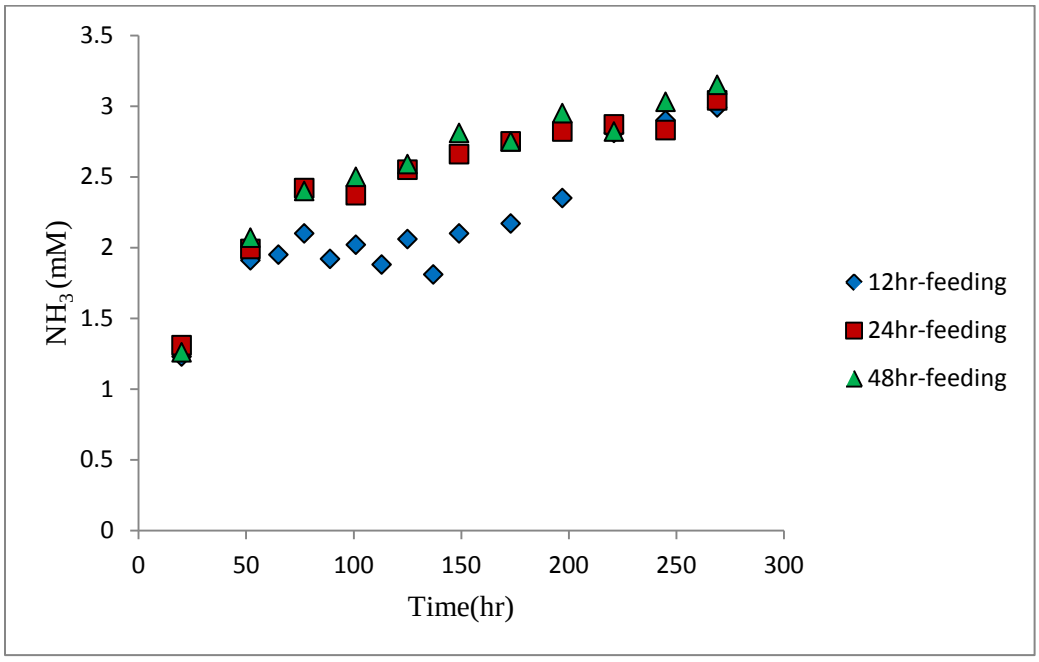

Figure 5.6: Time profile of NH_3 concentration of CHO cells in fed-batch culture at different time feeding intervals.

Based on the assumption that growth is limited when an unknown component in the regular SFX-CHO medium is being exhausted, the first attempt was using the same medium as feed in single-pulse additions' experiments. In order to eliminate culture dilution effect, pulsing with concentrated medium with different quantities and at different time periods was examined. Figure 5.7 presents the comparison of total viable cell concentration in 4 occasions of single-pulse feeding. Although the cell growth rate was equal in all cultures, contrary to the expectations the highest cell peak was achieved in batch run (feeding at t=0) with higher concentrated feed (30mL/L). However the high density condition was not stable and the density decline occurred much faster. Good viable cell density and viability was attained in batch culture with feeding 5mL/L (as recommended by the medium manufacturer) as well. The volumetric cell hour results also verify better performance for both batch culture runs, however, the difference is not significant (Figure 5.8). Glucose and glutamine concentration data of all runs exhibit almost identical consumption rate with no exhaustion, except that the last run began with slightly higher initial glutamine concentration (Figures 5.9 and 5.10). While using equal amount of glutamine in each spinner, maximum ammonia accumulation exceeded 3mM in the last batch (Figure 5.11) containing more concentrated feed (30mL/L). This high value of ammonia could be attributed to the presence of other amino acids such as asparagine, glutamate, aspartate present at high concentration in the feed medium (data not shown). The metabolism of these amino acids via the TCA cycle is expected to result in higher ammonia production. Since inhibition effect of amino acids in high concentrations are not known, rapid drop of viability in the last run could arise from the inhibitory role of ammonia at this level. Due to improvement in the peak cell density in batch culture containing concentrated feed without any reduction in the specific growth rate that could possible occurred due to hyperosmolality (Min Lee et al. 2009), the use of higher quantity of concentrated feed medium in various culture modes was examined. As mentioned before a simple batch culture run was used as a control.

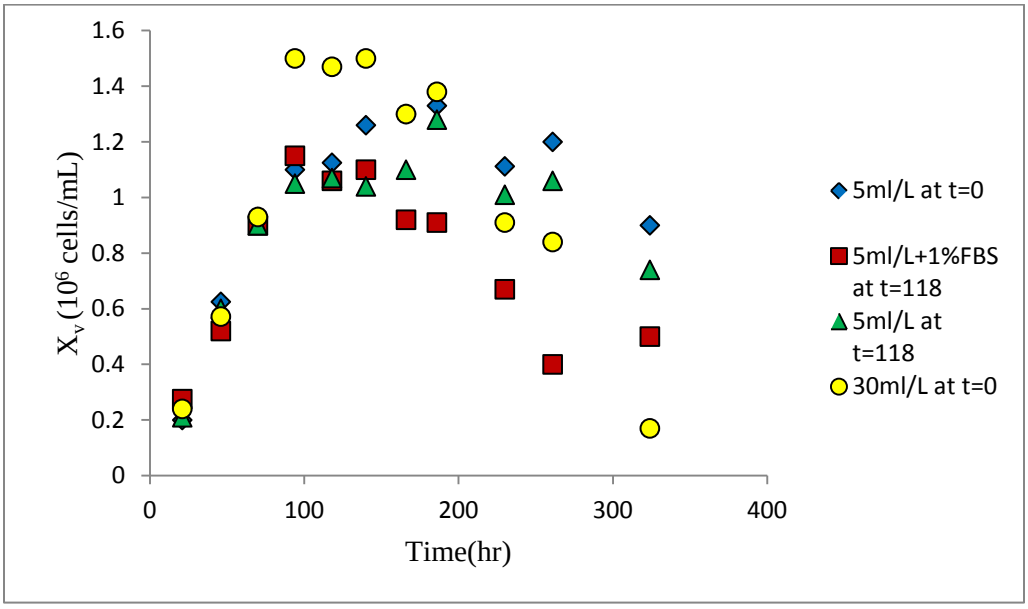

Figure 5.7: Time profile of total viable cell concentration on 4 occasions of single-pulse feeding.

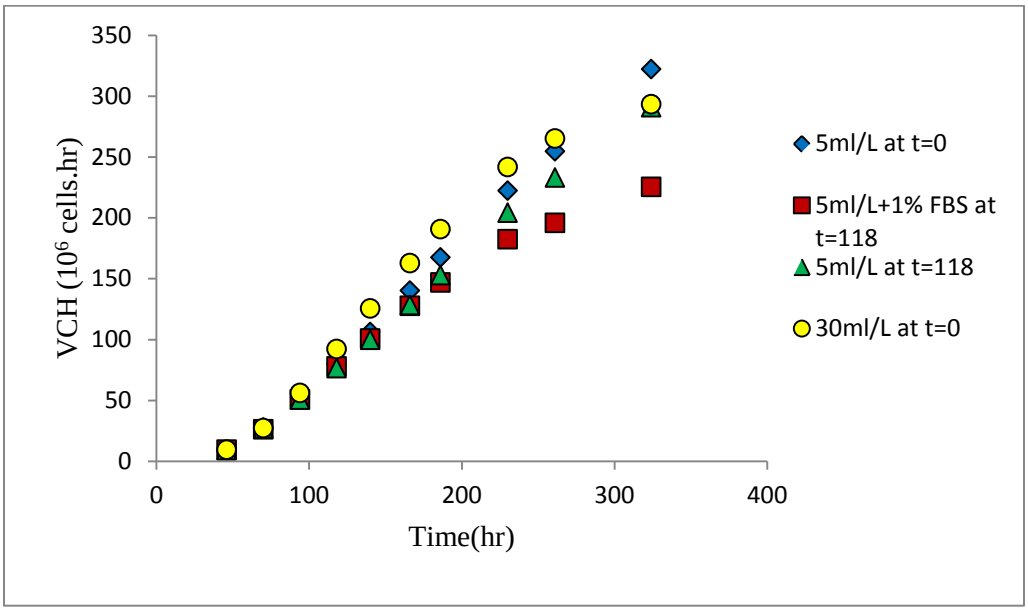

Figure 5.8: Time profile of volumetric cell hour on 4 occasions of single-pulse feeding.

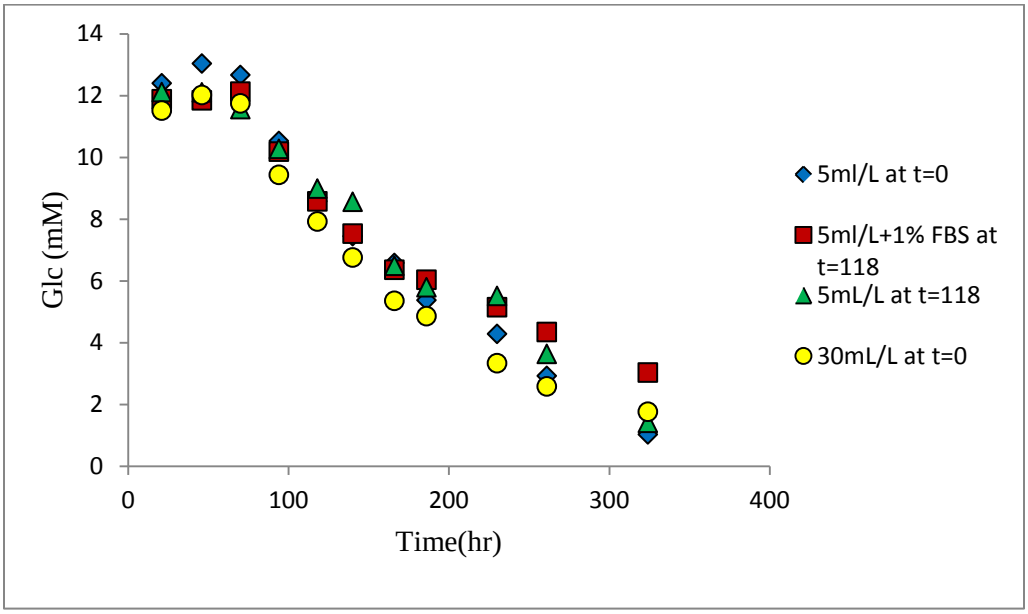

Figure 5.9: Time profile of glucose concentration on 4 occasions of single-pulse feeding.

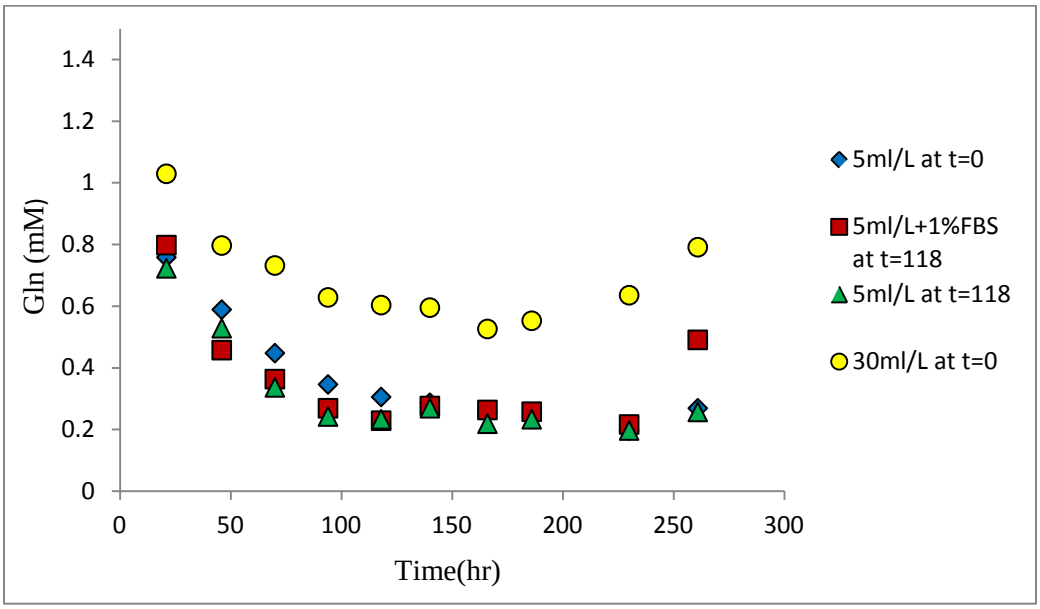

Figure 5.10: Time profile of glutamine concentration on 4 occasions of single-pulse feeding.

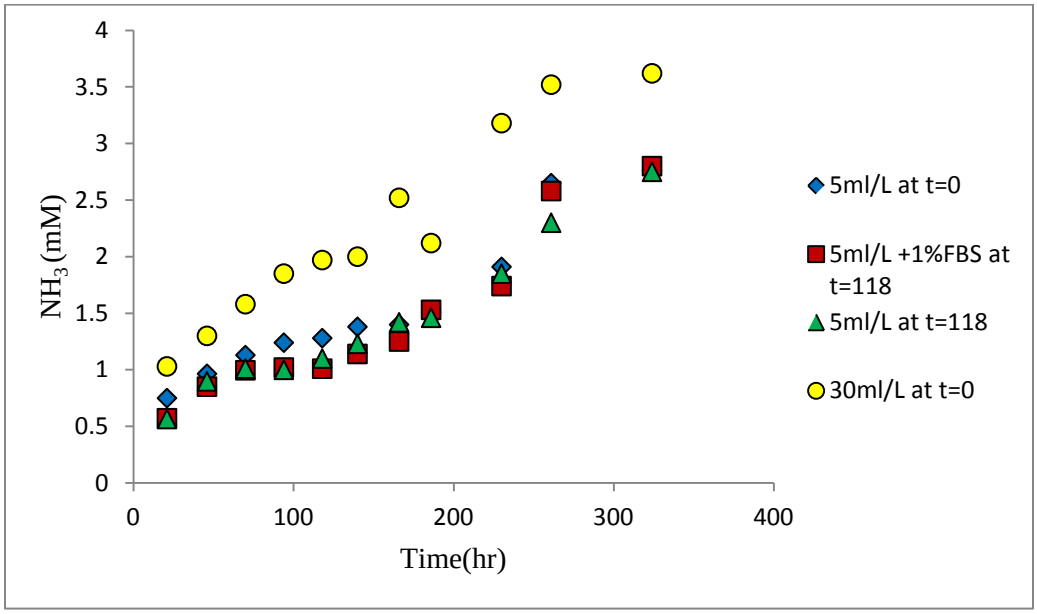

Figure 5.11: Time profile of NH_3 concentration on 4 occasions of single-pulse feeding.

Despite the differences between the spinner conditions in terms of concentrated feed used, feeding time, and operation mode, similar results were obtained for total viable cell concentrations and volumetric cell hours as well as shown in Figures 5.12 and 5.13. Glucose consumption rate was also the same in all spinners (Figure5.14). Additionally, in all above-mentioned experiments the initial glutamine concentration was equal, however, in contrast to simple batch culture in which glutamine was consumed as usual, it has been produced in the other 3 cultures (Figure 5.15). The production of glutamine could be associated with reversing of the glutamine deamination reaction by glutamine ammonia lyase. Consequently higher levels of ammonia could have been produced by amino acids metabolism (Figure 5.16). It was noteworthy that high ammonia accumulation in two pulse-fed spinners (at t=0 and t=48) had no remarkable effect on the viable cell profile.

Besides, the batch experiments conducted with regular and concentrated (2X and 5X) SFX-CHO medium did not show any significant improvement (data not shown). In case of the 2 spinner culture with 1X and 2X medium, similar results was obtained for viable cell density data, while no growth was observed with 5X medium. No growth occurred in flask

culture as well. It is hypothesized, based on discussions with the manufacturer, that at 5X concentrations, precipitation of medium components may have occurred thus explaining the lack of growth.

In addition, high serum level of 10% was also carried out to investigate whether growth is limited by the depletion of some component in the serum. Although cell adaptation was not possible in a serum free environment, enhancement of the serum up to 10% did not improve the growth and maximum cell density (data not shown). The aforementioned experiments seems to suggest that cell growth inhibition may not be related to depletion of a medium or serum component (Zhu et al. 2005) but it may rather be related to extracellular stimuli (Chong et al. 2011) or to the formation of inhibitory byproducts other than ammonia or lactate since the latter did not reach inhibitory levels. Hence in subsequent studies other effects (cell density, CO_2, O_2) were examined either individually or in combination.

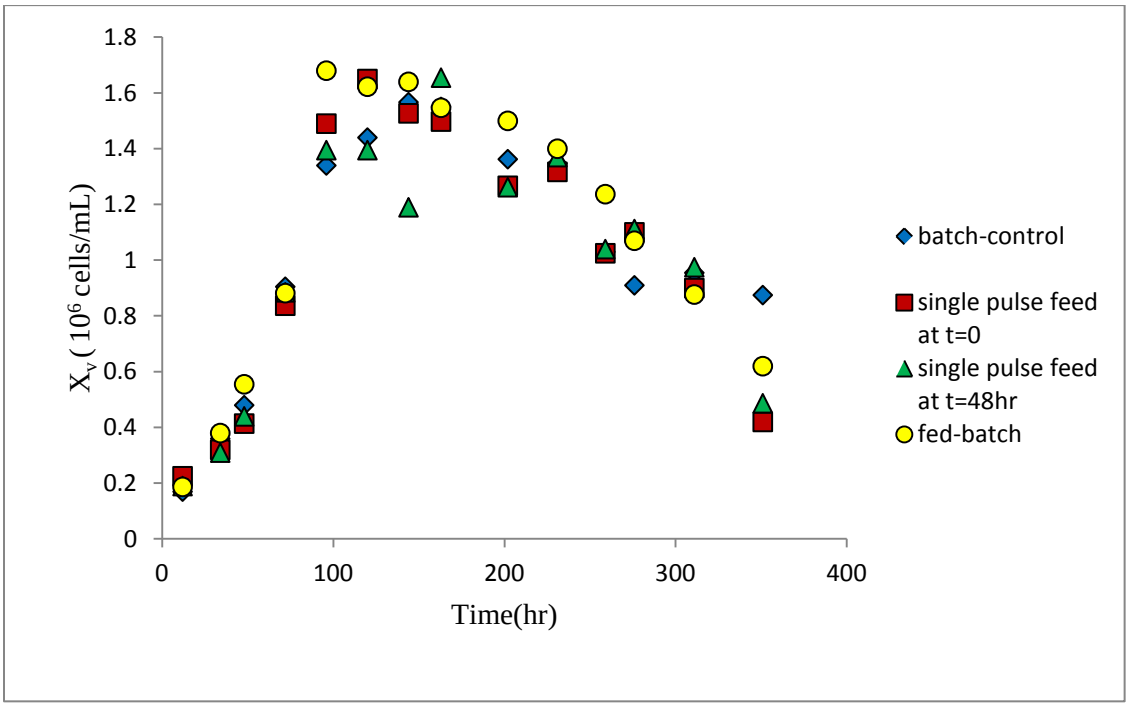

Figure 5.12: Time profile of total viable cell concentration on 4 occasions of concentrated medium feeding.

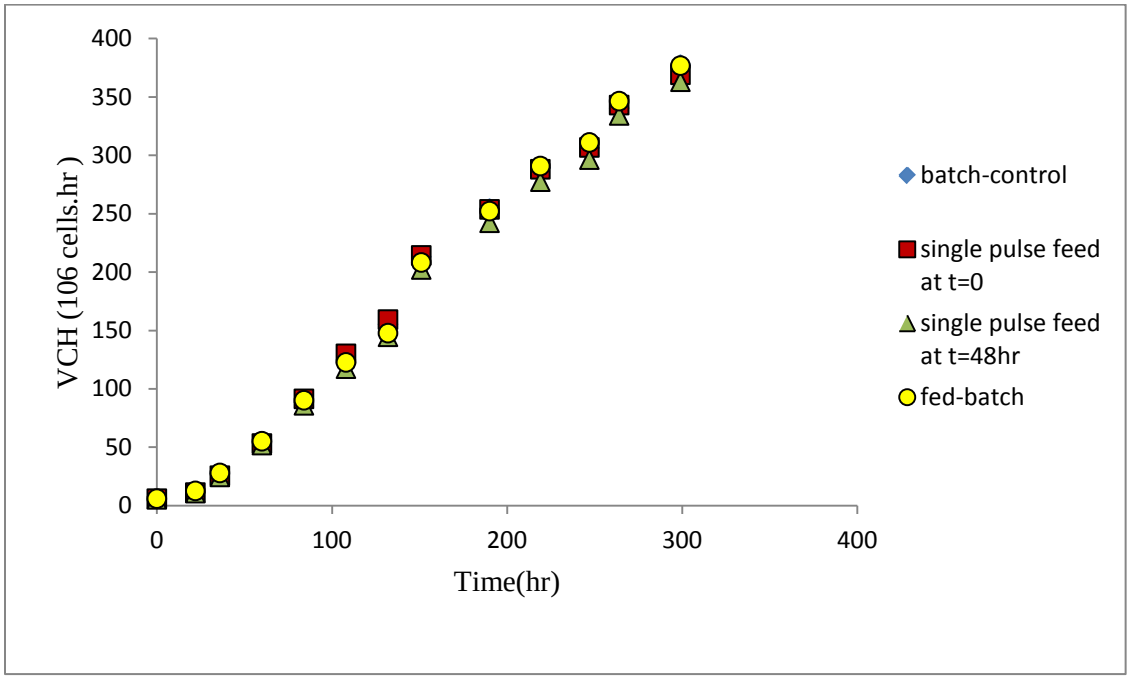

Figure 5.13: Time profile of volumetric cell hour on 4 occasions of concentrated medium feeding.

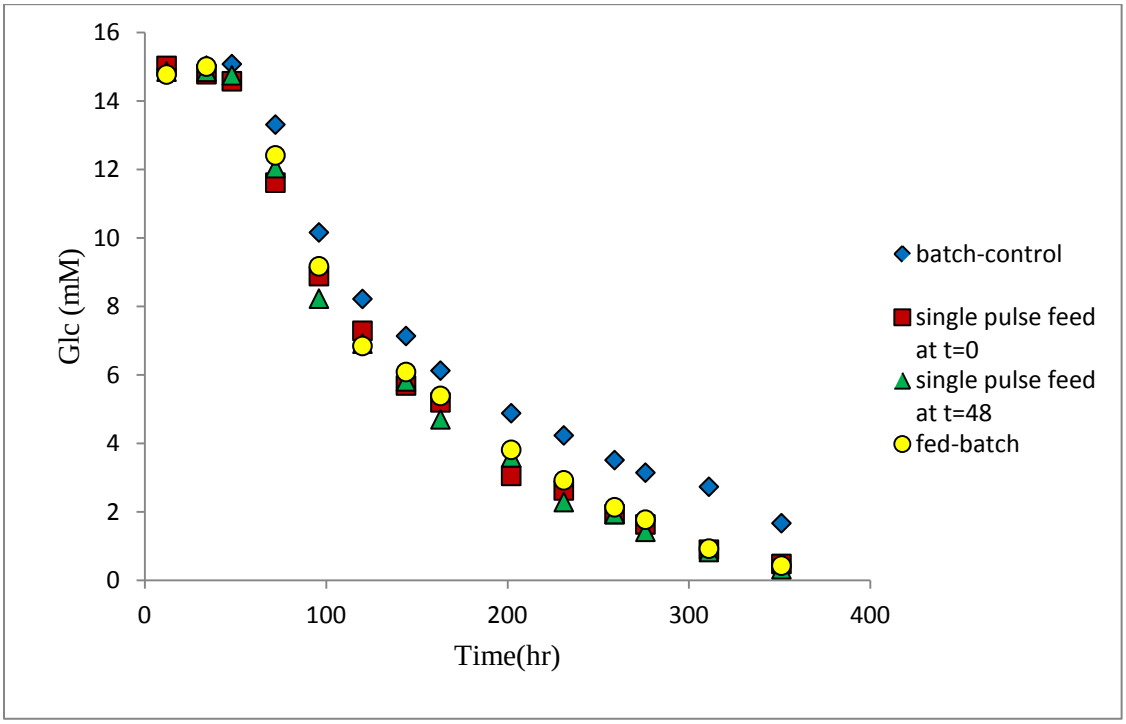

Figure 5.14: Time profile of glucose concentration on 4 occasions of concentrated medium feeding.

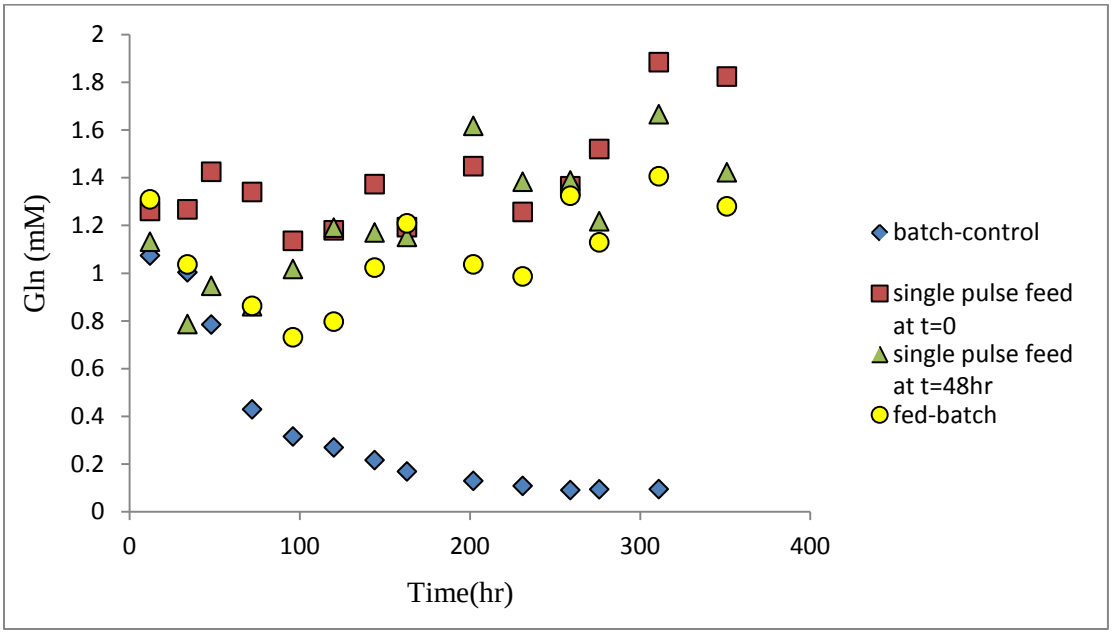

Figure 5.15: Time profile of glutamine concentration on 4 occasions of concentrated medium feeding.

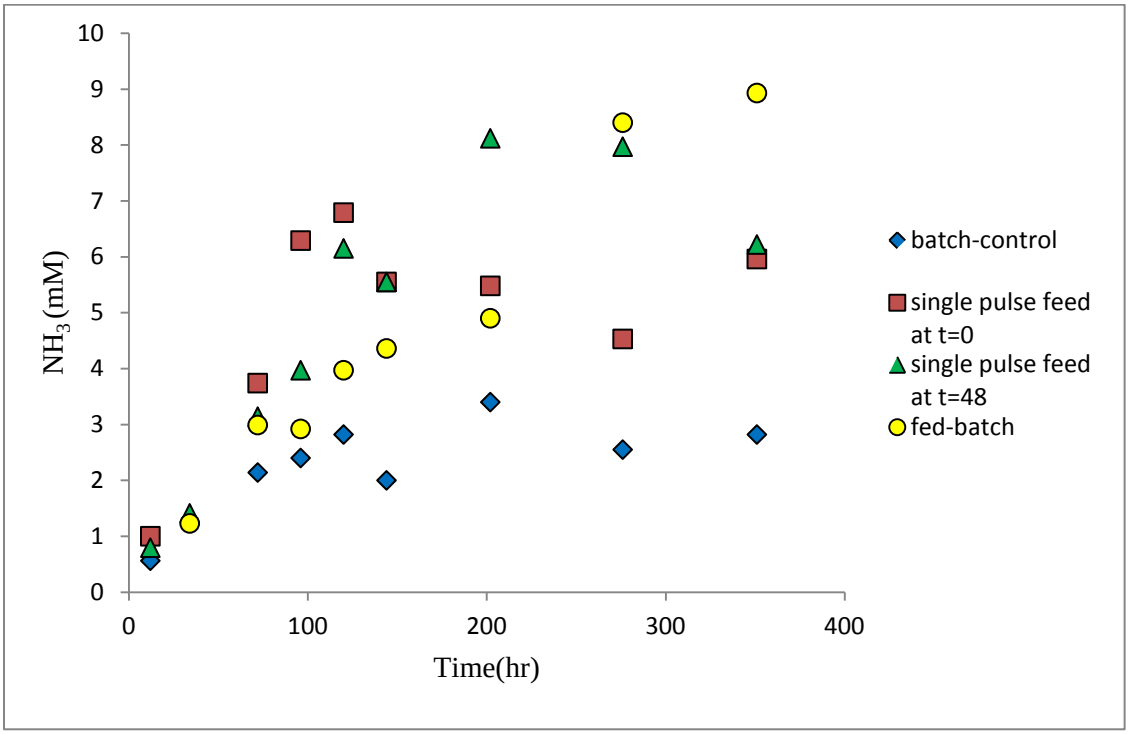

Figure 5.16: Time profile of NH_3 concentration on 4 occasions of concentrated medium feeding.

Chapter 6
Cell Density Effect

6.1 Introduction

In Chapter 5, where the potential depletion of an essential nutrient was investigated it was found that growth arrest may not be directly related to such depletion. The metabolic behavior of culture at this point seems to indicate that the consumption of metabolites is applied for maintenance due to the observed stable high viability. Similar behavior was also seen in the culture with high level of serum (10%) further indicating that other factors rather than essential nutrients may be involved in cell growth arrest. There have been previous investigations regarding density-dependent growth inhibition (Hardy and Stark 2002; Lee 2002), however there is still uncertainty regarding the factors and growth regulation mechanism. Hence, as a next step, the effect of cell density on the specific growth rate and the onset of apoptosis were examined from two points of view. The first approach involved applying different seeding density. The second involved rejuvenating the culture at the time that the cell density peak is reached by diluting the culture using different supplements such as PBS or regular medium. The results achieved in these experiments were also subsequently applied in a proposed biomass mathematical model describing cell density effect on the growth and apoptosis initiation in the culture.

6.2 Materials and Methods

6.2.1 Medium Composition

In all experiments the regular medium SFX-CHO was used as the basal medium supplemented with 1% serum and 1mM of L-glutamine. However, in order to achieve consistency regarding nutrient availability in all cultures with different seeding density level, the ratio of serum and glutamine was adjusted according to the initial cell density.

Accordingly, the concentration of serum and glutamine was four-fold higher in the high seeding density culture (0.8×10^6 cells/mL) compared to the low-density seeding culture (0.2×10^6 cells/mL).

The culture medium in the dilution effect experiment consisted of a combination of the regular medium SFX-CHO (1X) and enriched medium (2X). The latter was used to prevent the depletion of any essential nutrient after diluting the culture. The diluting solution for the second set of experiments consisted of phosphate-buffered saline (1×PBS) from Sigma or regular medium SFX-CHO, both supplemented with or without serum and glucose. PBS is a water-based isotonic solution which can provide a constant pH and since it is non-toxic, PBS is generally used in bioresearch.

6.2.2 Experimental Design

In the first set of batch experiments for the assessment of the effect of initial cell density, cells were cultivated in 500mL spinner flask (Bellco Glass Inc., USA) at various seeding density, i.e. 0.2, 0.5, and 1×10^6 cells/mL. The inoculum preparation was based on centrifugation of the seed culture at 1000 rpm for 5 min, and re-suspending the cells in fresh medium to get similar culture conditions in all spinners. Due to loss of cells during centrifugation, the initial seeding density was somewhat less than the intended concentrations.

In the second set of experiments for assessing the effect of culture dilution the process was started as a simple batch culture in 2 spinners with initial culture volume of 400mL seeded with 0.2×10^6 cells/mL. Cell growth was tracked in the exponential phase and after the peak one-pulse feeding of either 100mL of fresh regular medium or 100mL of PBS containing 15mM glucose were added to each spinner. The cell physiological response was monitored and assayed through various analyses.

In order to ensure the reproducibility of the pulse-feeding experiments and to provide a clear possibility of enhancement of cell growth after dilution, another set of experiments was performed with two spinner cultures seeded with 0.3×10^6 cells/mL, but lower initial volume

of 250mL. The medium used in the two spinners was regular and enriched SFX-CHO (1X and 2X) respectively, supplemented with 2% serum. The reason for applying double concentrated medium was to ensure no exhaustion of any essential nutrient after diluting the culture. The volume of single pulse feeding was 250mL of PBS to reach to the same final volume of 500mL.

In all experiments, similar conditions inside the incubator were applied as described in Chapter 3. The running time of all cultures was nearly two weeks, with sampling everyday for cell count and subsequent analysis.

6.3 Results and Discussion

In the first set of experiments described above the total viable cell data over culture time for different seeding densities were assessed using the trypan blue exclusion method. The results are presented in Figure 6.1. Under all conditions examined, cells grew in an exponential manner reaching a peak, followed by a plateau phase and eventually declined due to death. However, discrepancies were observed in each phase of the 3 trials. The specific growth rate quantified using these data was affected by the initial cell density (Table 6.1). Increasing seeding density up to a certain point (from 0.15 to 0.3×10^6 cells/mL) led to an increase in the specific growth rate. Further increase in initial cell density (from 0.3 to 0.85×10^6 cells/mL) resulted in decreasing specific growth rate. Although a higher maximum cell density was achieved with increasing seeding density, the culture with high initial cell density (0.85×10^6 cells/mL) was no longer stable in the stationary phase, and entered the death phase at a higher rate. Similar results have been published regarding the influence of inoculum size(Lee 2002). Despite the cells' capabilities in secreting adequate growth factors which provide optimum conditions for growth in the lag phase, the apparent accumulation of toxic metabolites (Figure 6.5) restrained growth and accelerated the death rate. Moreover, nutrient uptake (Figure 6.3 and 6.4) and metabolic activity confirm the possibility of energy requirement for maintenance and high viability, rather than growth.

On the other hand the fluorescent imaging data analysis (Figure 6.2) showed that although the number of the initial apoptotic cells was higher at higher cell density, this number dropped significantly due to death and lysis of apoptotic cells. These observations further reinforced the possibility of cell to cell interaction leading to apoptosis. It was implicitly assumed that cell to cell interactions will become more pronounced as the cell density increases. Cell signaling is not limited only to stimulating growth, but it can also induce the intracellular processes of caspase activation that induce apoptosis and regulation of cell growth (Hardy and Stark 2002). The caspase-8 assay results of Flow Cytometry performed by Meshram (Meshram et al. 2009), also confirms that cells act indirectly as growth-inhibitor at high density by inducing apoptosis.

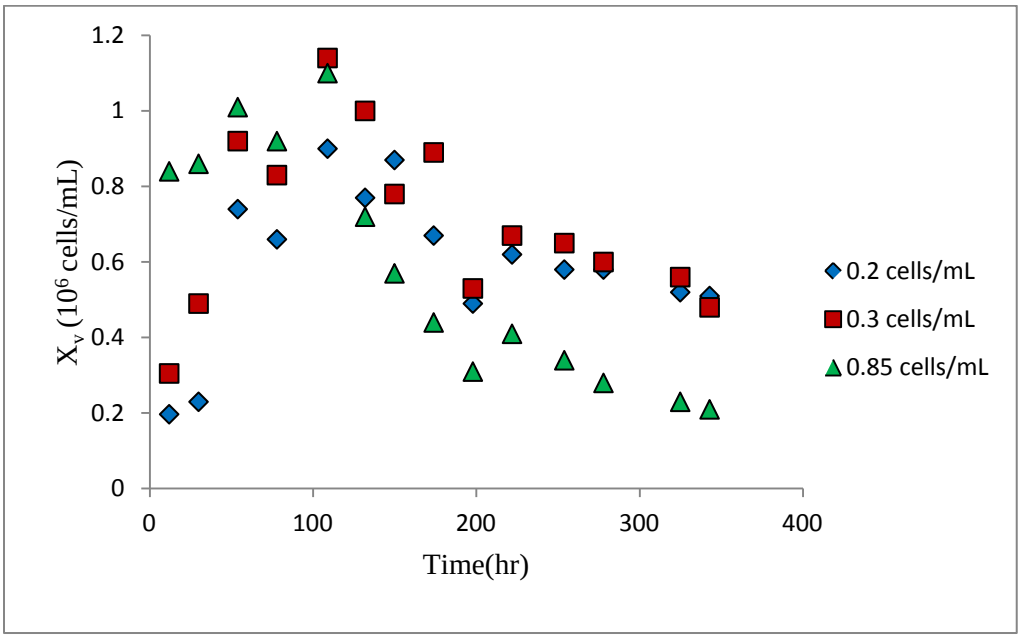

Figure 6.1: Time profile of total viable cell concentration cultured at different initial cell densities.

Table 6.1: The effect of initial cell density on specific growth rate.

Initial cell density (10^6 cells/mL)	Specific growth rate (h^{-1})
0.15	0.01919
0.30	0.02057
0.26	0.02377
0.85	0.00425

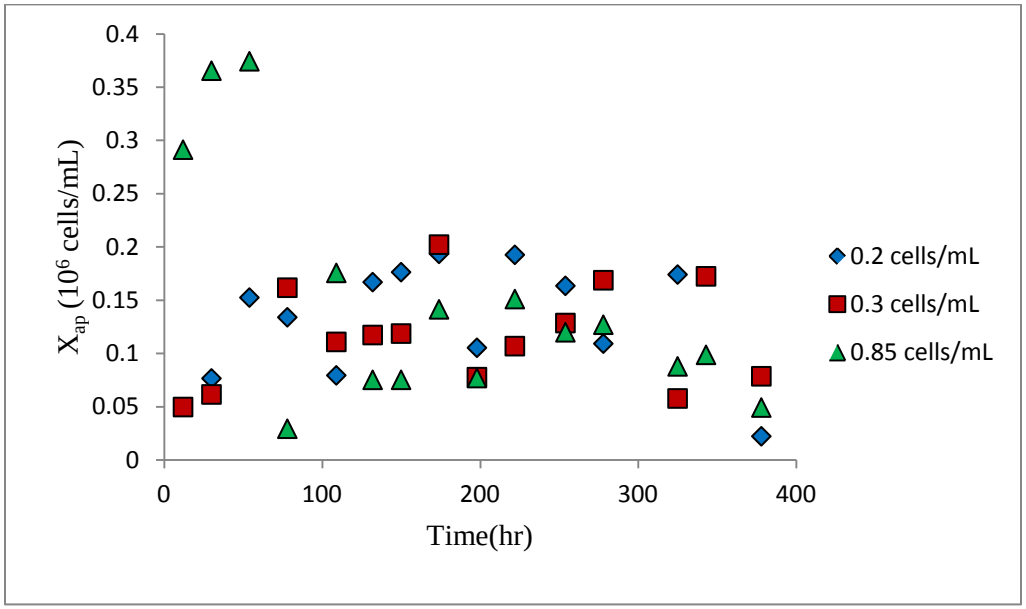

Figure 6.2: Time profile of total viable apoptotic cell concentration cultured at different initial cell densities.

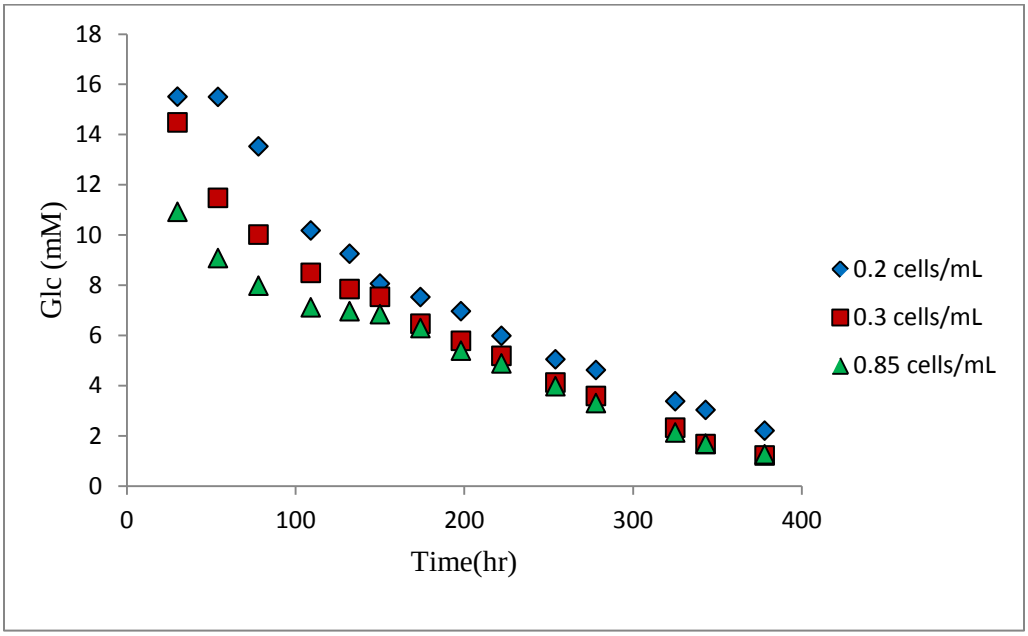

Figure 6.3: Time profile of glucose concentration cultured at different initial cell densities.

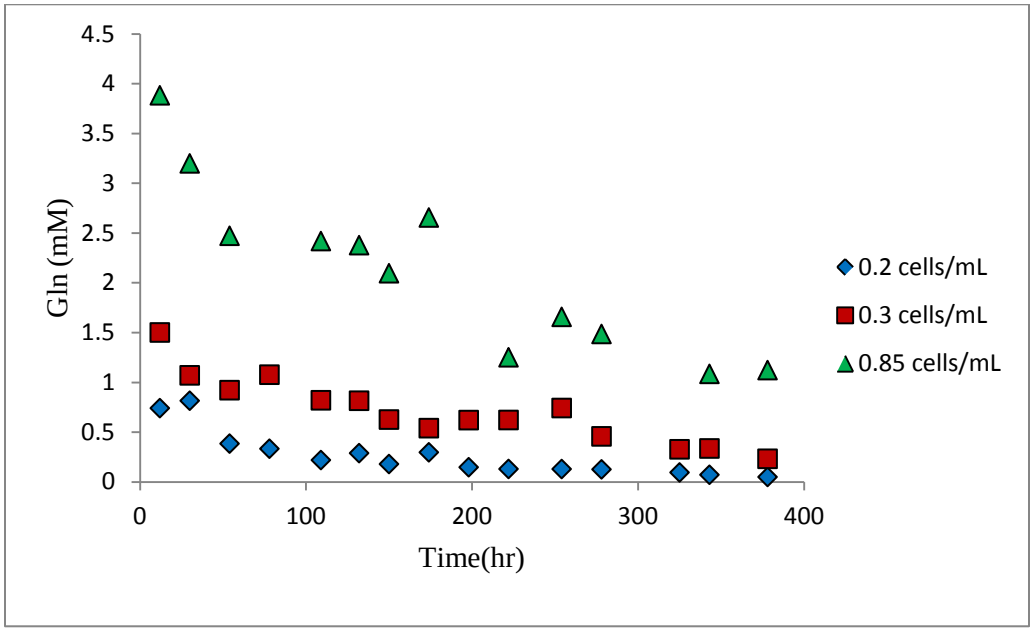

Figure 6.4: Time profile of glutamine concentration cultured at different initial cell densities.

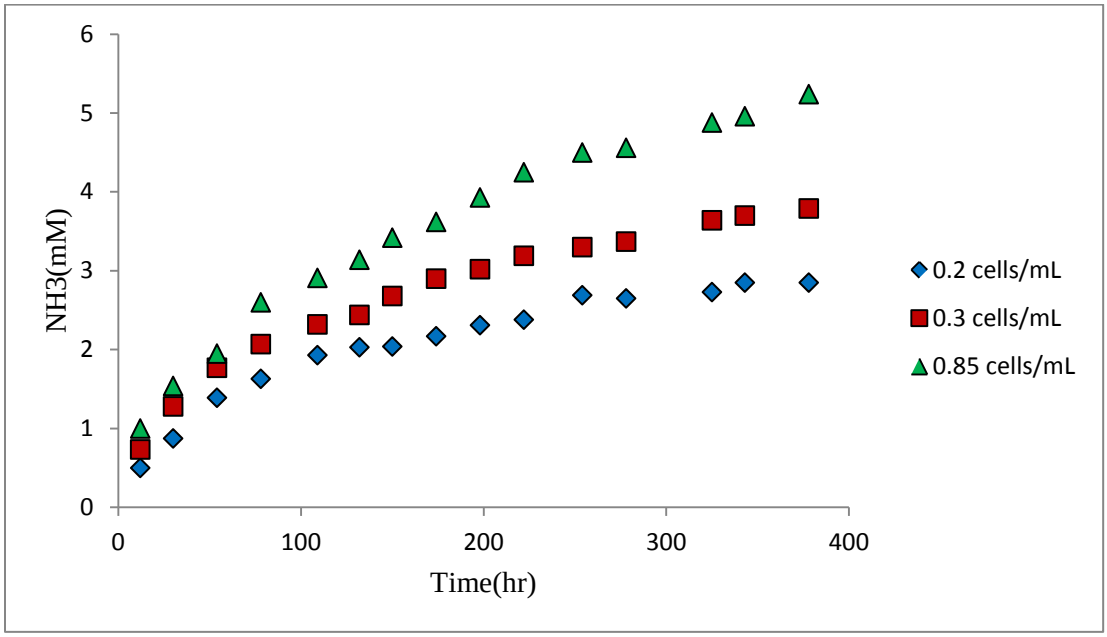

Figure 6.5: Time profile of NH_3 concentration cultured at different initial cell densities.

The next step was to examine whether the cells' physiological state is altered after diluting the culture thereby reducing the inhibiting effect of cell-density. Two spinner cultures similar in all respect except in diluting solution showed almost identical trend in total viable cell concentration (Figure 6.6). The culture was diluted with either regular medium (spinner 1) or PBS (spinner 2) after 110 hours of the cultivation, where cells surpassed the peak and viable cell number remained unchanged. While the cell density decrease with dilution was relatively low, the regeneration of cells was perceptible and the cell population rose to the saturation density, however in the second spinner (with PBS solution) cell revival was not as significant as in the first one. Recovery of the culture could be attributed to cell induction mechanism involving cells arrested in G_0 or G_1 phase to re-enter S and M phases and resuming proliferation. The occurrence of culture revival in the spinner diluted with PBS, despite the possibility that due to dilution an essential nutrient may have reached limiting levels, further suggests the possibility of cell-density inhibition effect. In a similar study performed by Thombre and Gadgil, the improvement in nutrient utilization and protein production was partially attributed to reduction in culture inhibitory concentration by diluting

the culture with PBS (Thombre and Gadgil 2011). Figure 6.7 also shows no depletion in glucose concentration even in diluting the culture with PBS and lactate concentration did not change significantly after dilution (Figure 6.8).

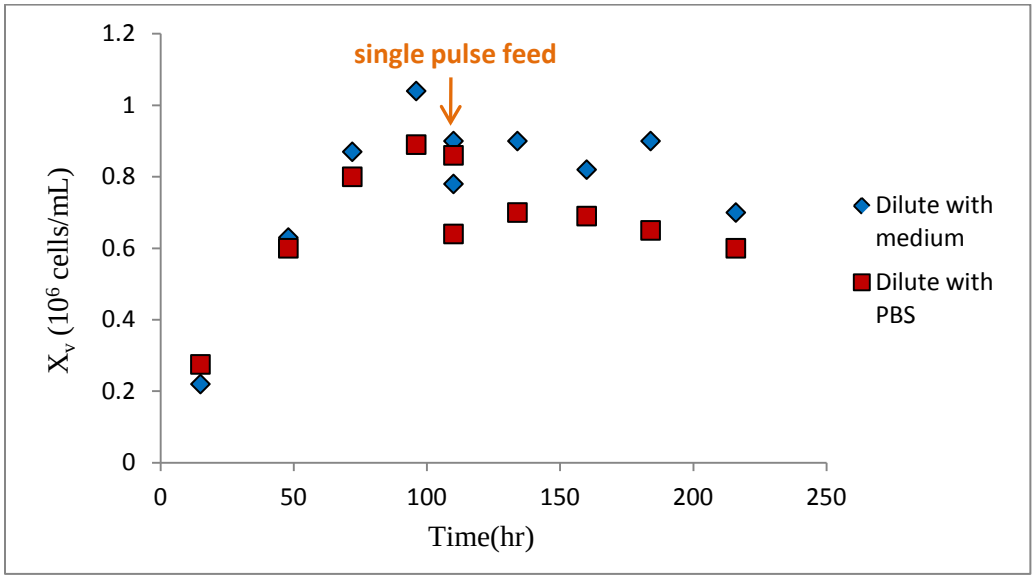

Figure 6.6: Time profile of total viable apoptotic cell concentration diluted with 100mL of normal medium and PBS at t=110 hr.

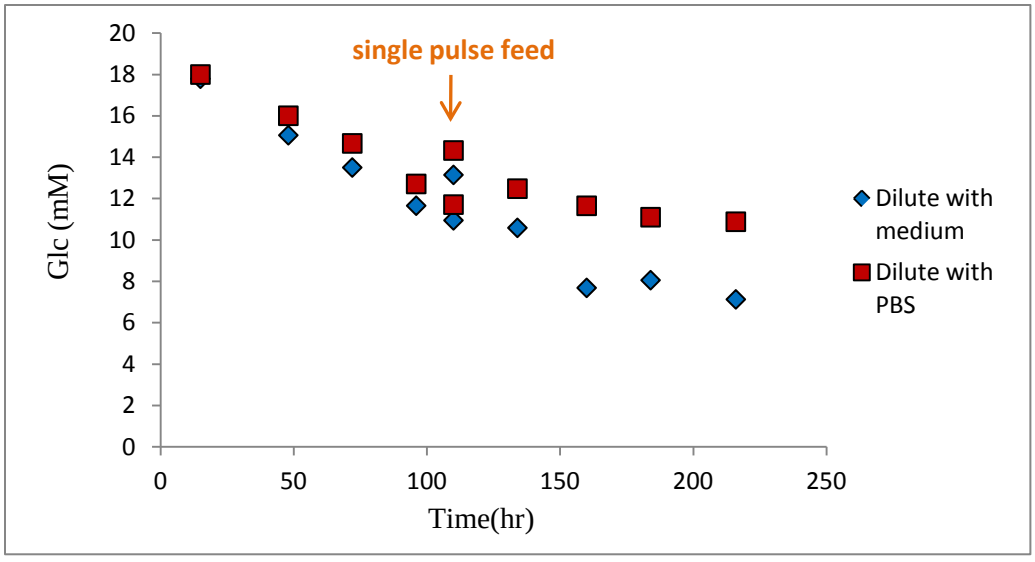

Figure 6.7: Time profile of glucose concentration diluted with 100mL of normal medium and PBS at t=110 hr.

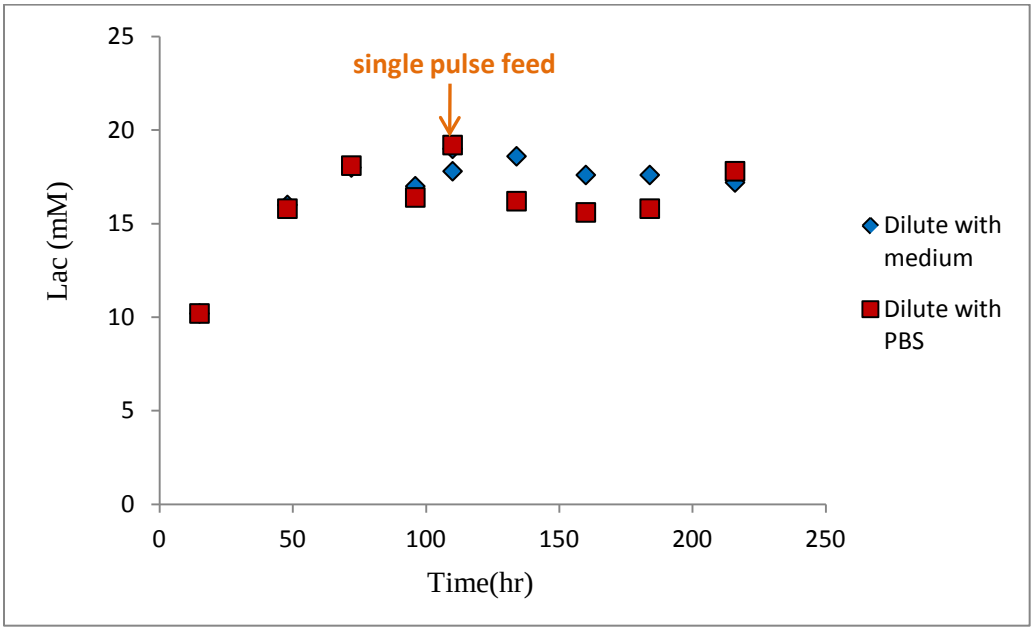

Figure 6.8: Time profile of lactate concentration diluted with 100mL of normal medium and PBS at t=110 hr.

Regarding this study, a similar set of experiments were performed with PBS dilution, except that the initial culture volume was lower (250 mL) and the medium concentration in one culture was doubled. Surprisingly, cell growth (Figure 6.9) in both culture vessels surpassed (2.5×10^6cells/mL) the maximum peak obtained in the previous batches. However the regeneration of cells after dilution was limited to 1.5×10^6cells/mL. Following these unexpected results that show a correlation between culture volume with growth it was hypothesized that growth inhibition could be associated to some inhibiting factors which accumulation depend on culture volume. It was also confirmed that although glucose concentration dropped with diluting the culture (Figure 6.10), the concentration remained above limiting levels.

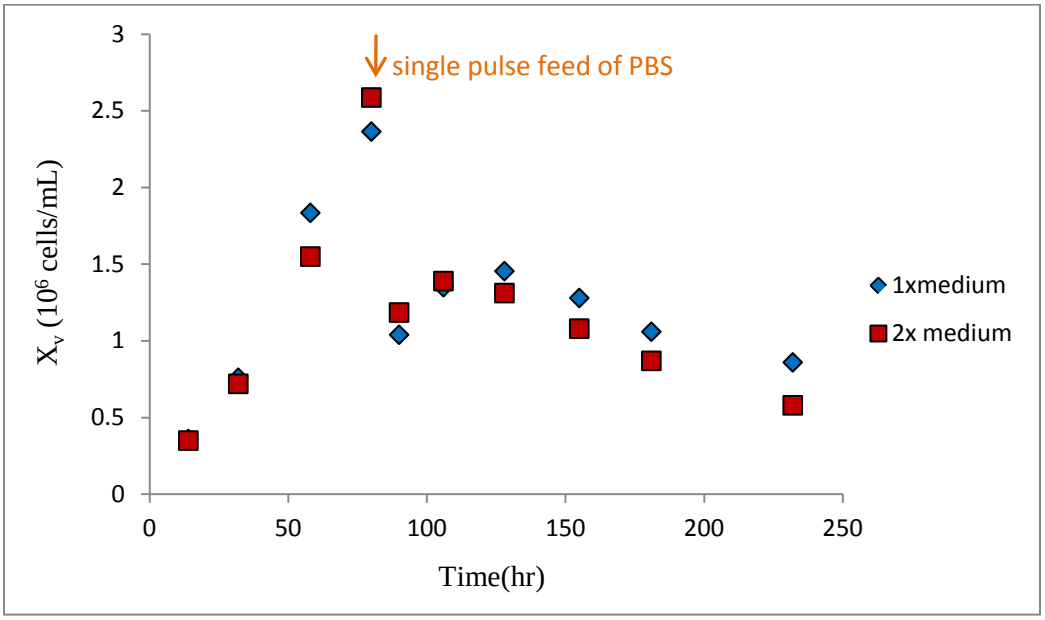

Figure 6.9: Time profile of total viable cell concentration diluted with 250mL of PBS at t=80 hr.

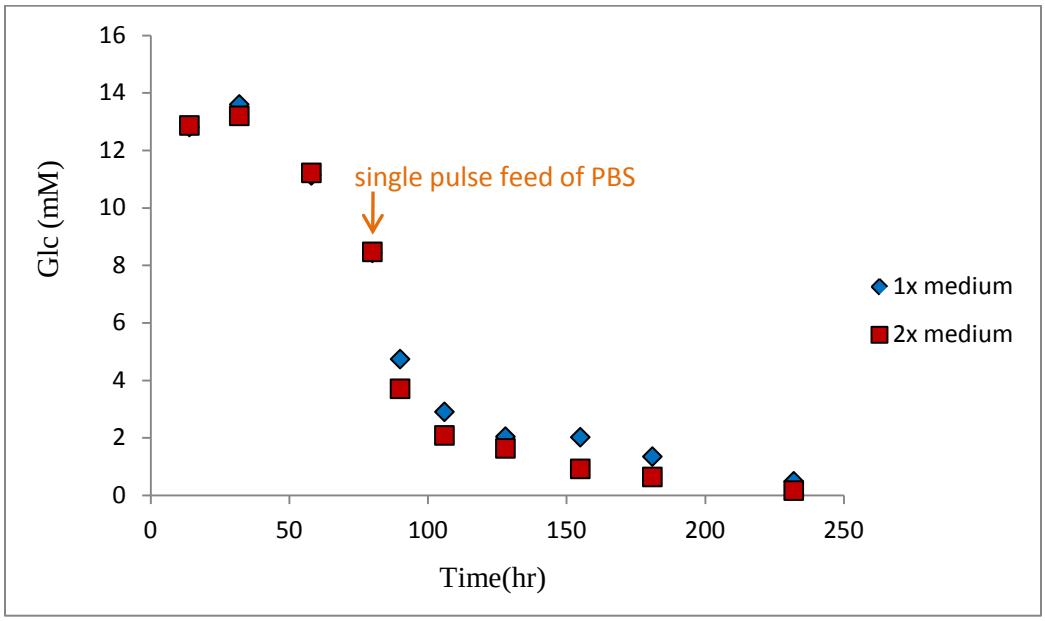

Figure 6.10: Time profile of glucose concentration diluted with 250mL of PBS at t=80 hr.

Chapter 7
Effect of Culture Volume

7.1 Introduction

In the experiments described in the previous chapter that were started with identical initial conditions but with different culture volumes, it was observed that the maximum cell density increased as the initial volume decreased. To interpret this volume effect, it was hypothesized that cells in each spinner were subjected to different environmental conditions which are directly related to the culture volume.

Environmental conditions affecting cell growth and protein synthesis is inevitable (Oliveira et al. 2008; Zhou et al. 2010). Due to dynamic changes in culture conditions involving various culture variables, it was difficult to accurately isolate these factors. Among the various variables that can impact growth, oxygen availability, carbon dioxide accumulation, osmolality and pH seem critical factors and expected to have a significant influence on cellular function (Zhu et al. 2005). Furthermore, it is hypothesized that gaseous components such as oxygen and carbon dioxide could be responsible for the observed volume effects since their accumulation or depletion will depend on the ratio between the surface-area available for mass transfer to the spinner volume. To address these volume related effects, the main strategy adopted was to diminish the effect of environmental factors by periodic perfusion of the culture with fresh medium after the peak cell density was reached. To investigate this strategy, three types of experiments were performed as follows: i) semi consecutive perfusion culture at two different initial volumes (250mL and 500mL); ii) one single full perfusion culture and iii) a fed-batch culture for comparison. Thus, the overall aim was an evaluation of culture lifetime by partial or complete replacement of the spent culture medium with fresh medium with or without changing the volume.

7.2 Materials and Methods

7.2.1 Medium Composition

Regular SFX-CHO medium was used as a basal medium for the adaptation and initiation of experiments, except that in the single full perfusion run, 2X concentrated was applied. The feed medium in the partial perfusion was regular (un-concentrated) medium, in the single full perfusion mode was 2X concentrate and in the fed-batch culture additions of 5X concentrate were used. The serum concentration in both initial medium and feed were 2% and the glutamine concentration was 1mM in the initial culture volume as well as in the feed.

7.2.2 Experimental Design

The first set of experiments was performed in two 500mL spinner flasks containing 250mL and 500 mL culture, respectively. Each spinner was inoculated with 2-day old cells growing in the exponential phase to give a seeding density of around 0.2×10^6 cells/mL and incubated under similar conditions as described previously. Viable cell density was measured every day and shortly after the time cells passed the peak. Periodically a part of the spent culture (50mL in the first spinner and 100 mL in the second one) was withdrawn and substituted with the same amount of fresh medium. It should be mentioned that the cells of the removed culture were not returned to the spinner. In order to mitigate cell loss with culture removal, the spinner was left un-agitated for a short time (10 min) to allow the cells to settle and the liquid removed from the top of the culture, however, there was a slight cell loss in each case of medium replacement. The partial renewal of the culture was performed every 48 hr based on the viable cell density amount. Although carbon dioxide was considered as one of the main factors influencing cell growth and viability, it was not feasible to measure and monitor CO_2 concentration throughout the process in the spinner flasks. However two factors, i.e. the dissolved oxygen concentration and the pH were measured with each sampling at the plateau and declining phases.

The evaluation of the culture condition effects on viable cell state was further pursued by running another set of experiments involving a single full perfusion operation (first spinner) and a fed-batch culture (second spinner) with 5X concentrated feed. The first culture was started with 500 ml of 2X concentrate SFX-CHO medium, and the fed-batch one was started with an initial volume of 300 mL normal SFX-CHO medium. The inoculation density (0.2×10^6 cells/mL) and incubator conditions were similar in both runs. Viable cell density was monitored by daily sampling. At the time point of 80 hrs when cell density reached its maximum, culture condition was manipulated in two ways. In the first spinner complete renewal of the culture was performed by centrifugation of the total culture, discarding supernatant and returning the cells in a same volume of fresh medium. In case of the second spinner, 4 times daily feeding of 50mL concentrated 5X SFX-CHO started at t=80hrs was performed. Samples of each run were taken aseptically every day for further analysis.

7.3 Results and Discussion

The results of total viable cell density for the 2 semi-perfusion runs are presented in Figure 7.1. Despite the first successive feeding resulting in the revival of the culture and high viability, no improvement was observed in the subsequent perfusions. Also, as shown in Table 7.1, at high cell density the dissolved oxygen concentration was not in the limiting range, as the levels ranged between 30%-90% of air saturation at which DO has no significant effect on cell metabolism (Trummer et al. 2006). On the other hand the pH level was found to be significantly below the optimal range for growth (6.80-7.60) as reported for a different CHO cell line (Link et al. 2004; Yoon et al. 2005). As stated above, although the CO_2 level in the culture was not identified, it was hypothesized that due to the slow removal of CO_2 through mass transfer and low driving force because of high CO_2 concentration in the gas phase at the culture surface (5%), accumulation of CO_2 may be inhibiting cell growth and cause a reduction in viability (Pattison et al. 2000). Apparently, the culture condition was not significantly refreshed in terms of CO_2 concentration in each perfusing environment and it returned to a critical inhibitory condition very fast. This could be attributed to high rate

of metabolic activity related to high amount of cells in which partial replenishment of the culture might not be sufficient to compensate (balance) for the elevated CO_2 . The lower cell density in the second spinner (500mL) compared to first one (250 mL) can be attributed to poorer CO_2 removal in the culture due to doubling of the culture height (less surface to volume ratio). Higher cell density in the first spinner led to higher consumption rate of glucose and glutamine in the post-exponential phase, so that glutamine was completely exhausted (Figure 7.2 and 7.3). However lactate and ammonia concentration are identical and below the inhibitory level in both cultures (Figure 7.4 and 7.5). Interestingly, in the first spinner as soon as glutamine and asparagine were depleted (near zero), the reaction of glutamate and aspartate was reversed to compensate this depletion (figure 7.6 and 7.7).

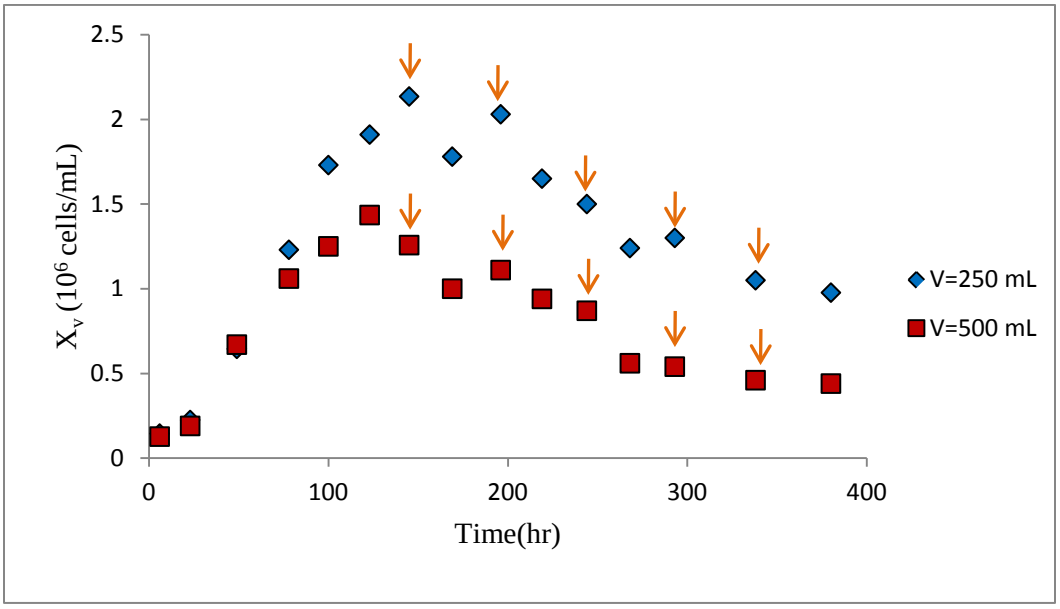

Figure 7.1: Time profile of total viable cell concentration in semi perfusion culture at two different volumes, V=250 mL, ΔV=50 mL(◆), V=500mL, ΔV=100 mL(■).

Table 7.1: Dissolved oxygen concentration (DO %) and pH of culture in two different volume.

	V=250mL		V=500mL	
Time	**DO%**	**pH**	**DO%**	**pH**
145	33.2	6.62	38.6	6.46
196	27.0	6.50	40.1	6.32
244	49.1	6.43	55.3	6.37
293	43.9	6.44	46.5	6.36
338	45.6	6.47	49.9	6.37

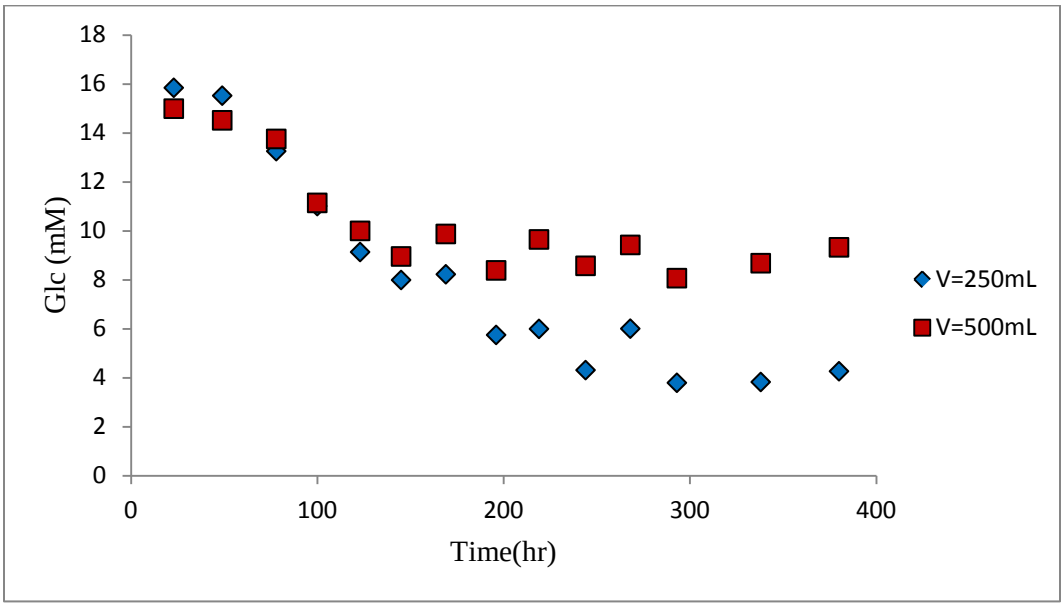

Figure 7.2: Time profile of glucose concentration in semi perfusion culture at two different volumes, V=250 mL, ΔV=50mL(◆), V=500mL, ΔV=100mL(■).

.

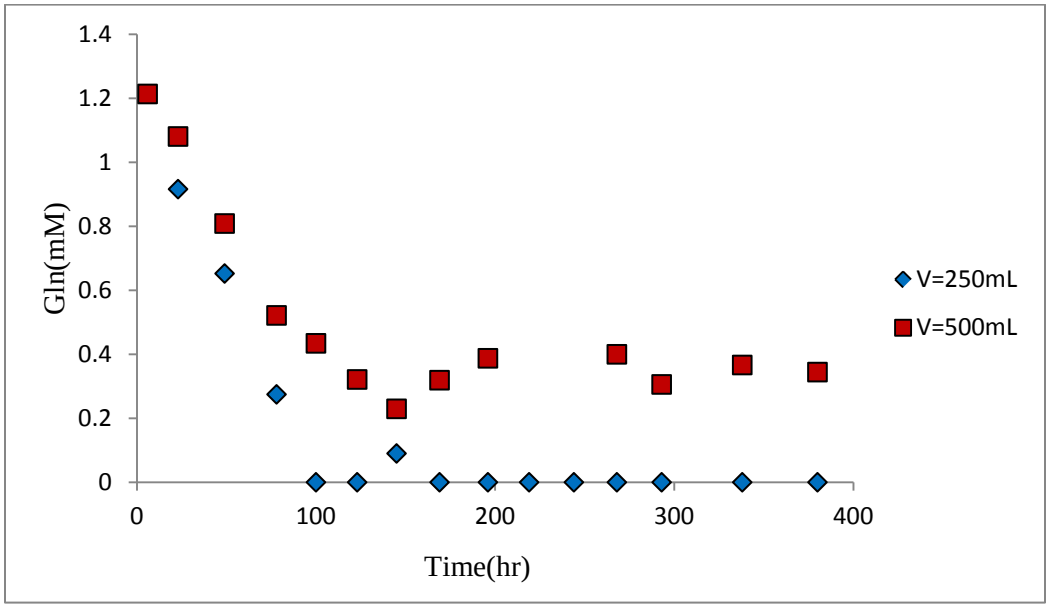

Figure 7.3: Time profile of glutamine concentration in semi perfusion culture at two different volumes, V=250 mL, ΔV=50 mL(◆), V=500mL, ΔV=100 mL(■).

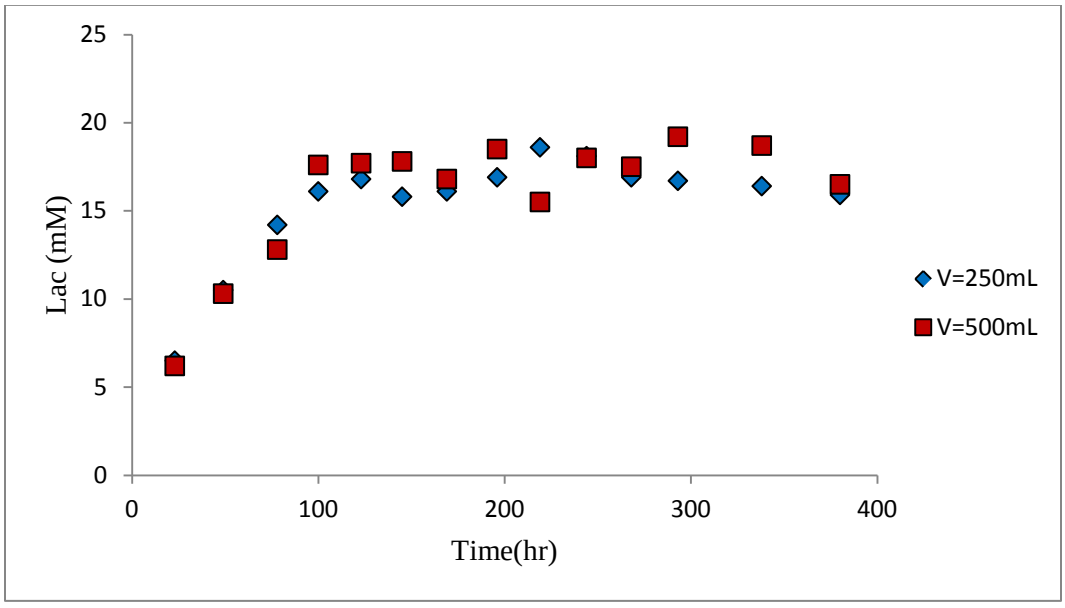

Figure 7.4: Time profile of lactate concentration in semi perfusion culture at two different volumes, V=250 mL, ΔV=50 mL(◆), V=500mL, ΔV=100 mL(■).

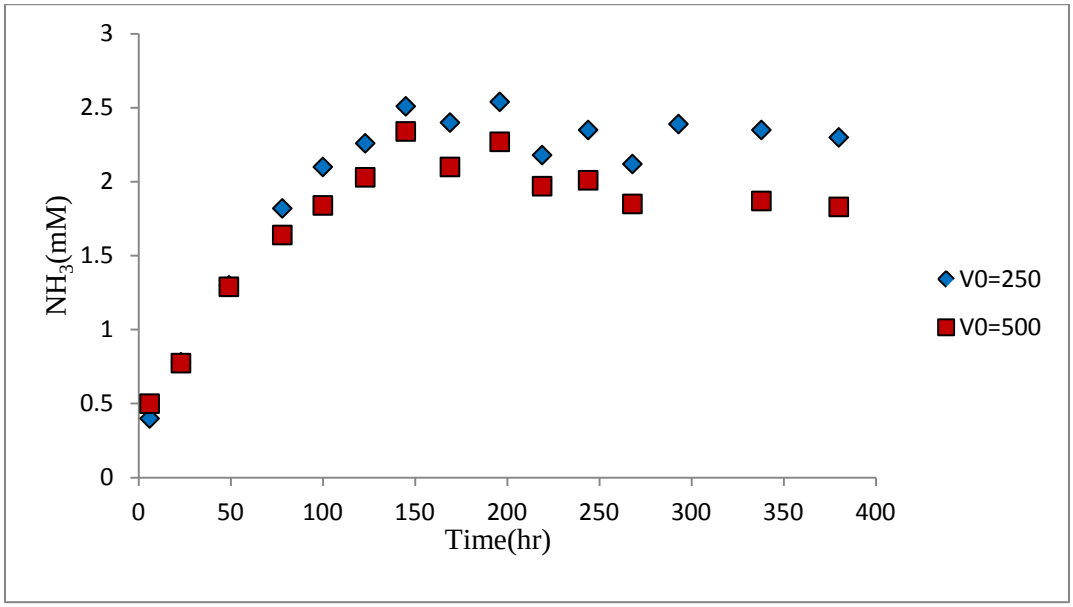

Figure 7.5: Time profile of NH_3 concentration in semi perfusion culture at two different volumes, V=250 mL, ΔV=50 mL(◆), V=500mL, ΔV=100 mL(■).

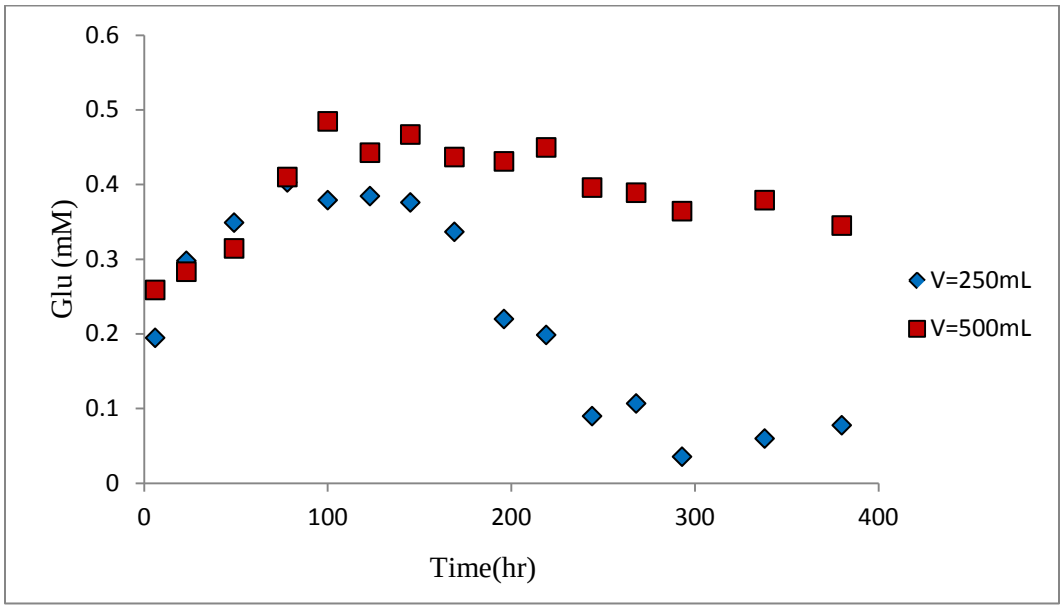

Figure 7.6: Time profile of glutamate concentration in semi perfusion culture at two different volumes, V=250 mL, ΔV=50 mL(◆), V=500mL, ΔV=100 mL(■).

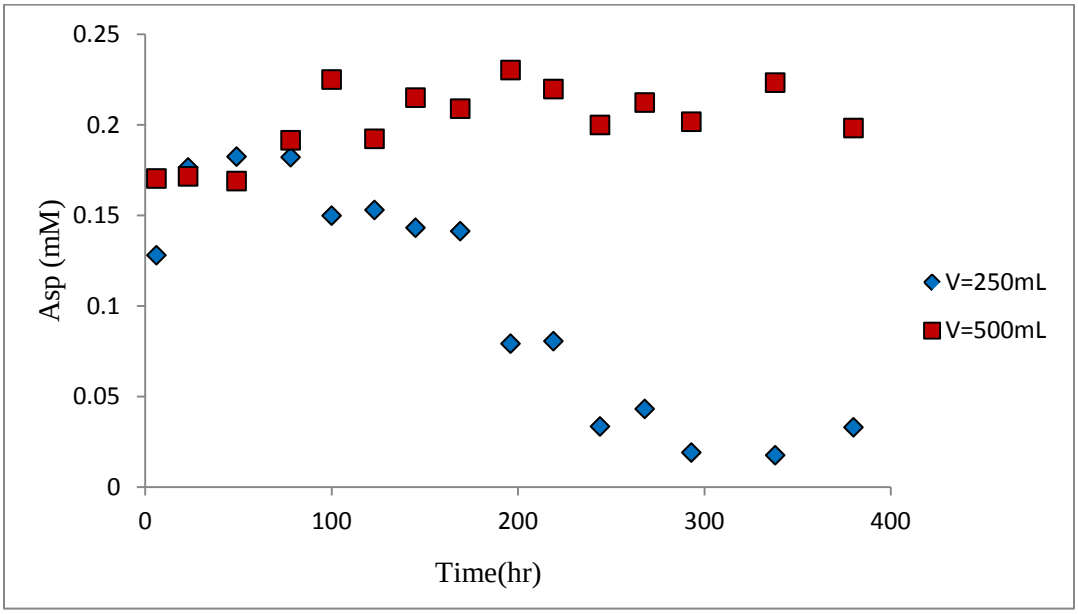

Figure 7.7: Time profile of aspartate concentration in semi perfusion culture at two different volumes, V=250 mL, ΔV=50 mL(◆), V=500mL, ΔV=100 mL(■).

The single full perfusion and fed-batch runs also show the volume effect on the total viable cell density (Figure7.8). While started with equal initial cell density, higher cell peak was achieved in the second spinner with lower initial volume (300mL). However, following the full perfusion at t=80h in which the total used medium was substituted with fresh medium, cell growth not only was renewed, but also cells could maintain higher density for longer time. Conversely, in the fed-batch run, no progress was observed in each feeding, and cells gradually entered the decline phase during which viable cell density and viability decreased. The consistent decline in growth occurring in fed-batch run after each feeding is possibly due to irreversible growth inhibition as the result of the progressive increase in volume, hence increasing accumulation of CO_2 as hypothesized above. Nevertheless, the volumetric cell hour profiles for both modes were similar (Figure 7.9), since the longevity of the perfusion run in the stationary phase compensated for the high peak of the fed-batch culture. Glucose data (Figure7.10) shows sufficient level beyond the limiting concentration, due to refreshing of the culture medium through either perfusion or periodic feeding. Glutamine consumption rate in perfusion culture is low (Figure 7.11), while it reached near zero in fed-batch culture

due to consumption and dilution. Figure 7.12 also depicts lactate production showing a high value of lactate at the early stage of the culture that could be attributed to the high initial cell density. It is also noticeable the fast rate of lactate production immediately after perfusion in which the concentration reached from near zero to over 10 mM in 24 hours. This enhancement of lactate demonstrates how fast cell culture condition changed due to metabolic activity of high viable cell concentration and it can be concluded that CO_2 accumulation could occur at a high rate as well.

Although nutrient supplementation is a main strategy to improve culture performance, the dominant role of culture conditions (temperature, dissolved oxygen and carbon dioxide, pH etc.) as critical factors for cell growth and metabolic activity should be taken into account to attain the goal of culture optimization. Considering the observed decline of the viable cell concentrations in fed-batch and perfusion cultures, it is evident that a seemingly irreversible growth arrest occurred during long-term periodic operations. This decline with each feed cycle coincided with a decrease of pH to growth-inhibiting level (pH< 6.6). Oncogene-induced growth arrest or replicative senescence under unfavorable environmental conditions has been reported previously (Ruiz et al. 2008). This irreversible growth arrest does not seem to be related directly to apoptosis; rather normal cells may be maintained in this arrested state for considerable time as a response to some cellular stress. Environmental stress related growth arrest of eukaryotic cells has been also observed previously with elevated temperature (Rincheval et al. 2002) and depression of pH (Cipollaro et al. 1986) as the stress factors. The study related to mitotic abnormalities caused by sublethal pH decline is particularly relevant for this work, since the depression of pH, of course, is inherently related to the accumulation of dissolved carbon dioxide in the medium. It is the accumulation of carbon dioxide that is modeled. Although this irreversible stoppage of eukaryotic cell proliferation is known, the exact mechanism of this event needs to be further investigated.

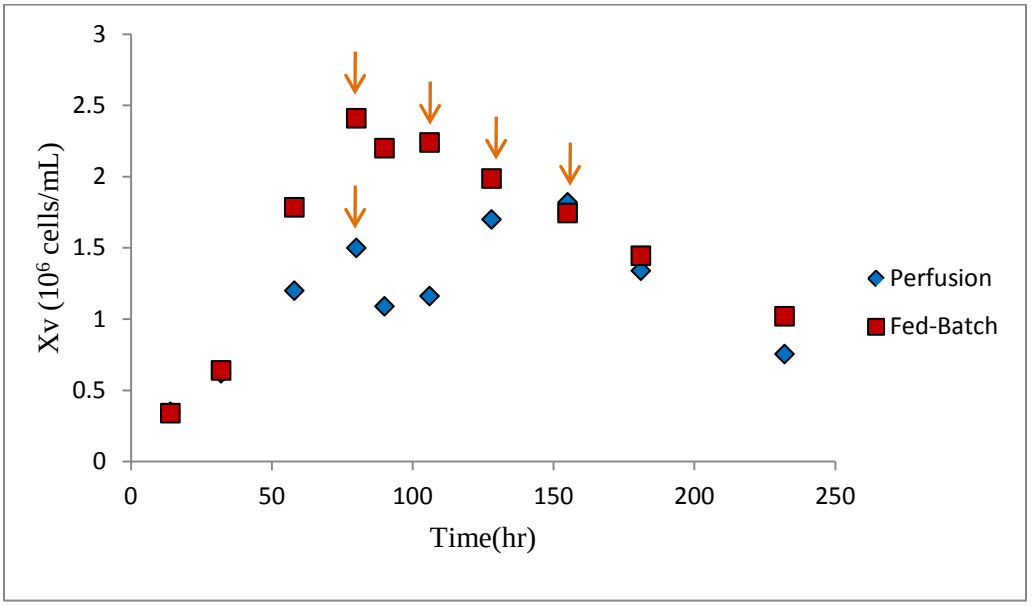

Figure 7.8: Time profile of total viable cell concentration in a single full perfusion and fed-batch culture start at t=80hr.

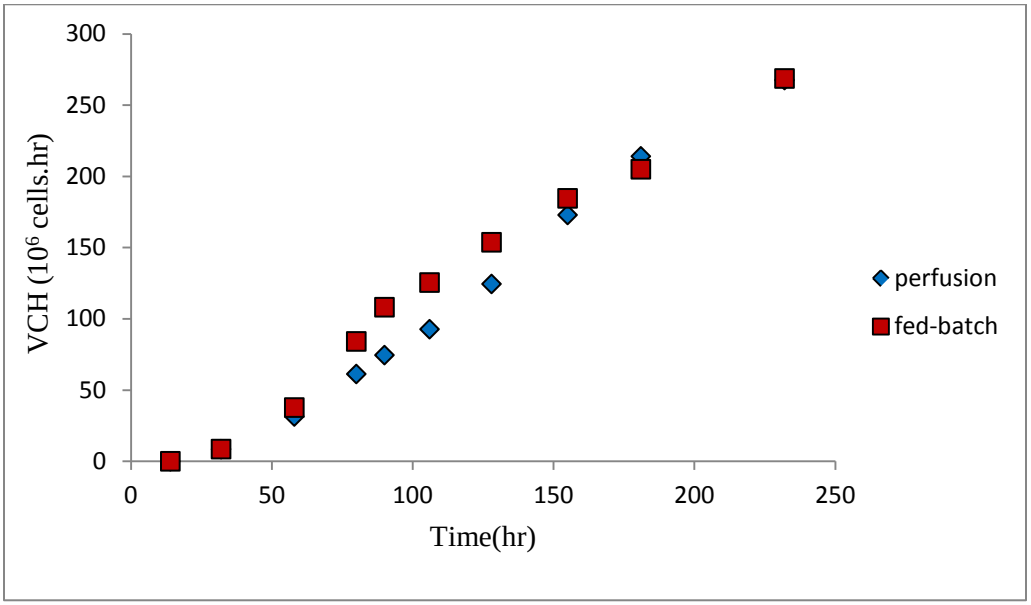

Figure 7.9: Time profile of volumetric cell hour in a single full perfusion and fed-batch culture start at t=80hr.

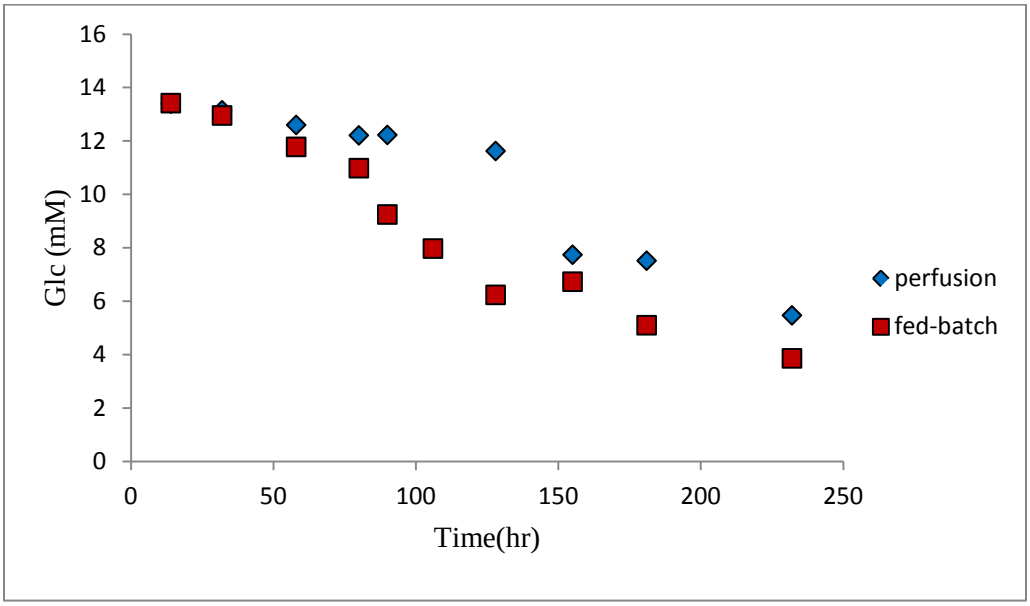

Figure 7.10: Time profile of glucose concentration in a single full perfusion and fed-batch culture start at t=80hr.

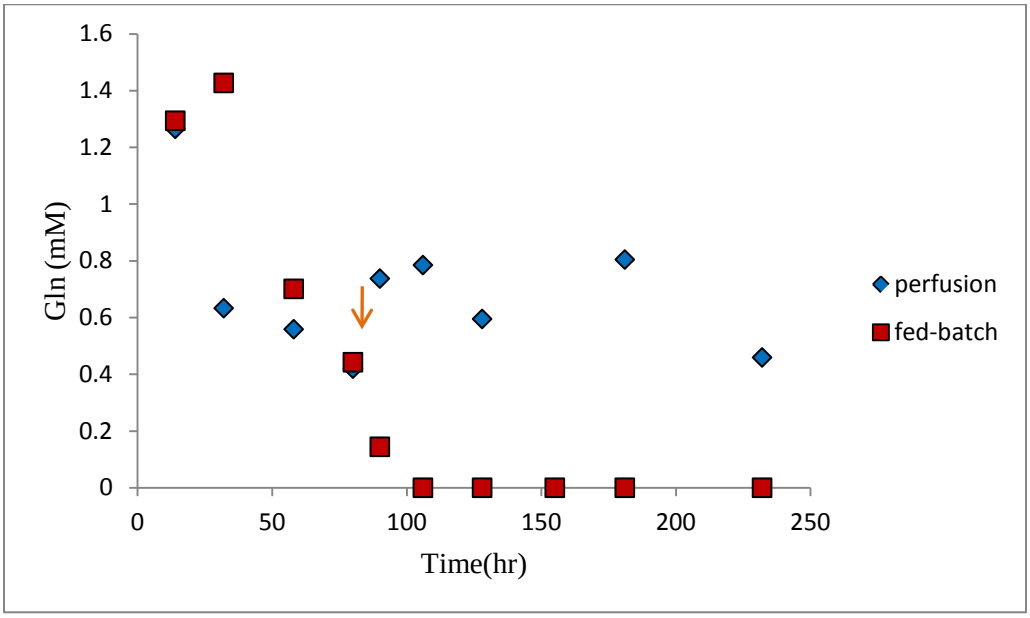

Figure 7.11: Time profile of glutamine concentration in a single full perfusion and fed-batch culture start at t=80hr.

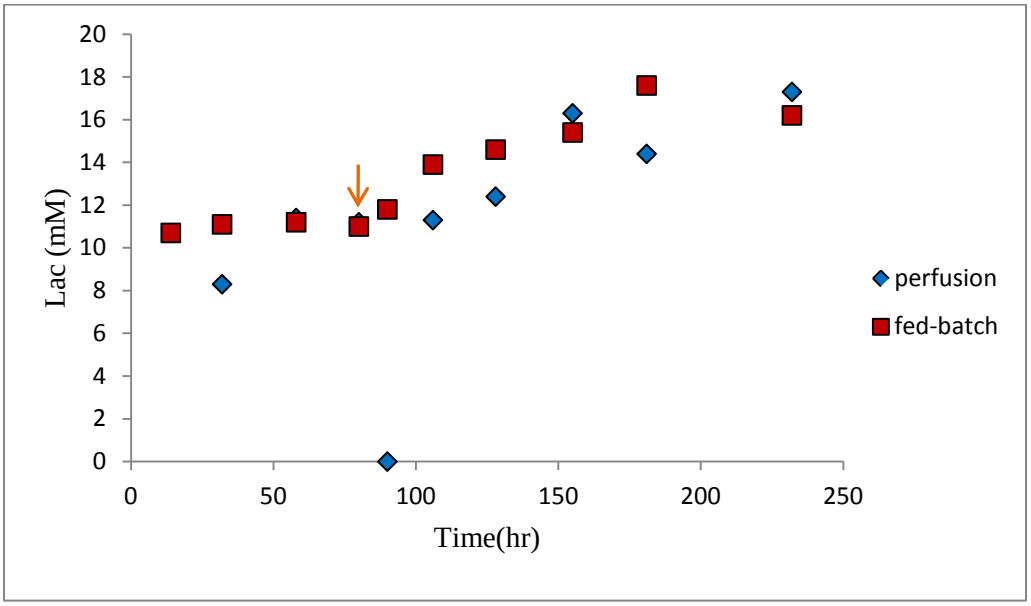

Figure 7.12: Time profile of lactate concentration in a single full perfusion and fed-batch culture start at t=80hr.

Chapter 8
Mathematical Modeling

8.1 Introduction

Mathematical modeling provides a logical and systematic method to identify and quantify key metabolites that have significant effects on cell growth and desired MAb production (Xing et al. 2010). Models can be also used for the design, control and optimization of the process. A variety of modeling techniques have been proposed for animal cell culture (Sidoli et al. 2004). Most of these studies have been limited to batch culture mode and have considered only one or two significant nutrients (such as glucose and glutamine) or the effect of primary byproducts such as lactate and ammonia. In the present study a systematic modeling approach is used that is based on Metabolic Flux Analysis (MFA). This analysis involves all amino acids contributing to the metabolic network and its key objective is to identify the key metabolites and metabolic events influencing the cell culture system. MFA can also be used to simplify the metabolic network by eliminating the insignificant fluxes. Then, on the basis of the reduced metabolic network, a set of macro-reactions connecting the input nutrients to output products can be formulated. The dynamic behavior of the significant extracellular metabolites can be predicted by a set of differential equations describing the mass balances corresponding to the identified macro-reactions. The metabolic flux analysis is based on a quadratic programming optimization. An additional part of the overall dynamic model is formulated to express the physiological state of cells within the population (dividing, resting and apoptotic). One of the goals of this biomass model is to relate biomass growth and apoptosis to cell density and to concentration levels of the key extracellular metabolites. Since MAb production is largely non-growth associated, the models for both normal and apoptotic cells are needed for predicting the MAb titer. Generally the cell concentration model for mammalian cell culture was the conventional kinetic model in which the growth rate was considered as a function of the limiting nutrient concentration, i.e. glucose or glutamine. In this study, based on the experimental results obtained in Chapter 4,

regarding essential nutrient starvation, none of the significant nutrients were found to be limiting. The proposed cell concentration model was established and modified upon our observation in each set up experiment and eventually finalized in a way to integrate all the significant variables influencing cell growth and behavior. The parameters of the dynamic model were estimated via Metropolis-Hastings algorithm and nonlinear optimization function in MATLAB software. The dynamic model were applied to both batch and fed-batch mode with different initial concentration of nutrients. Some parts of mathematical modeling have been published previously (Naderi et al. 2011). Relevant paragraphs from the publication are reproduced verbatim in this chapter.

8.2 Materials and Methods

In order to estimate the parameters of the model, the Metropolis-Hastings algorithm has been employed. This method developed by Metropolis et al. (1953) and generalized by Hastings (1970) is based on Markov Chain Monte Carlo (MCMC) methodology. Although various well-known parameter estimation techniques such as the least squares methods have been applied widely, many of these are not appropriate since they only provide accurate solutions for linear models with specific assumptions for measurement noise, e.g. normally distributed (Bischoff et al. 1991). Thus, these techniques find local, rather than global parameter estimates. Since the proposed dynamic model is a relatively complicated nonlinear model, these methods might not be appropriate for parameter estimation. Metropolis-Hastings algorithm not only is applicable to complicated models with nonlinear dependency on parameters, but it also provides estimates on the confidence intervals for each parameter (Jitjareonchai et al. 2006).

Metropolis-Hastings Algorithm is applied to draw a Monte Carlo sample from a posterior distribution. Assuming the proposal distribution for the model parameters, θ, is $q(\theta_n, \theta)$, then the acceptant probability is defined as:

$$\alpha(\theta_n, \theta^*) = \min\left\{\frac{\pi(\theta^*|\mathbf{y})q(\theta^*,\theta_n)}{\pi(\theta_n|\mathbf{y})q(\theta_n,\theta^*)}, 1\right\},$$

where $\theta^*$is the proposed parameter drawn from the proposal distribution, **y** is the variable vector, and $\pi(\theta|\mathbf{y})$ is the posterior distribution. The steps of the Metropolis-Hastings Algorithm are summarized as follows:

1) Initialize $n = 0$ and θ_n,
2) Sample θ^* from $q(\theta_n, \theta)$,
3) Sample u from $U(0,1)$; (Uniform distribution between 0 and 1),
4) If $u \leq \alpha(\theta_n, \theta^*)$ then set $\theta_{n+1} = \theta^*$,
5) Else, set $\theta_{n+1} = \theta_n$,
6) Set $n = n + 1$ and go to step 2.

Generally the first partial of iteration n is considered as burn-in and discarded from parameter samples in order to reduce the effect of selected initial guess of parameters. Eventually, the final parameter value and confidence intervals can be obtained from the probability distribution function of the accepted θs.

8.3 Metabolic Flux Analysis

The metabolic network chosen for CHO cell line has been adapted from Gao et al. (Gao et al. 2007) and it is schematically shown in Figure 8.1. This network consists of glycolysis, TCA cycle, and amino acids metabolism which are the most important pathways for energy, biomass and MAb production. The pentose phosphate pathway, which is the main source of 5-carbon sugars for nucleotide synthesis, is lumped into the biomass production flux. All the 19 amino acids are included in the metabolic network except tryptophan which has an insignificant contribution to energy and protein production (Gambhir et al. 2003). This network involved 30 metabolites via 34 fluxes corresponding to 34 bioreactions. The stoichiometric equations listed in Appendix C correspond to the key fluxes of carbon and nitrogen containing compounds considered in CHO cells.

Model development comprised two steps involving metabolic flux analysis and formulation of dynamic equations. In metabolic flux analysis, the internal flux distribution was computed using the metabolic network, stoichiometric balances and experimental data.

First, a mass balance for each metabolite in the network was derived. The result was a set of linear equations which can be expressed in a matrix form as follows:

$$\frac{d\boldsymbol{\psi}(\boldsymbol{t})}{d\boldsymbol{t}} = \boldsymbol{r}\boldsymbol{X}_{\boldsymbol{v}}(\boldsymbol{t}) \quad \textbf{(1)}$$

In Equation 1, $\boldsymbol{\psi}$ is the vector of intracellular and extracellular metabolite concentrations and *t* is the time interval specified for each phase of cell cultivation, i.e. exponential or post-exponential phase, in a batch system. $\boldsymbol{r}$ is the vector of specific uptake/production rate of each metabolite. $X_v(t)$ is the viable cell concentration which varies with culture time. Assuming that $\boldsymbol{r}$ is constant during the time interval between 0 to *t*, the integration of Equation (1) gives:

$$\int_0^t \boldsymbol{d\psi}(\boldsymbol{t}) = \boldsymbol{r}\int_{\boldsymbol{0}}^{\boldsymbol{t}} \boldsymbol{X}_{\boldsymbol{v}}(\boldsymbol{t})\boldsymbol{dt} \quad \textbf{(2)}$$

The integral term on the right hand side is referred to as the viability index or the volumetric cell hours (Dutton et al. 1998). To estimate the volumetric cell hours, the integrand is assumed to be the sum of piecewise continuous exponential functions with characteristic, but variable specific growth rates on the interval between *t* and $t + \Delta t$. Based on Equation (2) and the measured values of metabolites and viable cell density, the elements of the vector $\boldsymbol{r}$ were calculated for each extracellular metabolite. It should be noted that under balanced growth condition, e.g. during exponential growth, it was assumed that the intracellular metabolites are at a quasi-steady state implying that the net conversion rate of intracellular metabolites is zero (Gambhir et al. 2003; Provost and Bastin 2004). Considering the expected changes in cellular metabolism during the culture process, two distinct phases can be considered in the analysis: exponential and post-exponential phase and hence two sets of $\boldsymbol{r}$ can be obtained for each phase separately (Gao et al. 2007; Dorka et al. 2009). The transition from one phase to the next can be attributed to cessation of growth due to change in culture condition and consequently to the need for the cell to adapt to new conditions.

The next step was the computation of the intracellular fluxes in each phase by applying a steady-state mass balance equation for each metabolite. This was accomplished by setting the

conversion/production rate, *r(m),* of each metabolite according to the appropriate stoichiometric relationship as follows (Bonarius et al. 1996):

$$r(m) = \sum_{i=1}^{34} \alpha_{i,m} j_i \quad \textbf{(3)}$$

Where *r* is the net uptake or production rate of metabolite *m* and $\alpha_{i,m}$ is the stoichiometric coefficient for metabolite m=(1,2,…,30) in reaction *i*=(1,2,...,34). The constant, $\alpha_{i,m}$ has a negative value for any metabolite being consumed, while it is positive for metabolites that are produced. The term, j_i is the intracellular flux for reaction i. The complete set of mass balances for all metabolites using Equation (3) can be expressed in a matrix form as follows:

$$\boldsymbol{r} = \boldsymbol{Aj} \quad \textbf{(4)}$$

Where $\boldsymbol{r}$ is the vector of average uptake or production rates obtained from experimental data, $\boldsymbol{A}$ is the stoichiometric coefficient matrix of all bioreactions and $\boldsymbol{j}$ is the vector of intracellular fluxes. Since the system of equations is underdetermined, there will be more than one solution to this problem. An optimization strategy was used to calculate the fluxes by imposing constraints related to the directions of the reactions. This means mathematically that all calculated fluxes should be greater or at least equal to zero. Quadratic programming was used to minimize the target function:

$$\text{Min}(\boldsymbol{r} - \boldsymbol{Aj})^T \, (\boldsymbol{r} - \boldsymbol{Aj}) \quad \textbf{(5)}$$

If the number of active constraints for the solution of Equation (5) is greater than the number of degree of freedom i.e. 34 (reactions) - 30 (metabolites) = 4, then the solution is unique. In order to avoid the complexity of the dynamic model to be derived based on the network, insignificant fluxes were eliminated to derive a simpler metabolic network. This reduction was based on excluding the fluxes contributing less than 1% of the total sum of the fluxes. The reduced reaction network was the basis for the formulation of dynamic mass balances of extracellular metabolites. This network contained a set of elementary flux modes which were systematically combined to extract macroscopic reactions that directly correlated the substrates to the products.

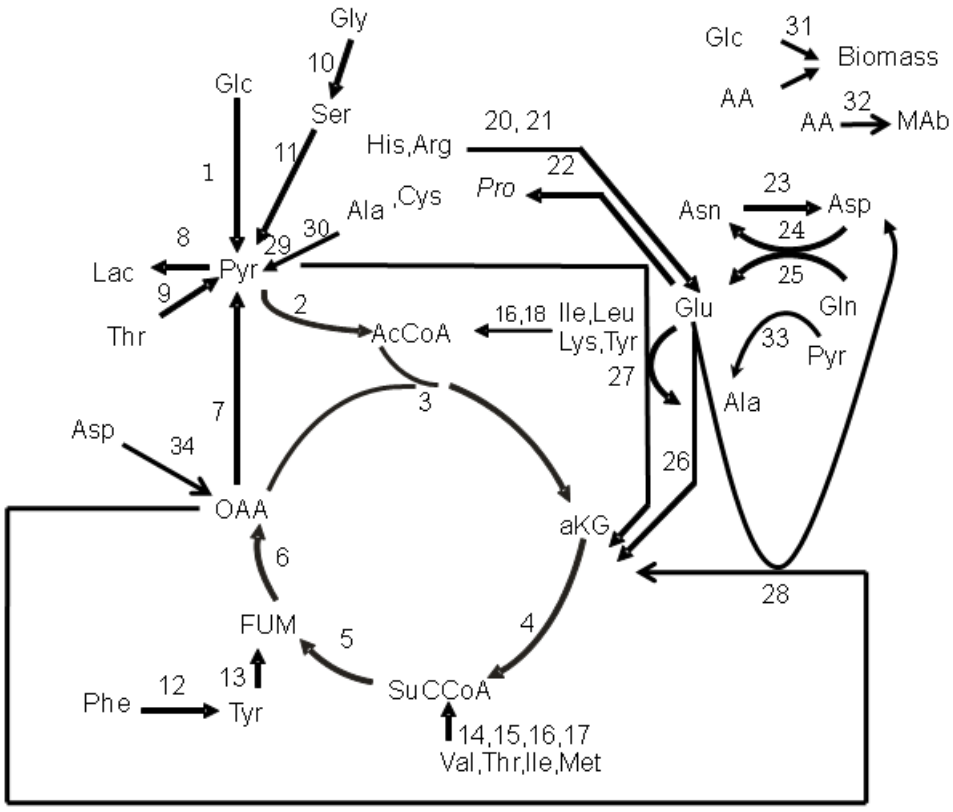

Figure 8.1: Metabolic Network Applied for CHO Cells (Adapted from Gao et al., 2007).

8.4 Metabolic Dynamic Model Development

The dynamic model was constructed based on the following macroscopic mass balances for each extracellular species:

$$\frac{d\boldsymbol{\xi}(t)}{dt} = \boldsymbol{K}\boldsymbol{r_E}(t) + \boldsymbol{u}(t) \qquad \textbf{(6)}$$

$\boldsymbol{\xi} = (\xi_1, \xi_2 \ldots \xi_i)^T$ is the vector of extracellular metabolites concentration and is a subset of the vector $\boldsymbol{\psi}$ in Equation (1). $\boldsymbol{r_E} = (r_1, r_2 \ldots r_i)^T$ is the vector of the macro-reaction rates and $\boldsymbol{K}$ refers to the stoichiometric coefficients of the matrix of the macroscopic reactions. $\boldsymbol{u(t)}$ is the vector representing the net exchange rate of the species with the surroundings. Except for CO_2 gas exchange, this term is zero for all metabolites. Due to the difficulty in measuring gas

concentrations in a spinner flask, CO_2 is not predicted by the model. Hence, the general matrix form of the model is expressed as follows:

$$\frac{d\boldsymbol{\xi}(t)}{dt} = \boldsymbol{K}\boldsymbol{r}_{\boldsymbol{E}}(t) \quad \textbf{(7)}$$

The next step of the model identification procedure is to determine the fundamental reaction kinetics. The kinetic functions are non-linear and often not well-known. In order to avoid the complexity of the model and identifiability problems of kinetic parameters, the Michaelis-Menten equation will be the preferable choice. This general kinetic function has been shown to be a logical compromise to capture complex kinetics in bioprocesses, and the dynamic models based on this kinetic structure has been shown in the past to provide an adequate fit with experimental data (Gao et al. 2007; Dorka et al. 2009). Therefore, the general expression of Monod kinetics is assumed for all the reactions as follows:

$$r_i(t) = a_{ig}\left[\prod_{i=1}^{n}\frac{m_i}{m_i + k_i}\right]X_g + a_{ing}\left[\prod_{i=1}^{n}\frac{m_i}{m_i + k_i}\right]X_{ng} \quad \textbf{(8)}$$

Where $r_i(t)$ is the reaction rate for i^{th} reaction; m_i and k_i are the corresponding metabolite concentration and half-saturation constant, respectively. As shown in Equation (8), each metabolic equation contains "growth associated" and non-growth associated or maintenance terms. To model the fate of metabolites, it was assumed that growing cells (X_g) and non-growing cells (X_{ng}), both normal and apoptotic, may metabolize nutrients at different rates.

Hence, a_{ig} and a_{ing} are the maximum rate at which the reaction can proceed, while X_g and X_{ng} are the viable growing and non-growing cell concentrations. Due to high substrate concentration in the exponential phase in which the majority of cells are growing, the nonlinear term of the growth associated part will be close to one, so Equation (8) can be simplified to:

$$r_i(t) = a_{ig}X_g + a_{ing}\left[\prod_{i=1}^{n}\frac{m_i}{m_i + k_i}\right]X_{ng} \quad \textbf{(9)}$$

The values of fluxes were obtained by applying quadratic programming using the function qp in MATLAB. Initial estimates of the parameters of the nonlinear dynamic model were obtained using available experimental data and Markov Chain Monte Carlo based methods using the Metropolis Hastings algorithm (Chib and Greenberg 1995; Berg 2004) respectively. The final parameter values were estimated using the *fmincon* function in MATLAB program that involves a nonlinear optimization for which the initial guesses were assumed to be equal to the estimates obtained from the Metropolis-Hastings algorithm. The variables, X_g and X_{ng} are associated with the growing and non-growing subpopulations in the culture and were obtained based on the defined cell concentration model which is described in the following section.

8.5 Cell Concentration Model

Development of models of cell growth is often challenging and problematic, particularly if the bioprocess is imperfectly known (Grosfils et al. 2007). For the CHO cell culture used in the current work growth could not be related directly to key nutrient concentrations. This was observed in the experiments at different concentrations of glucose and glutamine described in Chapter 4. When glucose, glutamine and asparagine were provided at higher concentration levels and were not depleted at any point during operation, cell growth seemed to be independent of these nutrients, but it could be correlated with cell density (Ruaan et al. 1993). The results also showed that the maximum cell density was very similar for all experiments possibly indicating a limitation in a nutrient that is not measured. Only at lower initial glucose concentration (4mM), glucose depletion significantly affected viability and the initiation of apoptosis. Therefore, a logistic model expressing the fraction of dividing cells seemed appropriate for describing time dependent profiles of normal and apoptotic sub-populations in batch or fed-batch culture. Glucose exhaustion related effects occurring when operating at low initial concentration of glucose were also incorporated into this logistic model. By its general nature a logistic model provides a means for the optimum estimation of growth and it can be readily extended to describe a variety of mammalian cell culture (Goudar et al. 2005). Since it was observed that MAb production was not only dependent on

growing cells, three subpopulations of live cells contributing in MAb secretion were quantified and modeled: normal growing, normal resting and apoptotic cells.

Fluorescent microscopic imaging was applied to discriminate and quantify each subgroup. Figures 8.2a and 8.2b show typical fluorescent photomicrographs of CHO cells stained with fluorescent dyes on the 3rd and 9th days of the culture. During the early stage of culture, when cells are in an exponential growth phase, the majority of the cell population comprises normal growing cells; however there is always a low number of apoptotic cells. This apoptotic sub-population slowly increases and reaches a maximum shortly after the total cell density peaks. In the late stages of culture, normal growing cells are replaced by normal resting cells, presumably due to G_0 cell cycle phase arrest, while the apoptotic cell pool is replaced by dead cells. Glucose was found in experiments to be highly correlated to cell death. Accordingly, it was hypothesized that the exhaustion of glucose that occurs during the course of a batch conducted with low initial glucose levels resulted in accelerated death possibly by autophagy (Hwang and Lee 2008). Accordingly, in the current study, autophagic death was modeled as a function of glucose depletion.

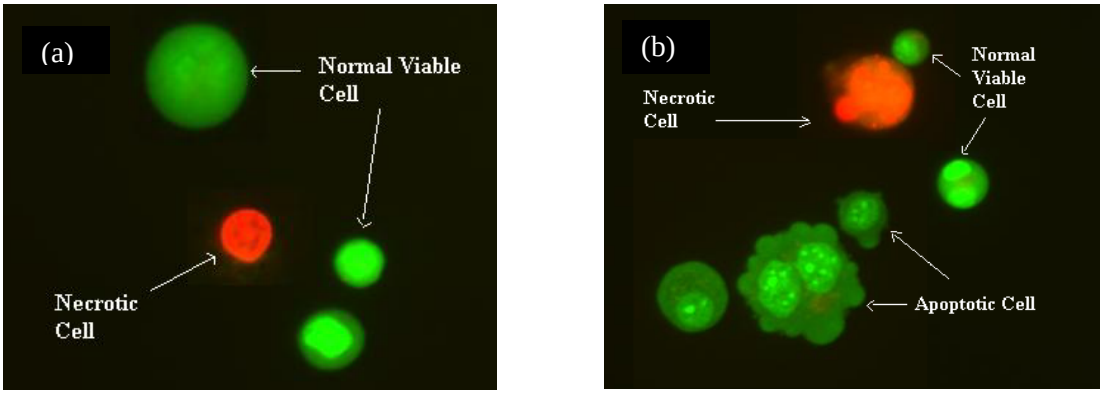

Figure 8.2: Fluorescent photomicrograph of CHO cells stained with Acridine Orange and Ethidium Bromide (a) at near maximum population density (day3), (b) in late culture (day 9).

Based on the observed dynamic profiles of cell sub-populations and significant nutrients and metabolites provided by various batch experiments at different glucose, glutamine and asparagine concentrations, a biomass model was developed as follows:

$$\frac{d(X_v)}{dt} = \mu\, f_{gr}\left(X_v - X_{ap}\right) - k_{D1}\, X_{ap}\, \frac{1}{1 + k_2\, e^{-\alpha N}} - k_{D2}\, X_{ap}\, \frac{1}{1 + k_3 e^{\left(\frac{Glc}{k_4}\right)}} \quad \textbf{(10)}$$

$$\frac{d\left(X_{ap}\right)}{dt} = k_{ap}\,(X_v - X_{ap})^2 - k_{D1}\, X_{ap}\, \frac{1}{1 + k_2\, e^{-\alpha N}} - k_{D2}\, X_{ap}\, \frac{1}{1 + k_3 e^{\left(\frac{Glc}{k_4}\right)}} \quad \textbf{(11)}$$

Where X_v and X_{ap} are the total viable and apoptotic viable cell concentration, respectively. μ is the specific growth rate and k_{ap} is the specific rate of apoptotic cell formation correspondingly. The difference between X_v and X_{ap} represents the concentration of healthy cells. The term, f_{gr}, indicates the fraction of dividing normal cells, and defines the population of growing cells, given by $X_g = f_{gr}\left(X_v - X_{ap}\right)$ and the non-growing cell population: $X_{ng} = X_v - X_g$. The differential equation for the fraction of dividing normal cells was derived from an analytical solution of a logistic model described by the Verhulst equation as follows:

$$\frac{df_{gr}}{dt} = -\mu f_{gr}(1 - f_{gr}) \quad \textbf{(12)}$$

In Equation (12), the initial growing fraction is the only calibrated parameter; its value is 0.87.

It was assumed that both growing and non-growing cells die through apoptosis. The rate of apoptotic cell formation was taken as a second order function of the normal cell density to represent cell to cell signaling and interaction effects that ultimately trigger apoptosis as

discussed in Chapter 6 (Hardy and Stark 2002; Lee 2002; Meshram et al. 2009). The rate of death, the second term in Equation 10 and 11, was found through correlation analysis to be a function of the ammonia concentration, *N*. The terms, k_{D1} and k_{D2} are the specific death rate constants and k_2 and α are the toxicity function constants in the death term. The parameters k_3 and k_4 are the autophagic and glucose saturation constants, respectively.

The effect of exhaustion in main nutrients has been discussed in Chapter 4. For instance, in the experiments performed at low glucose concentration (4mM), it was observed that the initiation of apoptosis and the death rate were much faster due to glucose exhaustion, while low glutamine levels had no apparent adverse effect on the culture. In fact, providing a low glutamine level led to lower ammonia accumulation, which resulted in longevity of the culture system. The third term in both models refers to the cell death rate and was significant at very low glucose concentration (nearly zero). This latter term can be related to death by autophagy as mentioned above (Hwang and Lee 2008).

The dynamic model for MAb is correlated with the combination of growing, resting and apoptotic cell populations as follows:

$$\frac{d(P)}{dt} = \alpha_g X_v \quad \textbf{(13)}$$

Where *P* refers to MAb concentration and α_g is the specific production rate for both growing and non-growing cells. Thus, the experimental data suggested that no significant difference in productivity rate of MAb was found among the different cells' subpopulations. This relationship of non-growth associated MAb production has been previously reported by Renard et al. (Renard et al. 1988). They were able to relate the integral of viable cell population to the concentration of MAb throughout the culture period.

Although the logistic model applied for describing the growth kinetics of CHO cell subpopulations represented the experimental data quite satisfactorily, it might not be appropriate for bioprocess control, especially in fed-batch operation. It is because the logistic model cannot properly capture the changes in cell growth after feeding fresh medium. Initially based on the experimental findings in chapter 5, it was assumed that the cell growth

depends on an unknown ingredient, and the cell culture supplementation strategy was performed with the aim of enriching the culture environment to prevent depletion of any essential component. Under the nutrient-dependency assumption, a kinetic model representing cell growth related to nutrient concentration was examined. Among various kinetic models (Annuar et al. 2008; Khavarpour et al. 2011), Tessier model was proposed due to a good fit to experimental data of batch culture and reaching faster to saturation level (Caramihai et al. 2010). This model incorporates the limiting substrate dependency based on an exponential function as follows:

$$f_{gr} = 1 - e^{\frac{-S}{k_s}} \quad \textbf{(14)}$$

Where S is the concentration of unknown component, and k_s is the Tessier constant. The consumption rate expression of S was also defined as:

$$\frac{dS}{dt} = -\mu a_s f_{gr}\left(X_v - X_{ap}\right) \quad \textbf{(15)}$$

in which a_s is the specific consumption rate of unknown component S. The concentration of S in the medium was arbitrarily considered to be 1mM. The parameter value of k_s and $a_s$were estimated based on the previous experimental data used for calibration.

Subsequent experimental results described in chapter 7, led us to introduce inhibitory agent in the kinetic model as an important factor rather than limiting component which restricted cell growth and viability. As explained in Chapter 7, the possible mechanism of inhibition was attributed to carbon dioxide accumulation during the culture process. In addition the volume effect was considered in a mass transfer term, as higher culture volume resulted in lower mass transfer of CO_2. For simplicity, a Tessier-type model as the one in Equation (14) was applied but instead of depletion of a substrate, the model assumed CO_2 accumulation as the inhibitory effect. Hence the fraction of dividing normal cells was described according to the following equation:

$$f_{gr} = 1 - e^{\frac{C-1}{k_c}} - k_a \int_0^t C dt \quad \textbf{(16)}$$

Where C is the inhibition factor concentration in the culture and k_c and k_a are the inhibitory and accumulation constants respectively. The integration term accounts for the accumulation effect of CO_2 causing irreversible cell damage. The net rate of production C was expressed in the following manner:

$$\frac{dC}{dt} = k_{11} f_{gr}\left(X_v - X_{ap}\right) + k_{22}(1 - f_{gr})\left(X_v - X_{ap}\right) + k_{33} X_{ap} - k_v(C - C_\infty) \qquad \textbf{(17)}$$

in which k_{11}, k_{22} and k_{33} are the specific production rate of CO_2 production by three subpopulation namely normal growing, normal non-growing and apoptotic cells. The last term refers to the removal of dissolved carbon dioxide of the culture to the outside. C_∞ is the CO_2 concentration in equilibrium with headspace gas phase. k_v is the mass transfer coefficient which has volume dependency.

8.6 Results and Discussion

8.6.1 Metabolic Network and Metabolite Model Development

Metabolic studies were performed in 500 mL spinner flasks. These stirred vessels have been well characterized (Qualitz 2005) and are believed to give representative performance of industrial scale operations. The scale-down of full-scale bioreactors to 50-500 mL volume for process analysis and optimization in medium to high-throughput screening studies has become standard practice in the biopharmaceutical industry (Kumar et al. 2004; Sucosky et al. 2004).

The flux distribution in the metabolic network was computed by optimizing Equation (4) via quadratic programming (Figure 8.3) using the MATLAB function *qp* (MATLAB 7.4). The results are shown in Appendix G. Since the metabolic flux distribution was found to be essentially identical for each phase of culture, i.e. exponential and post-exponential phase, a single metabolic network could be constructed for the entire culture. This network was also similar to the one obtained for hybridoma cells (Dorka et al. 2009) with slight differences of

an additional significant flux for asparagine (flux 34) while negligible proline uptake which was found significant with hybridoma.

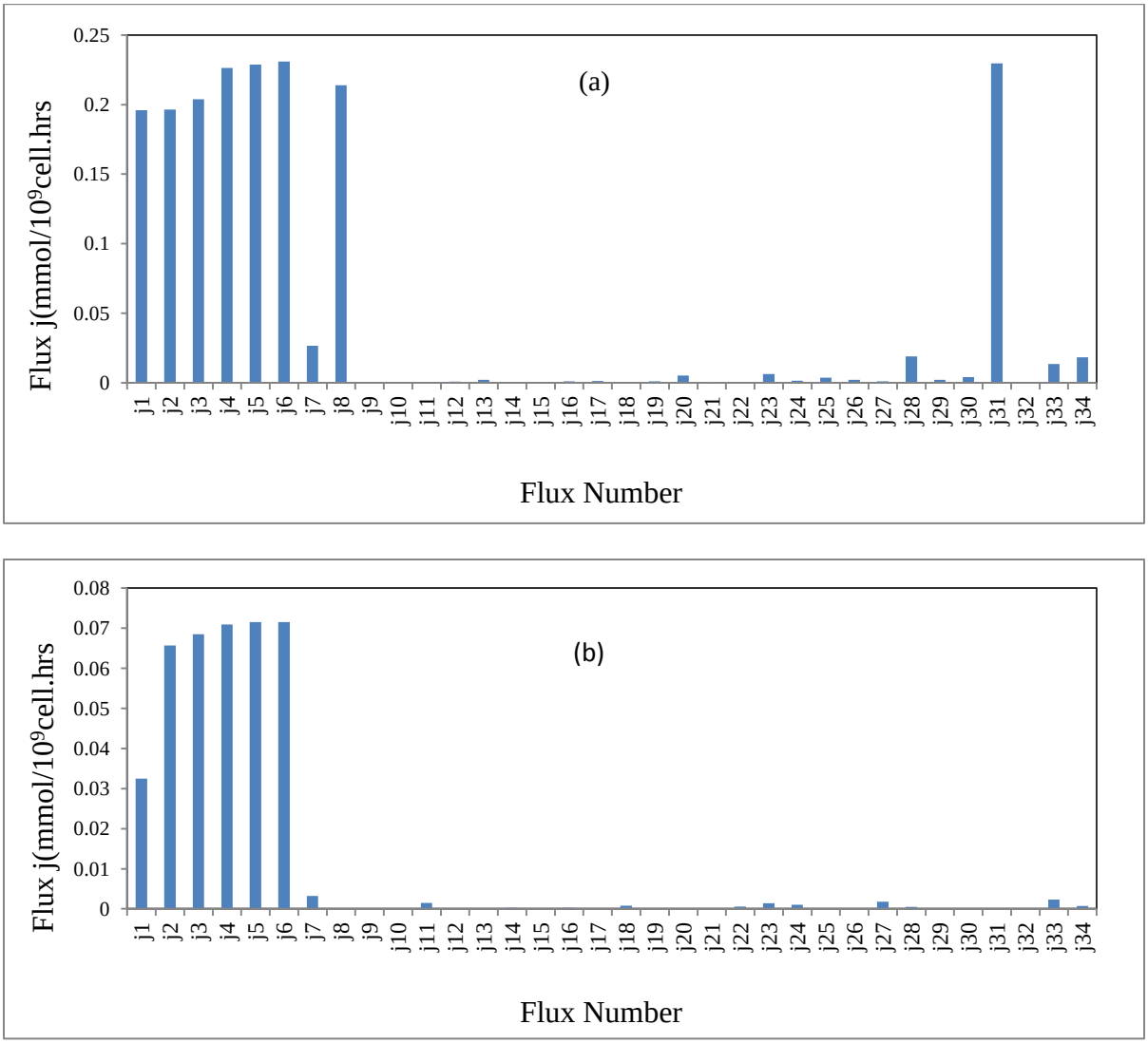

Figure 8.3: Distribution of fluxes for batch process for (a) Exponential Phase, (b) Post-Exponential Phase.

To test uniqueness of the resulting flux distribution for the current case with 30 equations and 34 unknowns, the number of active constraints should be larger than (n_i=34)-(n_m=30)=4. The number of active constraints was equal to 5 verifying that the solution is unique. The

insignificant fluxes (being less than 1% of total flux) were excluded to obtain a simpler metabolic network of elementary bioreactions (Figure 8.4).

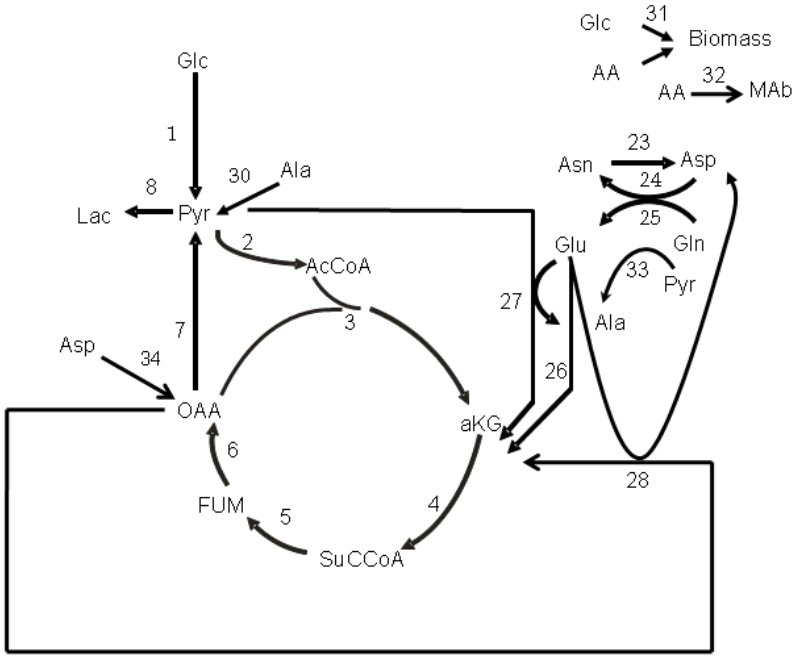

Figure 8.4: The simplified metabolic network for CHO cells

The systematic combination of these significant bioreactions resulted in a set of fundamental macro-reactions of extracellular metabolites shown in Table 8.1 (Dochain 2008). In general, we have chosen flux directions in accordance with published reports and with the apparent trends exhibited by the metabolites related to a particular flux. However, in two instances we have investigated the possibility of flux inversion when the culture passes from the exponential to the post-exponential phase: glutamine to glutamate (flux 25) and pyruvate to lactate (flux 8) conversions. To account for these cases, we have preformed flux analysis by assuming the reverse direction. In case of glutamate-glutamine we have found no difference in the results whereas in the lactate-to-pyruvate case we have found that the reversal is possible in the post-exponential phase but the resulting flux had a very small, insignificant value. In view of the flux value being small and the fact that lactate does not

decrease noticeably during the post-exponential phase we have not implemented this directional switch.

Table 8.1: Significant macro-reactions of extracellular metabolites.

E_1:	Glc → 2Lac
E_2:	Glc → $6CO_2$
E_3:	Glu → Lac + 2 CO_2 + NH_3
E_4:	Asn → Asp + NH_3
E_5:	Gln → $2NH_3$ + 5 CO_2
E_6:	Ala → NH_3 + 3 CO_2
E_7:	Gln + 0.5Glc → Glu + Ala
E_8:	Asp→ NH_3 + 4 CO_2

Accordingly, a dynamic mass-balance equation was established for each significant metabolite from macro-reactions (Table 8.2). As shown, the model provides two distinct terms for each metabolic rate: a "growth associated" term corresponding to growing cells (X_g) and a "non-growth associated" or maintenance term attributed to the population of non-growing cells (X_{ng}), which contains normal resting and apoptotic cells. In these equations, $X_g = f_{gr}(\boldsymbol{X}_v - X_{ap})$ and $X_{ng} = X_v - X_g$. Since the specific metabolic rates of apoptotic cells and normal resting cells were found to be nearly equal, these two subpopulations were merged into a unique population (X_{ng}) with identical parameters to simplify the model.

Table 8.2: Dynamic model of significant metabolites.

Glucose	$\frac{dGlc}{dt}=-a_{11}X_g-\left[\frac{a_1\,Glc}{k_{Glc}+Glc}+0.5\,\frac{a_7\,Glc.Gln}{(k_{Glc}+Glc).(k_{Gln}+Gln)}\right]X_{ng}$
Lactate	$\frac{dLac}{dt}=a_{22}\,X_g+\left[2.\frac{a_2\,Glc}{k_{Glc}+Glc}+\frac{a_3\,Glu}{k_{Glu}+Glu}\right]X_{ng}$
Glutamine	$\frac{dGln}{dt}=-a_{33}X_g-\left[\frac{a_5\,Gln}{k_{Gln5}+Gln}+\frac{a_7\,Glc.Gln}{(k_{Glc}+Glc).(k_{Gln}+Gln)}\right]X_{ng}$
Glutamate	$\frac{dGlu}{dt}=a_{44}\,X_g+\left[-\frac{a_3\,Glu}{k_{Glu}+Glu}+\frac{a_7\,Glc.Gln}{(k_{Glc}+Glc).(k_{Gln}+Gln)}\right]X_{ng}$
Asparagine	$\frac{dAsn}{dt}=-a_{55}X_g-\frac{a_4\,Asn}{k_{Asn}+Asn}\,X_{ng}$
Aspartate	$\frac{dAsp}{dt}=a_{66}X_g+\left[\frac{a_4\,Asn}{k_{Asn}+Asn}-\frac{a_8\,Asp}{k_{Asp}+Asp}\right]X_{ng}$
Alanine	$\frac{dAla}{dt}=a_{77}X_g+\left[-\frac{a_6\,Ala}{k_{Ala}+Ala}+\frac{a_7\,Glc.Gln}{(k_{Glc}+Glc).(k_{Gln}+Gln)}\right]X_{ng}$
Ammonia	$\frac{dNH_3}{dt}=a_{88}X_g+\left[\frac{a_3\,Glu}{k_{Glu}+Glu}+\frac{a_4\,Asn}{k_{Asn}+Asn}+2\,\frac{a_5\,Gln}{k_{Gln5}+Gln}+\frac{a_6\,Ala}{k_{Ala}+Ala}+\frac{a_8\,Asp}{k_{Asp}+Asp}\right]X_{ng}$

8.6.2 Parameter Estimation

The 9 differential equations for the extracellular metabolites were solved simultaneously along with the two differential equations that describe the viable (X_v) and apoptotic (X_{ap}) biomass (Equations 10 and 11). Model parameter calibration was performed using one data set, 1mM glutamine with 14 mM glucose (Naderi et al. 2010). For each parameter in the model, a 95% confidence interval was estimated by the Gibbs sampling version of the Metropolis-Hastings algorithm (Jitjareonchai et al. 2006). For each parameter, a normalized triangular probability distribution was used as the proposal density function. Altogether 6000 iterations were performed. The first 2000 iterations were used as burn-in to establish the

model variance. The parameter values obtained by this algorithm were then used as initial guesses for a more refined search conducted with the *fmincon* function in MATLAB (Appendix H). The coefficients, shown in Appendix H, were employed unadjusted for both the growth and the post-exponential phases of the culture.

8.6.3 Model Validation

In order to test the validity of the model, predictions were generated for a set of experimental conditions that were not used for the model calibration step explained in the previous section. Accordingly, the macroscopic model was used to predict the dynamic cell behavior for batch cultures with different glutamine and glucose concentration ratios. The results are compared with the calibration in Figure 8.5. The model validation shows good agreement with experimental measurements of cell growth and metabolite uptake. Glutamine consumption was higher at higher initial concentration (4mM), resulting in high ammonia levels as the byproduct of oxidative deamination mechanism. It seems that oxidative deamination of glutamine, forming glutamate and eventually α-ketoglutarate, provides entry into the citric acid cycle. This becomes the dominant energy yielding metabolism. Reitzer et al. (Reitzer et al. 1979) showed that glutamine rather than glucose was the main energy source for Hela and that glucose was essential for ribose synthesis as a precursor for nucleic acids in growing cells. The switch from glycolysis to glutaminolysis was explained in that study by the decreased need for nucleotide synthesis in resting cells. However, the accumulation of ammonia at toxic levels could affect the viability of the culture significantly. In case of lower glutamine concentration the accumulation of ammonia was less significant.

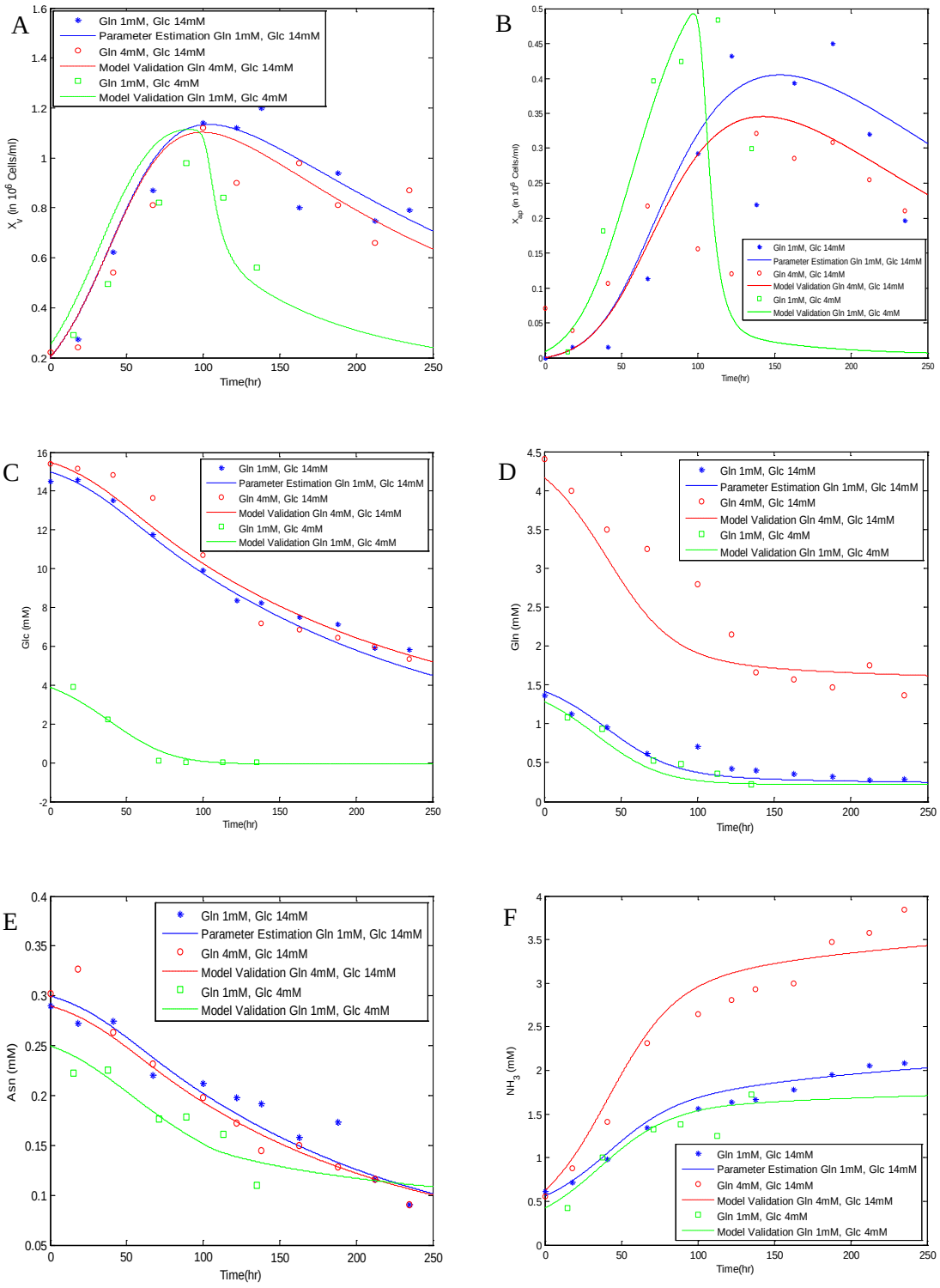
A
Gln 1mM, Glc 14mM
Parameter Estimation Gln 1mM, Glc 14mM
Gln 4mM, Glc 14mM
Model Validation Gln 4mM, Glc 14mM
Gln 1mM, Glc 4mM
Model Validation Gln 1mM, Glc 4mM
Time(hr)
B
Time(hr)
C
Glc (mM)
Time(hr)
D
Gln (mM)
Time(hr)
E
Asn (mM)
Time(hr)
F
Time(hr)

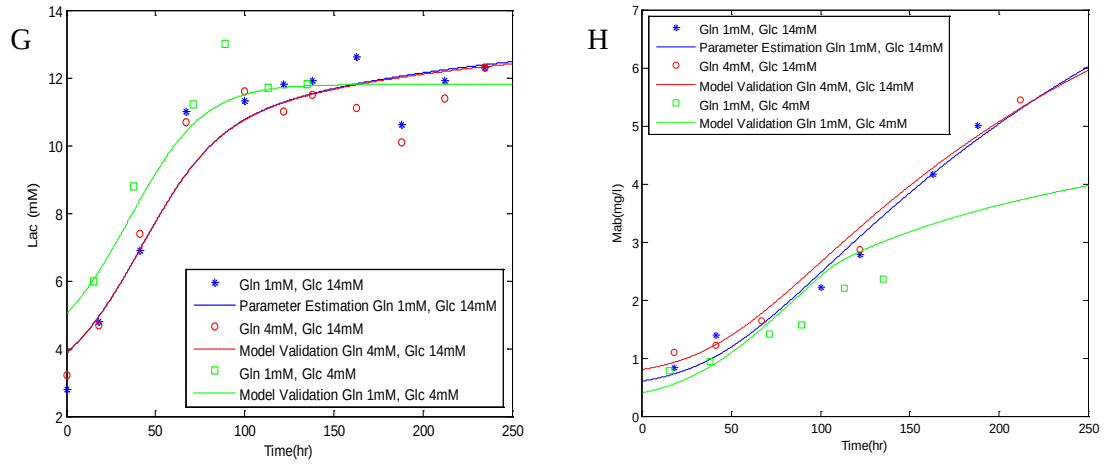

Figure 8.5: Model fitting and validation in batch culture using Logistic model : A) total viable cell, B) apoptotic cell, C) glucose, D) glutamine, E) asparagine, F) NH_3, G) lactate, H) MAb.

As shown on Figure 8.5, model simulation results have also been obtained for two different glucose levels, 4mM and 14mM. The model closely tracks cell subpopulation data and nutrient catabolism. However, the apoptotic state was not fully captured by the model, due to significant noise in fluorescent microscopy results. This noise was mostly due to the difficulty in distinguishing between normal and apoptotic cells based on blebbing patterns and due to the existence of clumps of cells. Blebbing in clumps was difficult to observe by microscopy. Considering 10 observations in 4 replicate runs, the standard error of the apoptotic cell assay was 8.4×10^4 cells/mL. The confidence interval of any single measurement ($\pm1.6\text{x}10^5$ cells/mL) was over 30% of the maximum estimated apoptotic population of 5.2×10^5 cells/mL. The total viable cell profile shows that glucose at low level (4mM) had almost no effect on the cell growth rate and the corresponding peak in cell concentration, but resulted in faster death rate as the viability declined dramatically after the stationary state. The temporal profile of significant amino acids, specifically glutamine was hardly affected by the different initial glucose concentration, implying that glutamine cannot be substituted for glucose. In contrast to hybridoma cells (Dorka et al. 2009), glucose has a critical role in CHO cell culture either in the growth or maintenance phase (Sun and Zhang

2004). Although the biomass model was affected by the concentrations of ammonia and glucose only (see Equations 10 and 11), due to the interrelationship among metabolites it was necessary to solve the entire metabolic network in order to calculate the concentrations of these two specific metabolites.

It seems that the cell-specific MAb productivities of growing and non-growing cells are essentially identical. Thus, we found that the differentiation between the two subpopulations with regard to MAb production was not necessary. However, this does not negate the significance of separately modeling the cell subpopulations, since the apoptotic state affects the overall viability thus indirectly impacting the overall productivity. The specific production rate of viable cells was 2.5×10^{-2} (mg MAb/hr.10^9 cells). It seems that the combination of the growing, resting and apoptotic cell populations was appropriate, since their cell specific productivities were not significantly different. In fact, modeling the two productivities separately did not improve the goodness of fit of the model.

Figure 8.6 shows model simulation of cell subpopulations and metabolites. The only difference from the previous model is applying Tessier's equation for the kinetic growth rate, while there is no change in the modeling of the metabolites. The model prediction shows good agreement with the experimental data, except for the apoptotic cell density due to high fluctuation in the experimental data. This model is comparable with the logistic model used previously (Naderi et al. 2011) and has the advantages of being able to describe fed-batch operation with respect to a substrate present in the medium, however we found that cell growth and viability is more dependent on an unknown inhibitory factor rather than on a nutrient.

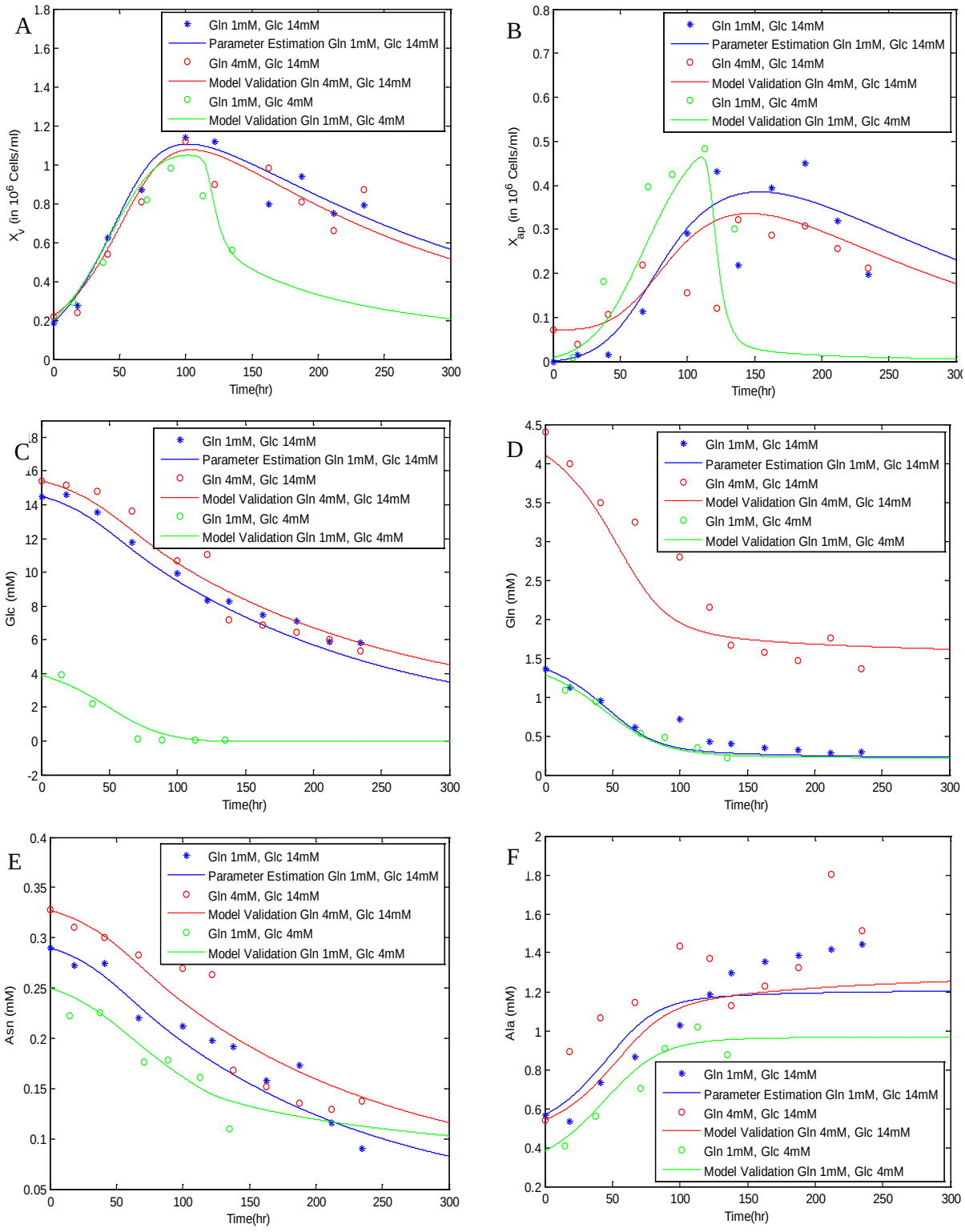
A
B
C
D
E
F
Gln 1mM, Glc 14mM
Parameter Estimation Gln 1mM, Glc 14mM
Gln 4mM, Glc 14mM
Model Validation Gln 4mM, Glc 14mM
Gln 1mM, Glc 4mM
Model Validation Gln 1mM, Glc 4mM
Time(hr)
Xv (in 10^6 Cells/ml)
Xap (in 10^6 Cells/ml)
Glc (mM)
Gln (mM)
Asn (mM)
Ala (mM)

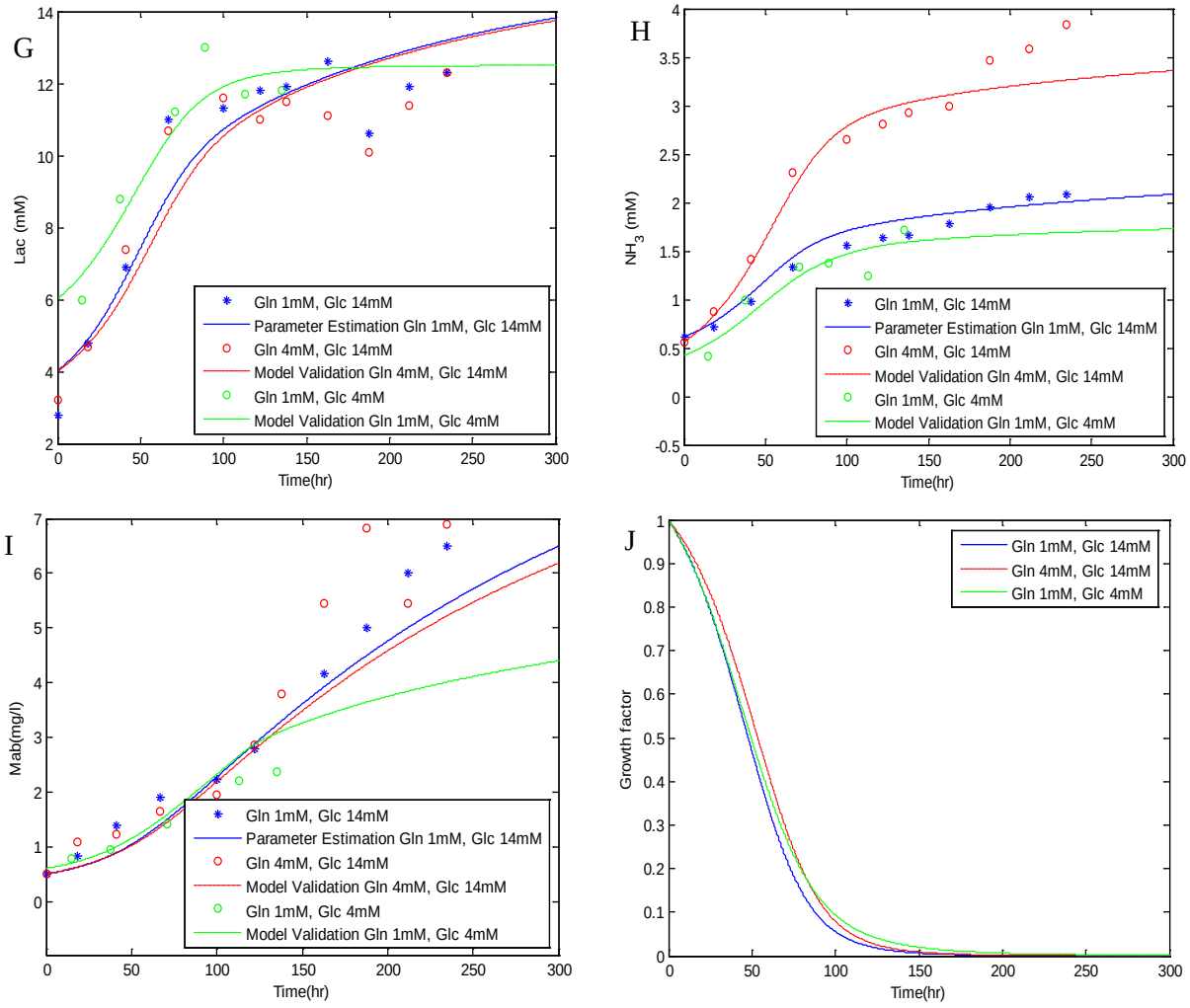

Figure 8.6: Model fitting and validation in batch culture using Tessier model : A) total viable cell, B) apoptotic cell, C) glucose, D) glutamine, E) asparagine, F) alanine, G) lactate, H) NH_3 I) MAb J) growth factor.

Augmenting the inhibitory effect of CO_2 in the dynamic model, the results for two periodic partial perfusion cultures at two different volume 250 and 500 mL are presented in Figure 8.7. It should be mentioned that all the parameters values are same as obtained in the previous batch culture, except the new parameters for inhibitory model ($k_{11,}$ k_{22}, $k_{33,}$ $k_{a,}$ $k_{v,}$ C_{∞}) estimated from partial perfusion data of a 500 mL culture. The model prediction shows good agreement with experimental data at both culture volumes. However, there is no

experimental data for apoptotic cell concentration and CO_2 to confirm the model prediction at the lower volume. The amino acids, glutamate and aspartate show gradual reduction as glutamine and asparagine concentrations decreased to near zero but cell continued growing. This consumption has been simulated in the model by reversing the two reactions E4 and E7, shown in Table 8.1, as glutamine and asparagine are depleted, while the fraction of growing cells is above zero. In addition, the model prediction for single full perfusion and fed-batch culture are presented in Appendix I and J.

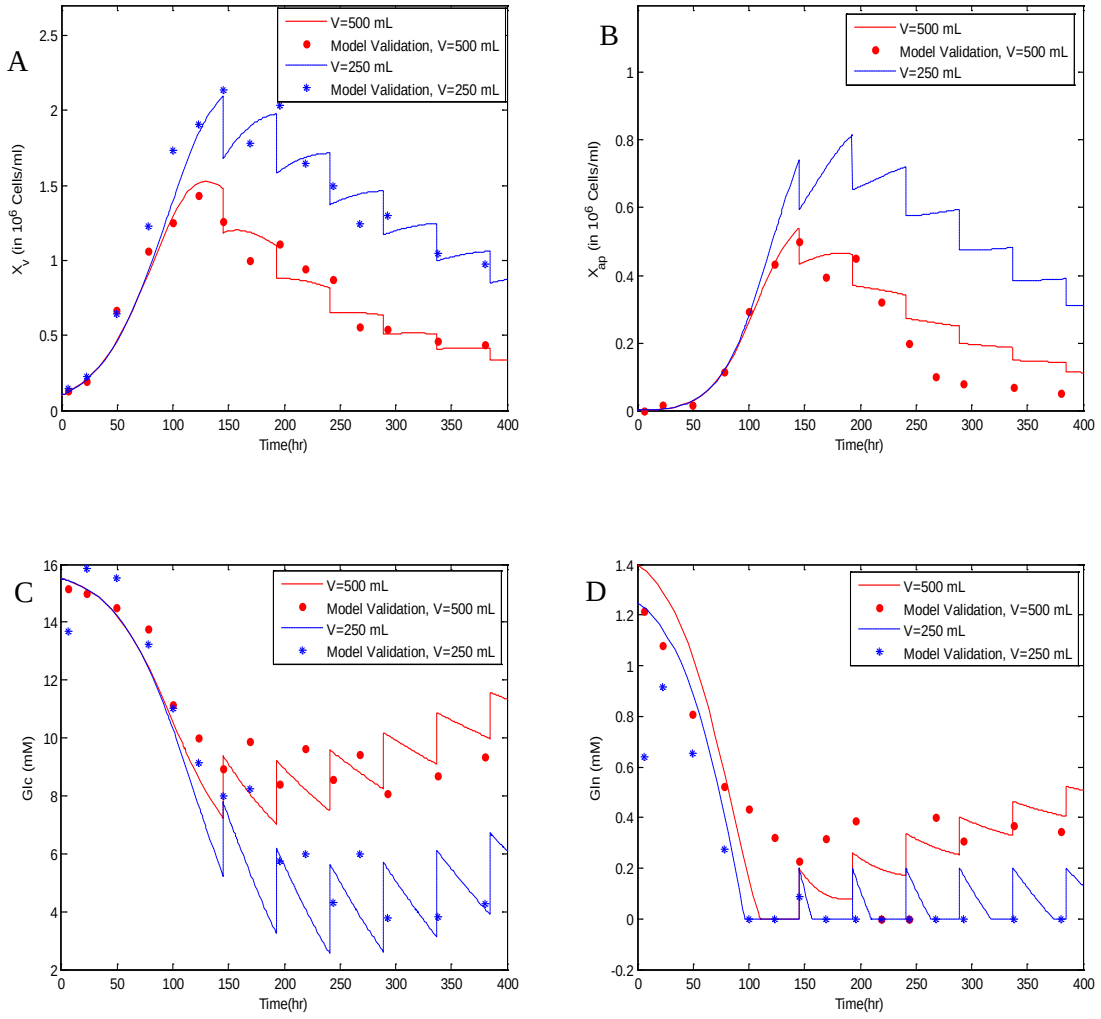

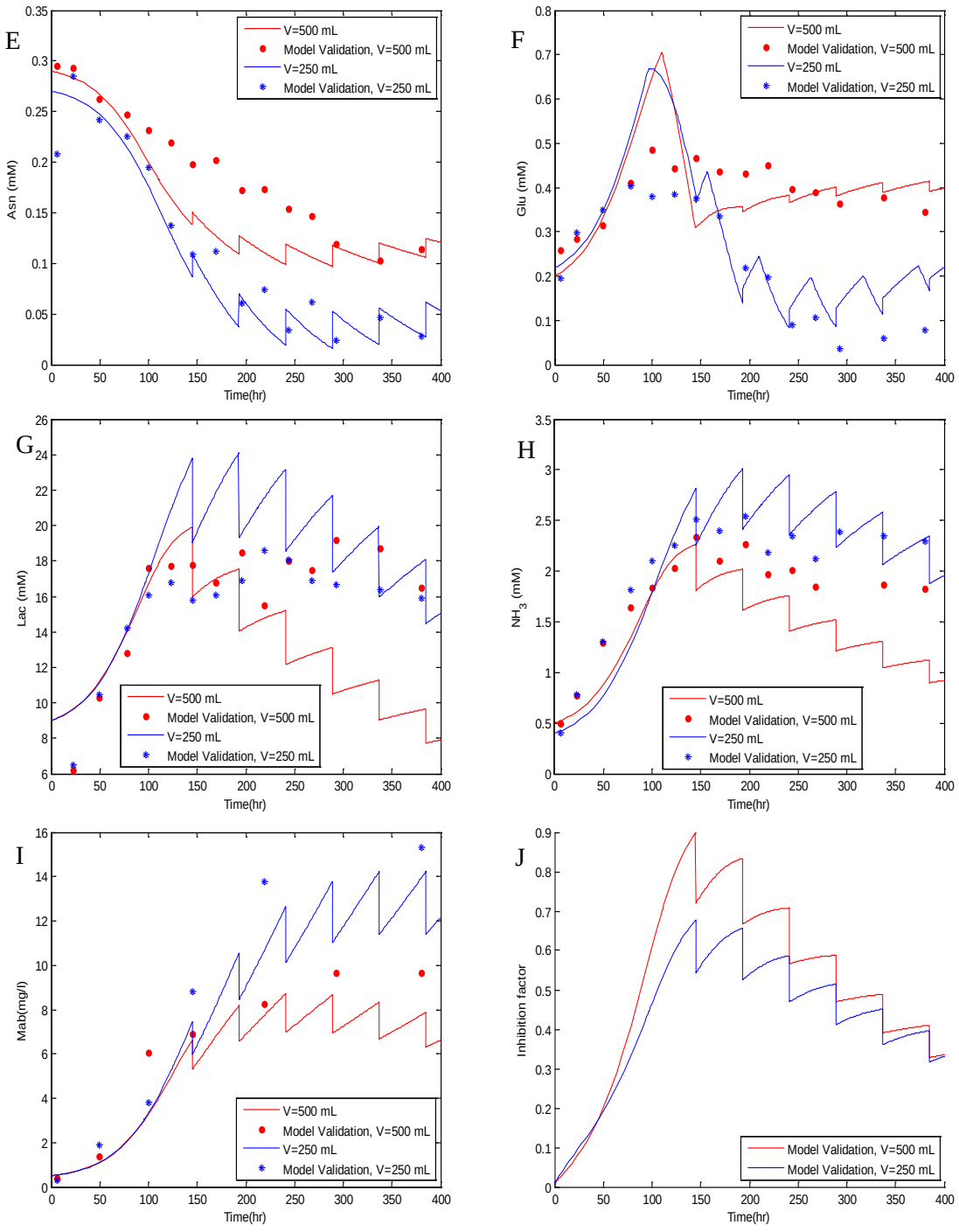

Figure 8.7: Model validation in periodic partial perfusion culture using Tessier-based model: A) total viable cell, B) apoptotic cell, C) glucose, D) glutamine, E) asparagine, F) glutamate, G) lactate, H) NH_3, I) MAb, J) inhibition factor.

Chapter 9
Conclusion and Recommendation

The main focus of this study was the dynamic analysis of the metabolic behavior of a CHO cell culture under different conditions. Various strategies for modifying the culture environment were employed in order to provide optimal conditions for continued growth, maintaining high viability, and MAb production. Statistical analysis based on paired comparison has confirmed the reproducibility of the data. The significant parameters affecting optimality were identified by applying metabolic flux analysis, and a kinetic model was developed describing cell metabolism and biosynthesis under different culture modes; batch, fed-batch, and perfusion processes. The important findings of this study are summarized below.

Although glutamine and asparagine are recognized as main energy and carbon sources, their depletion in the medium did not affect cell growth significantly. Glucose depletion accelerated the initiation and progress of apoptosis and eventual cell death. Unlike hybridoma cells, which show strong growth dependency on glutamine concentration, it is difficult to identify clear growth dependence to any significant nutrient in CHO cells. Although significant differences in glutamine utilization using 1mM and 4mM glutamine were observed, no improvement in growth or productivity occurred. The higher initial glutamine concentration resulted in higher ammonia production. This suggested that glutamine should be supplied at low concentration to avoid the adverse effect of ammonia on growth at high level. This condition also makes the cell to substitute and utilize other amino acids such as glutamate more effectively. It is remarkable that glucose metabolism is hardly affected by the higher initial glutamine levels. Since the nutrient requirements of growing and resting cells differ, modifications of the medium may be needed to optimize long-term propagation of cells by either fed-batch or perfusion methods. Similarly, the metabolism of the other amino acids, notably alanine, glutamate, asparagine and aspartate, was scarcely affected when the initial glutamine concentration was increased from 1mM to 4mM. However glucose concentration control is necessary to prevent cell death. This growth

limiting feature of glucose has been expressed in the biomass model, but was significant only at very low concentration of glucose. Employing sufficient level of glucose is recommended to avoid high lactate concentration and osmolality, but not in limiting concentration that may initiate apoptosis or autophagy.

Supplementation of culture with different regular and concentrated medium in various feeding strategies such as single-pulse feeding and fed-batch culture resulted in no appreciable improvement in cell growth, peak concentration, viability or MAb productivity. This implies that the main cell culture conditions (pH, CO_2 for example) need to be optimized/controlled to achieve the optimal results by nutrient supplementation. Reduction of pH due to possible accumulation of dissolved carbon dioxide was identified as a significant parameter which effectively inhibited cell growth. Although this suppression effect was mitigated by partial replacement of culture with fresh medium in the perfusion system, due to high cell density and subsequently high metabolic activity, following each perfusion instance the culture rapidly returned to undesirable conditions, so that gradually the cells lost their capability of regeneration. Irreversible loss in cell growth ability was observed in subsequent refreshment of the culture. This motivates the need for measuring CO_2 for optimal control and applying a strategy for its faster removal from a culture. A simple way might be decreasing slowly the CO_2 level in gas phase inside the incubator before cells reaching the peak. In addition gentle sparging of filtered nitrogen gas to the culture can accelerate the gas removal rate. This could also improve the mixing efficiency. In the proposed model, the cumulative effect of dissolved carbon dioxide on cell growth under metabolically stressful conditions was expressed. Although other byproduct metabolites, such as lactate and ammonia were not at the toxic levels, their effects on the metabolic activity were not negligible and all these factors need to be regulated for achieving improved environmental conditions.

Cell density also influenced cell growth and the evolution of programmed cell death. The postulate is that at high density the cells are arrested in G_1/G_0 phase through signaling mechanism. The balance between cell division and apoptosis was examined by diluting the culture near the peak. Dilution resulted in inducing cell proliferation. The results of flow

cytometry for caspase 8 activation also confirmed cell to cell interaction. However it was not possible to separate the effect of cell density from the effect of possible carbon dioxide accumulation, since diluting the culture also caused reduction of environmentally inhibitory concentrations. Also, the experiments conducting higher initial cell density cannot separate these two effects since more cells are expected to produce carbon dioxide at a faster rate. Also, although CHO cell lines are reported to be immortal, the behavior identified in this work seem to indicate senescence or aging of the culture. It is recommended that the reversibility of the growing and the non-growing populations should be further examined, since it has a profound effect on growth. For instance, a continuous culture operated, by proper manipulation of dilution rates, back and forth between different levels of cell concentration could help to further elucidate these reversibility effects. To the knowledge of the author this reversibility or lack of it with respect to growth or apoptosis has not been addressed thoroughly in the literature as yet, although an earlier study has referred to sublethal pH depression as a cause for irreversible growth arrest of mammalian cells.

The flux distribution estimated through metabolic flux analysis was found to be identical for each phase of the culture: exponential and post-exponential phases. This supported the construction of a single metabolic network for both phases. The flux directions were identified according to similar metabolic networks presented in previous studies, and the observed trends of measured metabolites. Based on the metabolic network, a dynamic model for each metabolite was developed. The simulation results showed that the model can describe the metabolic behavior of CHO cell adequately for each measured metabolite. In case of the two amino acids glutamate and aspartate, the model predictions indicate an increase of these two metabolites in the growth phase leveling off as the culture enters the stationary phase as observed in the different experiments. In fact the reaction occurs in both directions throughout the process, however in the exponential phase the rate of production is much faster, while in the post-exponential phase their consumption becomes dominant. The high consumption rate was significant at low culture volume (250mL) with high cell density (over 2×10^6 cells/mL), at very low glutamine and asparagine levels. This reversibility was

achieved in the model by changing the sign as the glutamine and asparagine concentrations reaching below a specified level, while the cell growth continues.

A novel approach was presented to differentiate between normal growing, normal resting and apoptotic cell subpopulations with unique specific metabolic rates. This division enabled the quantitative assessment of metabolic state of the cell culture at various times. An important finding was the apparent switch in the rate of metabolism as the culture ages and non-growing cells become predominant. Establishing sub-populations also eliminated the necessity for arbitrary division of the population into “exponential” and “post-exponential” phases.

A major issue was the high variability observed in the monoclonal antibody assay in the experiments. This caused uncertainty on the attained results and in difficulty in comparing the data from different experimental conditions. This variability could be attributed to the ELISA method regarding inconsistency in the reagents and standards and also the analysis of data. This is important especially when performing process optimization to ensure significant process improvement. Another issue may be the secretion of the MAb product from cells. Therefore, it is recommended to investigate further the analytical issue as well as the dynamics of MAb secretion under different operating conditions.

Another issue was the significant noise on the imaging results of apoptotic cells due to the difficulty in distinguish between apoptotic and normal cells, especially for the cell clumps at high cell density. Since apoptosis is a rapid cellular event and is actually a transient status of the cell life cycle, it is difficult to follow this process carefully. To get more consistency in the results, the provided MATLAB program should be modified to account for clumps by possible detection of inflection points around the clumps and also it is recommended to look for other feasible methods of detecting apoptosis.

Although the logistic equation for expressing the growing fraction of the viable population was applied successfully, due to the lack of inhibitory effect, this model cannot describe metabolic behavior appropriately, also it could not be applied for optimization of fed-batch culture with respect to addition of media. The final developed model accounts for the effect

of several significant factors on cell growth and metabolic activity and can simulate successfully the time profile of cell populations and major external metabolites. However the model simulation of some metabolites was inconsistent and needs to be modified to capture any significant variables affecting cellular behavior for accurate prediction. This model would be the basis for an optimal-control of a fed-batch or perfusion process provided that issues related to carbon dioxide inhibition can be addressed. In the presence of such inhibition, one possible optimal strategy could be periodic full perfusion of the culture as soon as inhibitory levels of pH are measured. Clearly this will result in progressively shorter periods of operation after each perfusion due to the progressive increase in cell mass with the corresponding increase in carbon dioxide production rates.

Appendix A

Nomenclature

α	toxicity function constant
α_g	specific production rate for both growing and non-growing cells
$\alpha_{i,m}$	stoichiometric coefficient for metabolite m in reaction i
a_{ig}	maximum rate of reaction for growing cells
a_{ing}	maximum rate of reaction for non-growing cells
a_s	specific consumption rate of unknown component S
μ	specific growth rate
$\boldsymbol{\xi}$	vector of extracellular metabolites concentration
$\boldsymbol{\psi}$	vector of intracellular and extracellular metabolite concentrations
$\boldsymbol{A}$	stoichiometric coefficient matrix of all bioreactions
C	inhibition factor concentration
C_∞	CO_2 concentration in equilibrium with headspace gas phase
f_{gr}	fraction of dividing normal cells
$\boldsymbol{j}$	vector of intracellular fluxes
j_i	intracellular flux for reaction i
k_2	toxicity function constant
k_3	autophagic constant
k_4	glucose saturation constant
k_{11}	specific production of CO_2 by normal growing cells
k_{22}	specific production of CO_2 by normal non-growing cells
k_{33}	specific production of CO_2 by apoptotic growing cells
k_a	accumulation constant
k_c	inhibitory constant
k_{D1}	specific death rate constant
k_{D2}	specific death rate constant

$\boldsymbol{K}$	stoichiometric coefficients of the matrix of the macroscopic reactions
k_{ap}	specific rate of apoptotic cell formation
k_{i}	half-saturation constant
k_s	Tessier constant
k_v	mass transfer coefficient
m_i	metabolite concentration
n	number of reactants in the ith reaction
N	Ammonia concentration
P	MAb concentration
$\boldsymbol{r_E}$	vector of the macro-reaction rates
r_i	reaction rate for i^{th} reaction
$\boldsymbol{r}$	vector of specific uptake/production rate of each metabolite
$r(m)$	net uptake or production rate of metabolite m
S	concentration of unknown component
t	time interval
$\boldsymbol{u}$	vector of net exchange rate of the species with the surroundings
X_{ap}	apoptotic viable cell concentration
X_g	viable growing cell concentration
X_{ng}	viable non-growing cell concentration
$X_{\boldsymbol{v}}$	viable cell concentration

Appendix B

Abbreviations Used In Metabolic Reactions

*α*KG	α-Ketoglutarate
AA	Amino Acids
AcCoA	Acetyl Coenzyme A
Asn	L-Aspargine
Ala	L-Alanine
Arg	L-Argenine
Asp	L-Aspartate
CO_2	Carbon Dioxide
Cys	L-Cysteine
FUM	Fumarate
Glc	Glucose
Gln	L-Glutamine
Glu	L-Glutamate
Gly	L-Glycine
His	L-Histidine
Ile	L-Isoleucine
Lac	Lactate
Leu	L-Leucine
Lys	L-Lysine
MAb	Monoclonal Antibody
Met	L-Methionine
NH_3	Ammonia
OAA	Oxaloacetate
Pro	L-Proline
Phe	L-Phenylalanine
Pyr	Pyruvate
Ser	L-Serine
Thr	L-Threonine
Tyr	L-Tyrosine
Val	L-Valine

Appendix C

List of Stoichiometric Equations

j_i (i=1,2,…,34)	Reaction
Central Metabolic Pathway	
j_1	GLC→ 2PYR + 2NADH + 2ATP
j_2	PYR→ AcCoA + CO_2+NADH
j_3	AcCoA + OAA→ aKG + NADH + CO_2
j_4	aKG→ SuCCoA+ NADH + CO_2
j_5	SuCCoA→ FUM + NADH
j_6	FUM→ OAA + NADH
j_7	OAA→ PYR + NADPH + CO_2
j_8	PYR + NADH→ LAC
j_9	THR→ PYR + CO_2 + NH_3 + 2NADH
j_{10}	2GLY→ SER+CO_2+NH_3 + NADH
j_{11}	SER→ PYR+NH_3
j_{12}	PHE→ TYR + NADH
j_{13}	TYR→ FUM + 2AcCoA + NH_3 + CO_2 + NADPH
j_{14}	VAL→ SuCCoA + CO_2 + NH_3 + NADPH
j_{15}	THR→ SuCCoA + NH_3
j_{16}	ILE→ SuCCoA + AcCoA + NADPH + NH_3
j_{17}	MET + O_2→ SuCCoA + SO_2 + NADPH + NH_3
j_{18}	LEU→ NH_3 + 3AcCoA + NADPH
j_{19}	LYS→ 2 AcCoA + 2CO_2 + 2NADPH + 2NH_3
j_{20}	HIS→ GLU+2NH_3+CO_2
j_{21}	ARG→ aKG + 2NH_3 + UREA + 3 NADH
j_{22}	GLU + ATP + 2 NADPH→ PRO
j_{23}	ASN→ ASP + ATP + NH_3
j_{24}	GLN + ASP + 2 ATP→ ASN + GLU
j_{25}	GLN→ GLU + ATP + NH_3
j_{26}	GLU→ AKG + NADPH + NH_3
j_{27}	PYR + GLU→ ALA + AKG
j_{28}	GLU + OAA→ ASP + AKG
j_{29}	CYS + O_2→ PYR + SO_2 + NADH + NH_3
j_{30}	ALA→ PYR + NADH + NH_3
j_{33}	Gln + Pyr→Glu+Ala
j_{34}	Asp →OAA+NH_3

List of Stoichiometric Equation (Cont'd)

j_i (i=1,2,…,33)	Reaction
Biomass Formation	
j_{31}	0.0508GLC +0.0577GLN +0.0133ALA +0.007ARG +0.006ASN+0.020lASP +0.0004CYS +0.0016GLU +0.0165GLY +0.0033HIS+0.0084ILE +0.0133LEU +0.0101LYS +0.0033MET +0.0055PHE+0.0081PRO +0.0099SER+0.008THR+0.004TYR+0.0096VAL→BIOMASS
Antibody Production	
j_{32}	0.0104GLN +0.011ALA +0.005ARG +0.0072ASN +0.0082ASP+0.005CYS +0.0107GLU +0.0145GLY +0.0035HIS +0.005ILE+0.0142LEU +0.0145LYS +0.0028MET +0.0072PHE +0.0148PRO+0.0267SER +0.0160THR +0.0085TYR +0.0189VAL→ MAb

Appendix D

A Typical Amino Acid Calibration Curve

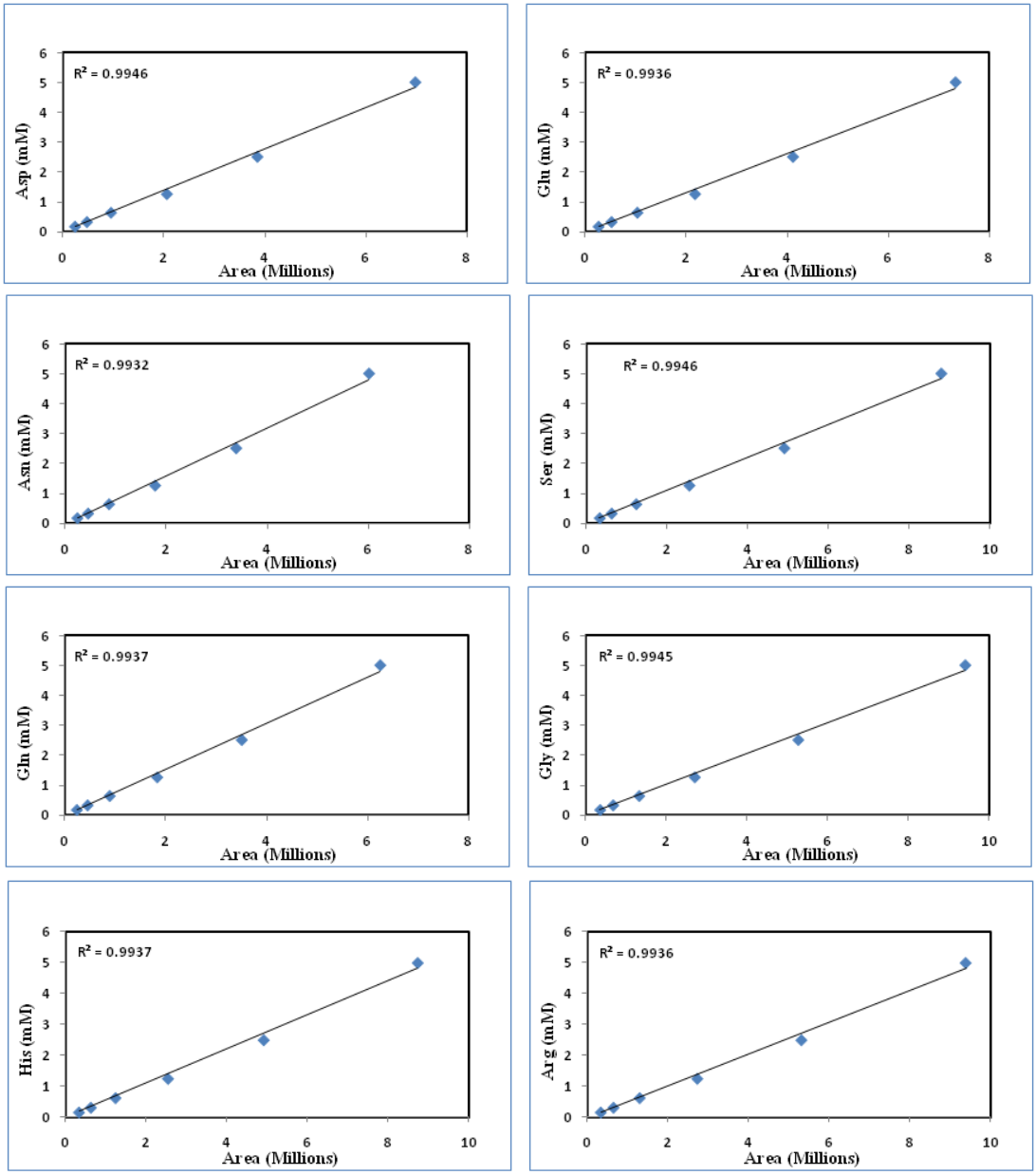

A Typical Amino Acid Calibration Curve (Cont'd)

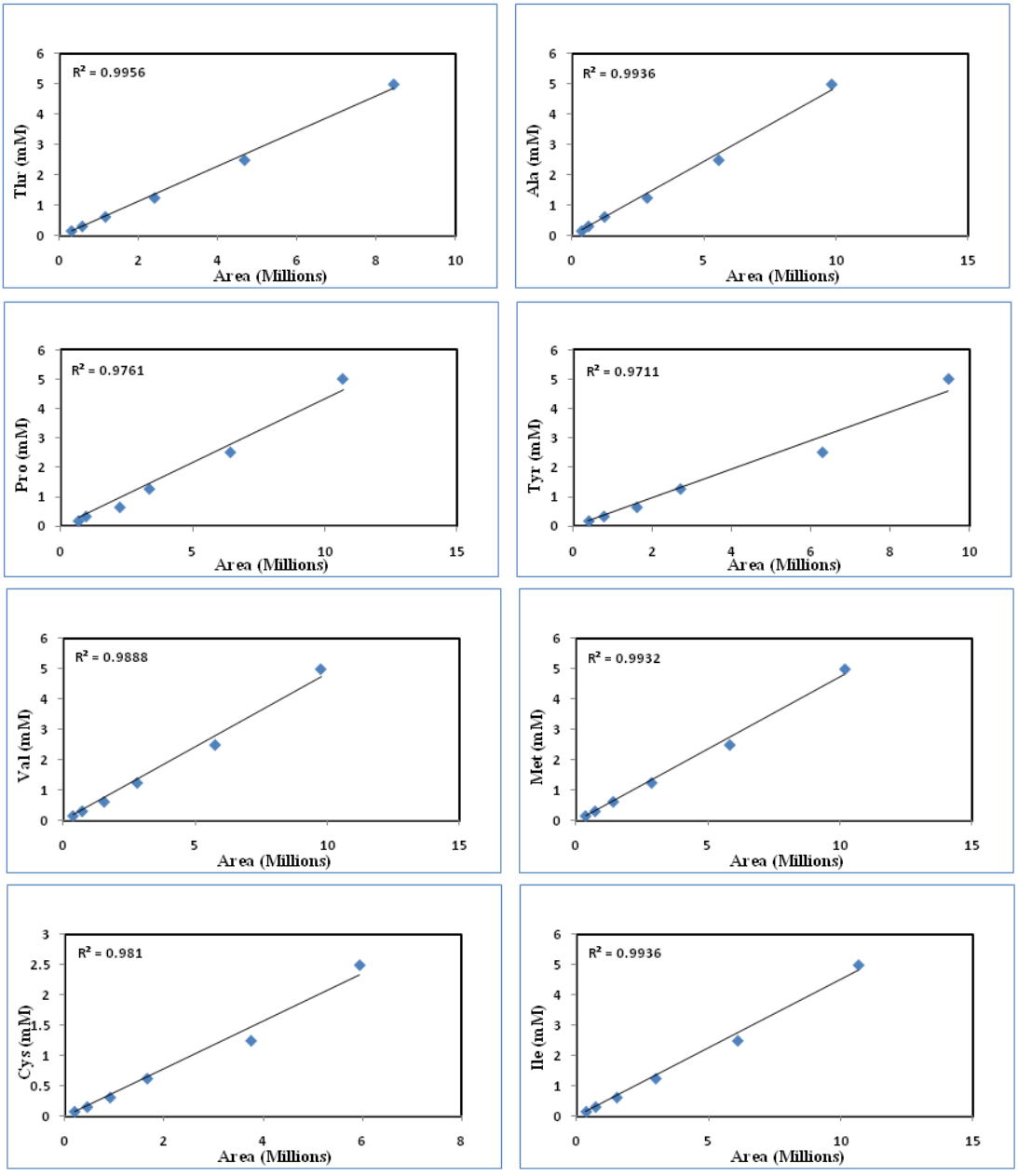

A Typical Amino Acid Calibration Curve (Cont'd)

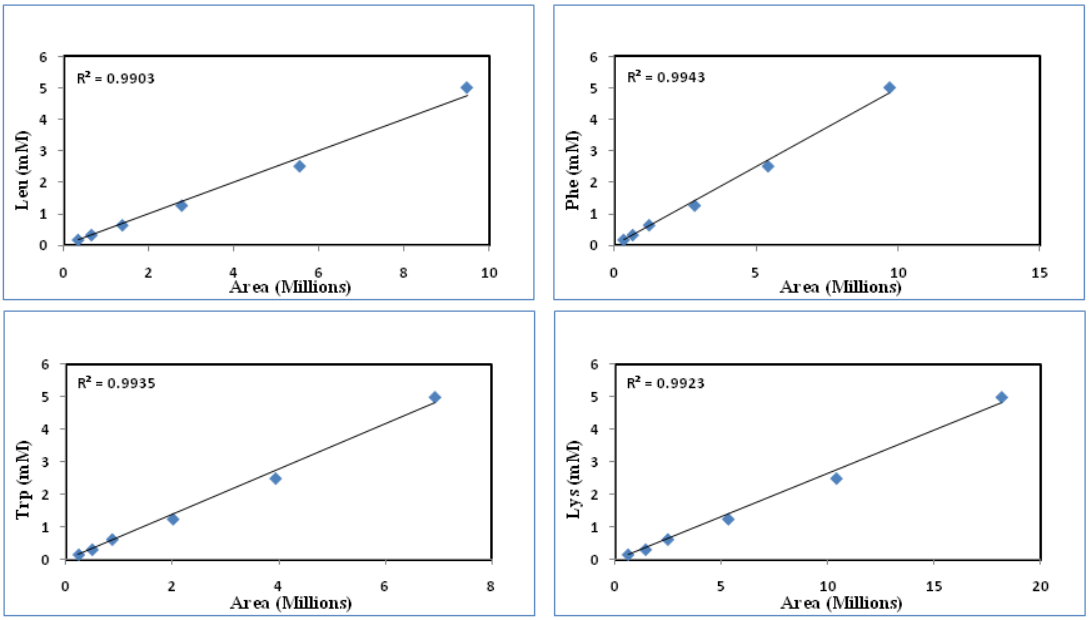

Appendix E

Analysis of Variance (ANOVA) for Glutamine and Glucose Effect

ANOVA Table for Glutamine Effect

95% Confidence Level $F_{0.05,2,20}=3.49$, $F_{0.05,10,20}=2.35$

Source of Variation	SS	df	Ms	F
Time	2.9867	10	0.2987	43.6189
Glutamine	0.0038	2	0.0019	0.2753
Error	0.1369	20	0.0068	
Total	**3.1279**	**32**		

ANOVA Table for Glucose Effect

95% Confidence Level $F_{0.05,3,30}=2.92$, $F_{0.05,10,30}=2.16$

Source of Variation	SS	df	Ms	F
Time	3.2302	10	0.323	49.3831
Glucose	0.0327	3	0.0109	1.6662
Error	0.1963	30	0.0065	
Total	**3.4591**	**43**		

Appendix F

Paired *t*-Test for Replicates

Batch Experiment with 1mM Glutamine, 14mM Glucose, 0.3mM Asparagine.

95% Confidence Level $t_{0.025,10}$=2.228

Variable	t_0
Xv	0.190217
Glucose	1.668696
Glutamine	0.582161
Lactate	0.411377
Ammonia	1.533644

Batch Experiment with 1mM Glutamine, 4mM Glucose, 0.3mM Aspargine.

95% Confidence Level $t_{0.025,5}$=2.571

Variable	t_0
Xv	0.2225
Glucose	0.820919
Glutamine	0.754354
Lactate	0.058513

Appendix G

Intracellular Fluxes j (*mmol/10^9 cell hours*)

j_i	j_{exp}	$j_{post\text{-}exp}$
j_1	0.196	0.0325
j_2	0.1964	0.0657
j_3	0.2039	0.0685
j_4	0.2264	0.0709
j_5	0.2287	0.0715
j_6	0.2309	0.0715
j_7	0.0266	0.0032
j_8	0.2138	0
j_9	0	0
j_{10}	0	0
j_{11}	0	0.0015
j_{12}	0.0009	0
j_{13}	0.0022	0
j_{14}	0	0.0003
j_{15}	0	0
j_{16}	0.001	0.0003
j_{17}	0.0013	0
j_{18}	0	0.0008
j_{19}	0.0011	0
j_{20}	0.0053	0
j_{21}	0.0004	0
j_{22}	0	0.0006
j_{23}	0.0063	0.0014
j_{24}	0.0014	0.001
j_{25}	0.0036	0.0001
j_{26}	0.0021	0.0001
j_{27}	0.0011	0.0018
j_{28}	0.0189	0.0005
j_{29}	0.0021	0
j_{30}	0.0042	0
j_{31}	0.2296	0
j_{32}	0	0
j_{33}	0.0135	0.0023
j_{34}	0.0184	0.0007

Appendix H

Parameters Value and Confidence Intervals

parameter	Value	Std.deviation	Confidence Intervals
a	1.397	0.521	1.02116
μ	0.042	0.00372	0.00729
a_1	0.0486	0.00535	0.01049
a_2	0.011538	0.000809	0.00159
a_3	0.0000502	2.39E-06	4.7E-06
a_4	0.001147	0.00241	0.00472
a_5	0.00123	0.000264	0.00052
a_6	0.0001469	0.000023	4.5E-05
a_7	0.001233	0.000419	0.00082
a_8	0.00107	0.00284	0.00557
a_{11}	0.1317	0.00891	0.01746
a_{22}	0.2451	0.01426	0.02795
a_{33}	0.0416	0.00476	0.00933
a_{44}	0.014839	0.000161	0.00032
a_{55}	0.002339	0.000365	0.00072
a_{66}	0.00994	0.00152	0.00298
a_{77}	0.0235	0.01426	0.02794
a_{88}	0.0416	0.00372	0.00729
a_g	0.025	0.000725	0.00142
a_s	0.94631		
C_∞	0.0983	0.0241	0.047236
k_{11}	0.0182	0.00163	0.003195
K_{22}	0.0082	0.00154	0.003018
K_{33}	0.00536	0.00072	0.001411
K_a	0.00277	0.00078	0.001529
k_{Glc}	2.41	0.359	0.70364
k_{Gln}	0.509	0.213	0.41748
k_{Gln5}	4.968	1.156	2.26576
k_{Glu}	0.223	0.00834	0.01635

Parameters Value and Confidence Intervals (Cont'd)

parameter	Value	Std.deviation	Confidence Intervals
k_{Asn}	0.096	0.0108	0.02117
k_{Asp}	0.0605	0.022	0.04312
k_{Ala}	0.109	0.205	0.4018
k_{D1}	0.009	0.0024	0.0047
k_2	5.42	0.764	1.49744
k_{D2}	0.15	0.005956	0.01167
k_3	0.05	0.00314	0.00615
k_4	0.017	0.0224	0.0439
k_{ap}	0.00933	0.001321	0.00259
k_c	0.64027	0.0968	0.189728
k_s	0.64027	0.0968	0.189728
k_v	0.0093	0.00152	0.002979

Appendix I

Model Prediction of Single Full Perfusion

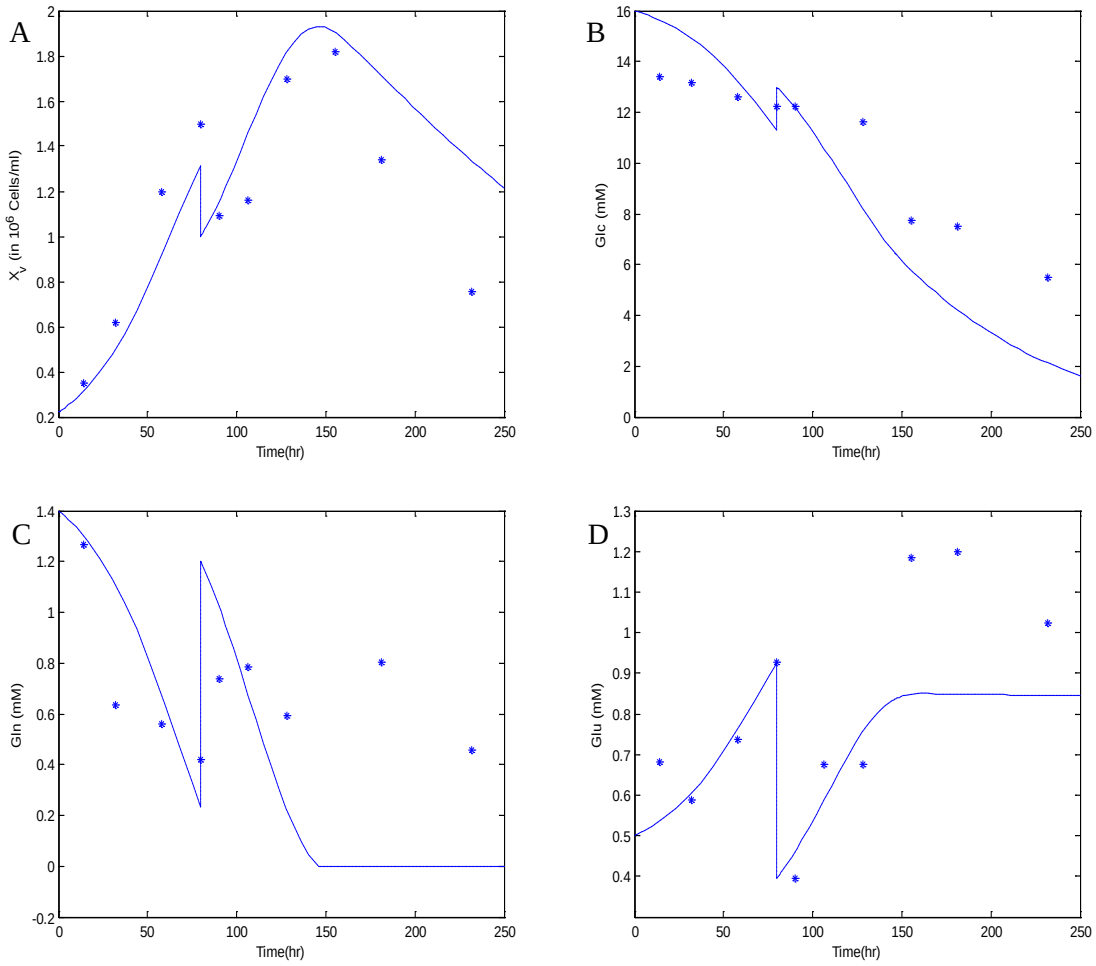

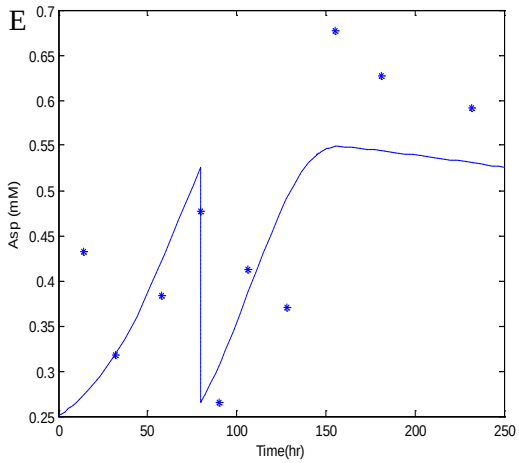
E
Asp (mM)
Time(hr)

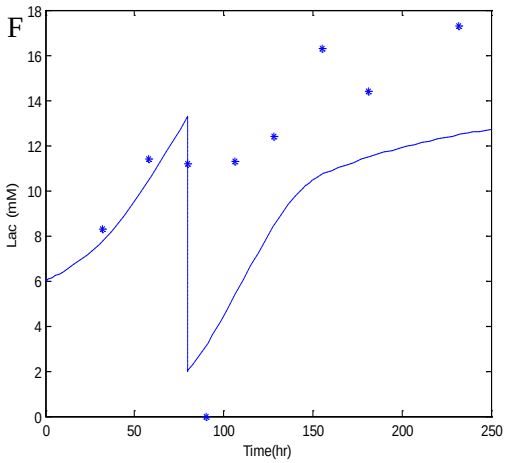
F
Lac (mM)
Time(hr)

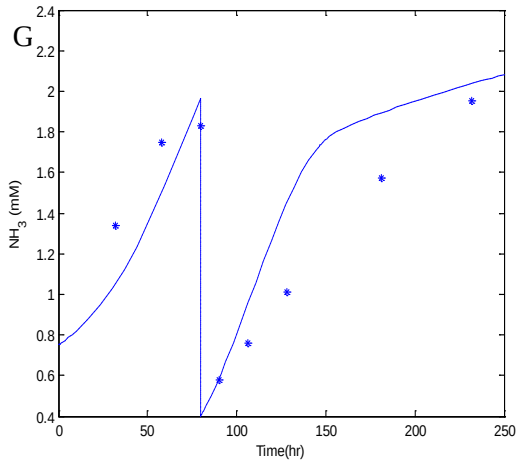
G
NH3 (mM)
Time(hr)

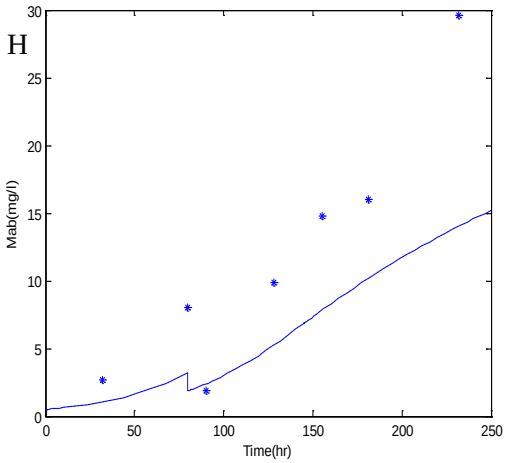
H
Mab(mg/l)
Time(hr)

Appendix J

Model Prediction for Fed-batch Culture

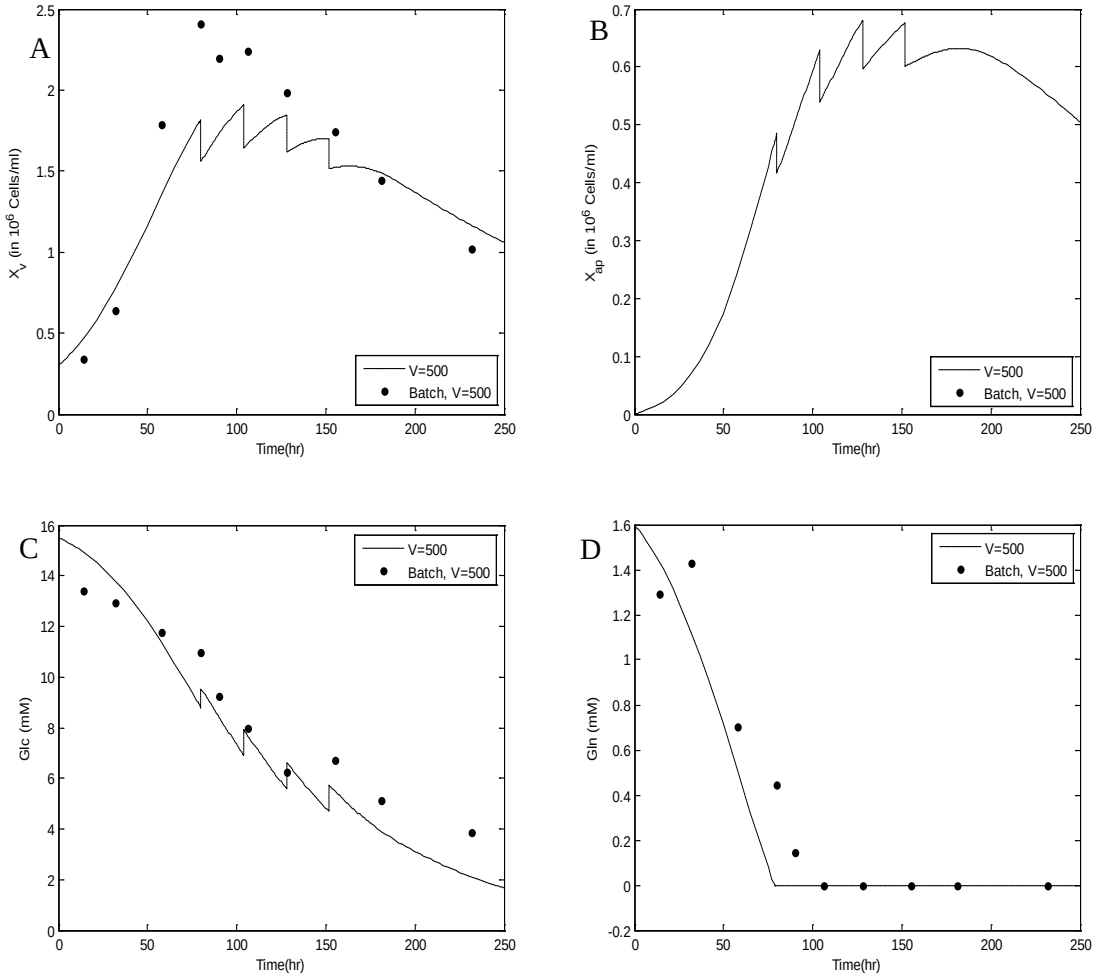

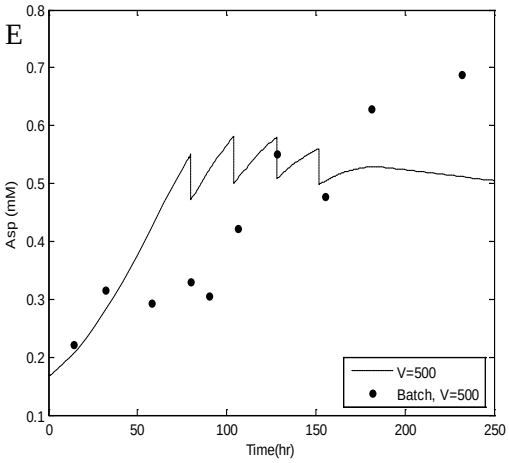
E
Asp (mM)
Time(hr)
V=500
Batch, V=500

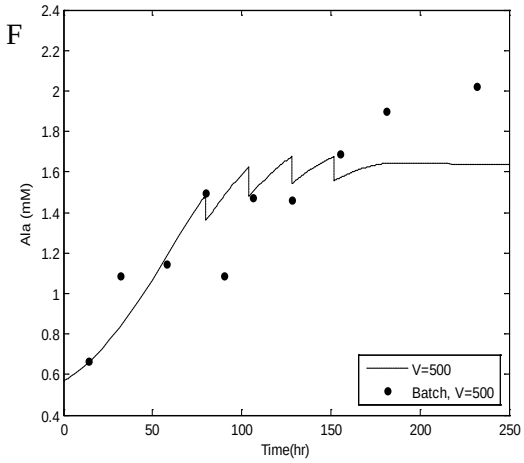
F
Ala (mM)
Time(hr)
V=500
Batch, V=500

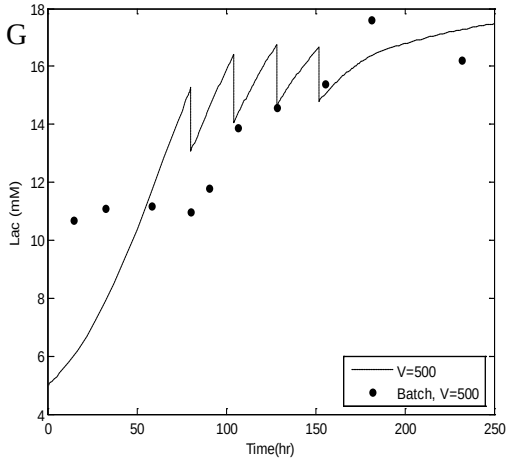
G
Lac (mM)
Time(hr)
V=500
Batch, V=500

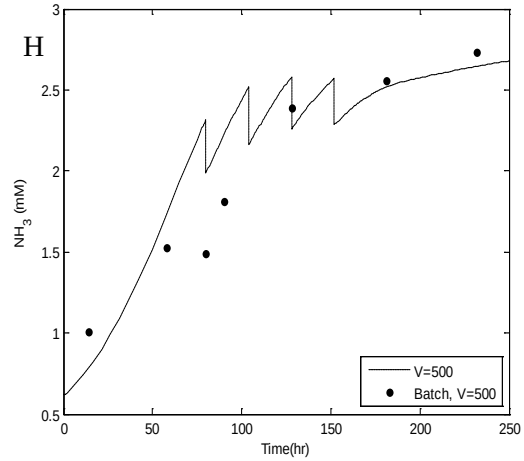
H
NH3 (mM)
Time(hr)
V=500
Batch, V=500

Appendix K

Experimental Results

Exp1-1(sp1) : Simple Batch Culture (Gln=1mM)

Concentration	0h	18h	41h	67h	100h	122h	138h	163h	188h	212h	235h
$X_v \times 10^6$	0.187	0.275	0.623	0.87	1.14	1.12	1.2	0.8	0.94	0.75	0.79
$X_d \times 10^6$	0.003	0	0.015	0.025	0.032	0.045	0.065	0.115	0.23	0.3	0.45
Total cells $\times 10^6$	0.19	0.28	0.64	0.90	1.17	1.17	1.27	0.92	1.17	1.05	1.24
Viability %	98.68	100.00	97.65	97.21	97.27	96.14	94.86	87.43	80.34	71.43	63.71
Normal Xv$\times 10^6$	0.19	0.26	0.61	0.76	0.85	0.69	0.98	0.41	0.49	0.69	0.59
Xap $\times 10^6$	0.00	0.02	0.02	0.11	0.29	0.43	0.22	0.39	0.45	0.06	0.20
Glc (mM)	14.51	14.58	13.54	11.78	9.92	8.35	8.26	7.51	7.13	5.92	5.84
Lac(mM)											
MAb(mg/l)		0.56	0.93		1.85	2.04		2.59	3.71		7.41
NH3(mM)	0.61	0.72	0.99	1.34	1.56	1.64	1.67	1.78	1.95	2.06	2.09
Gln(mM)	1.36	1.13	0.96	0.62	0.71	0.43	0.40	0.36	0.32	0.28	0.29
Asn(mM)	0.26	0.27	0.28	0.22	0.28	0.20	0.19	0.16	0.17	0.12	0.09
Asp(mM)	0.17	0.19	0.25	0.23	0.34	0.30	0.32	0.29	0.28	0.28	0.32
glu(mM)	0.22	0.37	0.43	0.49	0.79	0.71	0.77	0.74	0.72	0.69	0.81
Ser(mM)	0.46	0.46	0.56	0.57	0.81	0.50	0.48	0.41	0.35	0.30	0.29
Gly(mM)	0.26	0.26	0.31	0.31	0.59	0.51	0.57	0.67	0.73	0.79	1.04
His(mM)											
Arg(mM)	1.42	1.23	1.43	1.41	2.28	1.52	1.53	1.57	1.60	1.57	1.97
Thr(mM)	0.72	0.63	0.76	0.75	1.26	0.84	0.90	0.93	0.94	0.93	1.16
AlA(mM)	0.57	0.53	0.73	0.87	1.62	1.19	1.30	1.35	1.38	1.42	1.82
Pro(mM)	0.29	0.27	0.31	0.31	0.48	0.32	0.35	0.36	0.36	0.36	0.47
Tyr(mM)	0.60	0.44	0.50	0.45	0.75	0.52	0.55	0.54	0.54	0.63	0.75
Val(mM)	1.19	0.98	1.14	1.11	1.77	1.19	1.25	1.27	1.27	1.28	1.57
Met(mM)	0.37	0.31	0.35	0.33	0.47	0.30	0.36	0.35	0.32	0.32	0.40
Cys(mM)											
Ile(mM)	1.16	0.93	1.08	1.01	1.51	1.01	1.12	1.11	1.05	1.06	1.28
Leu(mM)	1.99	1.58	1.83	1.74	2.54	1.70	1.90	1.84	1.78	1.81	2.12
Phe(mM)	0.78	0.64	0.74	0.72	1.09	0.74	0.82	0.82	0.81	0.83	0.95
Trp(mM)	0.19	0.15	0.16	0.15	0.22	0.14	0.16	0.16	0.17	0.17	0.18
Lys(mM)	1.11	0.99	1.15	1.17	1.90	1.27	2.40	2.31	2.49	2.55	1.74

Exp1-1(sp2) : Simple Batch Culture (Gln=1mM)

Concentration	0h	18h	41h	67h	100h	122h	138h	163h	188h	212h	235h
Xv × 10^6	0.265	0.262	0.615	0.937	1.2	0.98	1.13	0.92	0.9	0.65	0.89
Xd × 10^6	0.005	0.003	0.015	0.025	0.035	0.052	0.055	0.082	0.21	0.24	0.35
Total cells × 10^6	0.27	0.26	0.63	0.96	1.24	1.03	1.19	1.00	1.11	0.89	1.24
Viability %	98.15	99.05	97.62	97.40	97.17	94.96	95.36	91.82	81.08	73.03	71.77
Normal Xv× 10^6	0.25	0.25	0.51	0.85	1.04	0.83	0.73	0.44	0.50	0.53	0.66
Xap × 10^6	0.02	0.01	0.10	0.09	0.16	0.15	0.40	0.48	0.40	0.12	0.23
Glc (mM)	14.92	14.18	14.77	13.00	10.72	9.25	9.08	8.10	7.21	6.37	7.15
Lac(mM)	2.80	4.80	6.90	11.00	11.30	11.80	11.90	12.60	10.60	11.90	12.30
MAb(mg/l)		0.93	1.24		2.47	3.09		2.78	5.87		9.27
NH3(mM)	0.52	0.70	1.04	1.39	1.55	1.59	1.62	1.82	1.86	2.03	1.80
Gln(mM)	1.48	1.28	0.83	0.63	0.39	0.44	0.33	0.35	0.30	0.28	0.29
Asn(mM)	0.30	0.33	0.26	0.23	0.20	0.17	0.14	0.15	0.13	0.12	0.09
Asp(mM)	0.17	0.20	0.23	0.28	0.23	0.32	0.24	0.29	0.33	0.28	0.32
glu(mM)	0.23	0.29	0.52	0.64	0.56	0.68	0.58	0.68	0.71	0.69	0.81
Ser(mM)	0.51	0.53	0.48	0.57	0.47	0.54	0.38	0.40	0.34	0.30	0.29
Gly(mM)	0.29	0.31	0.29	0.31	0.35	0.48	0.42	0.59	0.64	0.79	1.04
His(mM)											
Arg(mM)	1.55	1.45	1.40	1.38	1.44	1.59	1.19	1.40	1.39	1.57	1.97
Thr(mM)	0.79	0.77	0.67	0.74	0.69	0.91	0.69	0.85	0.82	0.93	1.16
AlA(mM)	0.63	0.83	0.76	0.82	0.93	1.29	0.98	1.23	1.22	1.42	1.82
Pro(mM)	0.32	0.30	0.25	0.29	0.24	0.39	0.28	0.33	0.32	0.36	0.47
Tyr(mM)	0.54	0.43	0.32	0.53	0.31	0.62	0.45	0.49	0.46	0.63	0.75
Val(mM)	1.31	1.17	0.96	1.09	0.97	1.27	1.01	1.16	1.10	1.28	1.57
Met(mM)	0.44	0.37	0.31	0.32	0.30	0.36	0.26	0.31	0.29	0.32	0.40
Cys(mM)											
Ile(mM)	1.69	1.32	1.16	1.14	1.01	1.26	1.00	1.18	1.10	1.23	1.50
Leu(mM)	2.26	1.97	1.58	1.65	1.52	1.83	1.46	1.82	1.55	1.81	2.12
Phe(mM)	0.93	0.82	0.67	0.71	0.69	0.79	0.65	0.96	0.68	0.83	0.95
Trp(mM)	0.23	0.18	0.12	0.15	0.13	0.16	0.14	0.24	0.12	0.17	0.18
Lys(mM)	1.29	2.17	1.19	1.23	1.05	1.38	2.03	1.51	1.20	2.55	1.74

Exp1-1(sp3) : Simple Batch Culture (Gln=2mM)

Concentration	0h	18h	41h	67h	100h	122h	138h	163h	188h	212h	235h
Xv × 10^6	0.287	0.285	0.62	1.06	0.99	1.09	1.15	0.89	0.9	0.73	0.72
Xd × 10^6	0	0	0.008	0.018	0.033	0.062	0.09	0.112	0.18	0.21	0.37
Total cells × 10^6	0.29	0.29	0.63	1.08	1.02	1.15	1.24	1.00	1.08	0.94	1.09
Viability %	100.0	100.0	98.8	98.38	96.82	94.62	92.74	88.82	83.33	77.66	66.06
Normal Xv× 10^6	0.25	0.25	0.60	0.97	0.94	0.69	0.93	0.54	0.81	0.56	0.51
Xap × 10^6	0.04	0.04	0.02	0.09	0.05	0.40	0.22	0.35	0.09	0.17	0.21
Glc (mM)	14.95	13.61		12.6	11.12	11.33	9.83	8.09	6.93	6.30	5.11
Lac(mM)	3.10	5.00	7.20	12.0	11.70	11.60		10.80	11.50	12.70	12.20
MAb(mg/l)		0.56	0.83		1.39	1.39		2.64	2.92		6.26
NH3(mM)	0.61	0.79	1.19	1.64	1.97	1.90	2.18	2.37	2.58	2.52	2.73
Gln(mM)	2.26	2.06	1.62	1.26	1.06	0.91	1.04	0.75	0.88	0.69	0.49
Asn(mM)	0.33	0.29	0.27	0.27	0.25	0.20	0.21	0.15	0.15	0.17	0.08
Asp(mM)	0.20	0.18	0.24	0.28	0.29	0.26	0.30	0.30	0.37	0.40	0.29
glu(mM)	0.25	0.26	0.46	0.62	0.67	0.63	0.70	0.68	0.84	0.65	0.64
Ser(mM)	0.45	0.50	0.51	0.57	0.55	0.48	0.54	0.39	0.42	0.33	0.21
Gly(mM)	0.29	0.29	0.29	0.32	0.44	0.48	0.65	0.63	0.91	0.87	0.72
His(mM)											
Arg(mM)	1.33	1.35	1.33	1.38	1.78	1.44	1.79	1.45	1.93	1.62	1.30
Thr(mM)	0.69	0.72	0.69	0.74	0.87	0.82	1.06	0.86	1.16	0.93	0.78
AlA(mM)	0.70	0.62	0.72	0.90	1.26	1.18	1.72	1.45	1.98	1.59	1.37
Pro(mM)	0.26	0.29	0.30	0.31	0.32	0.33	0.43	0.38	0.48	0.44	0.34
Tyr(mM)	0.34	0.49	0.49	0.56	0.51	0.44	0.68	0.50	0.70	0.51	0.51
Val(mM)	1.05	1.14	1.12	1.14	1.19	1.22	1.57	1.20	1.62	1.10	1.08
Met(mM)	0.35	0.38	0.37	0.34	0.34	0.39	0.40	0.34	0.43	0.33	0.28
Cys(mM)											
Ile(mM)	1.06	1.09	1.16	1.11	1.05	1.03	1.34	1.06	1.36	0.93	0.90
Leu(mM)	1.84	1.89	1.83	1.78	1.80	1.88	2.24	1.79	2.26	1.61	1.56
Phe(mM)	0.74	0.81	0.79	0.77	0.77	0.83	0.96	0.77	1.00	0.70	0.70
Trp(mM)	0.16	0.19	0.17	0.16	0.14	0.20	0.19	0.15	0.20	0.15	0.16
Lys(mM)	1.10	2.38	1.21	2.13	1.23	1.00	1.76	2.22	1.89	1.24	1.19

Exp1-1(sp4) : Simple Batch Culture (Gln=4mM)

Concentration	0h	18h	41h	67h	100h	122h	138h	163h	188h	212h	235h
Xv × 10^6	0.22	0.24	0.54	0.81	1.12	0.9	1.31	0.98	0.81	0.66	0.87
Xd × 10^6	0.003	0	0.015	0.04	0.037	0.055	0.097	0.1	0.12	0.15	0.29
Total cells × 10^6	0.22	0.24	0.56	0.85	1.16	0.96	1.41	1.08	0.93	0.81	1.16
Viability %	98.88	100.00	97.30	95.29	96.80	94.24	93.11	90.74	87.10	81.48	75.00
Normal Xv× 10^6	0.15	0.20	0.43	0.59	0.96	0.78	0.99	0.69	0.50	0.40	0.66
Xap × 10^6	0.07	0.04	0.11	0.22	0.16	0.12	0.32	0.29	0.31	0.26	0.21
Glc (mM)	15.42	15.17	14.82	13.66	10.70	11.03	7.19	6.85	6.44	6.00	5.36
Lac(mM)	3.20	4.70	7.40	10.70	11.60		11.50	11.10	10.10	11.40	12.30
MAb(mg/l)		0.83	1.39		1.39	2.78		4.17	5.00		8.34
NH3(mM)	0.56	0.88	1.41	2.31	2.65	2.81	2.93	3.00	3.47	3.58	3.84
Gln(mM)	4.41	5.15	4.81	3.25	2.80	2.15	1.66		1.47	1.75	1.36
Asn(mM)	0.33	0.35	0.37	0.28	0.27	0.26	0.17		0.14	0.13	0.14
Asp(mM)	0.22	0.23	0.30	0.32	0.34	0.29	0.28		0.27	0.30	0.31
glu(mM)	0.24	0.31	0.57	0.69	0.80	0.67	0.64		0.60	0.67	0.70
Ser(mM)	0.46	0.62	0.73	0.66	0.65	0.48	0.38		0.29	0.31	0.20
Gly(mM)	0.16	0.23	0.42	0.37	0.48	0.48	0.43		0.58	0.81	0.79
His(mM)											
Arg(mM)	1.34	1.90	2.02	1.65	1.72	1.58	1.15		1.23	1.60	1.63
Thr(mM)	0.70	0.99	1.03	0.88	0.95	0.96	0.67		0.72	0.94	0.79
AlA(mM)	0.54	0.89	1.06	1.14	1.44	1.37	1.13		1.32	1.80	1.51
Pro(mM)	0.27	0.42	0.42	0.36	0.39	0.33	0.29		0.31	0.40	0.31
Tyr(mM)	0.44	0.65	0.80	0.72	0.69	0.46	0.45		0.48	0.63	0.43
Val(mM)	1.07	1.54	1.60	1.42	1.36	1.18	0.95		1.05	1.34	1.05
Met(mM)	0.41	0.60	0.50	0.43	0.45	0.35	0.32		0.29	0.37	0.29
Cys(mM)											
Ile(mM)	1.16	1.55	1.50	1.29	1.26	1.04	0.86		0.88	1.13	0.91
Leu(mM)	1.80	2.69	2.55	2.22	2.11	1.79	1.46		1.52	1.88	1.56
Phe(mM)	0.75	1.06	1.05	0.96	0.92	0.80	0.63		0.67	0.82	0.70
Trp(mM)	0.18	0.25	0.25	0.22	0.19	0.16	0.13		0.15	0.16	0.13
Lys(mM)	1.09	2.45	2.59	2.55	2.51	1.22	1.06		1.13	1.46	1.16

References

Altamirano, C., Paredes, C., Illanes, A., Cairo, J. J. and Godia, F. 2004. Strategies for fed-batch cultivation of t-PA producing CHO cells: substitution of glucose and glutamine and rational design of culture medium. *J Biotechnol* **110**(2): 171-179.

Annuar, M. S. M., Tan, I. K. P., Ibrahim, S. and Ramachandran, K. B. 2008. A kinetic model for growth and biosynthesis of medium-chain-length poly-(3-hydroxyalkanoates) in Pseudomonas putida. *Brazilian Journal of Chemical Engineering* **25**(2): 217-228.

Arden, N. and Betenbaugh, M. J. 2004. Life and death in mammalian cell culture: strategies for apoptosis inhibition. *Trends Biotechnol* **22**(4): 174-180.

Bailey, J. E. 1998. Mathematical modeling and analysis in biochemical engineering: past accomplishments and future opportunities. *Biotechnol Prog* **14**(1): 8-20.

Berg, B. A. 2004. Markov Chain Monte Carlo Simulations and Their Statistical Analysis. New Jersey, World Scientific.

Bidlingmeyer, B. A., Cohen, S. A. and Tarvin, T. L. 1984. Rapid analysis of amino acids using pre-column derivatization. *J Chromatogr* **336**(1): 93-104.

Birch, J. R. and Racher, A. J. 2006. Antibody production. *Adv Drug Deliv Rev* **58**(5-6): 671-685.

Bischoff, W., Cremers, H. and Fieger, W. 1991. Normal distribution assumption and least squares estimation function in the model of polynomial regression *Journal of Multivariate Analysis* **36**(1): 1-17.

Boghigian, B. A., Seth, G., Kiss, R. and Pfeifer, B. A. 2010. Metabolic flux analysis and pharmaceutical production. *Metab Eng* **12**(2): 81-95.

Bonarius, H. P., Hatzimanikatis, V., Meesters, K. P., de Gooijer, C. D., Schmid, G. and Tramper, J. 1996. Metabolic flux analysis of hybridoma cells in different culture media using mass balances. *Biotechnology and Bioengineering* **50**(3): 299-318.

Bonarius, H. P., Ozemre, A., Timmerarends, B., Skrabal, P., Tramper, J., Schmid, G. and Heinzle, E. 2001. Metabolic-flux analysis of continuously cultured hybridoma cells using (13)CO(2) mass spectrometry in combination with (13)C-lactate nuclear magnetic resonance spectroscopy and metabolite balancing. *Biotechnology and Bioengineering* **74**(6): 528-538.

Breckenridge, D. G., Germain, M., Mathai, J. P., Nguyen, M. and Shore, G. C. 2003. Regulation of apoptosis by endoplasmic reticulum pathways. *Oncogene* **22**(53): 8608-8618.

Browne, S. M. and Al-Rubeai, M. 2007. Selection methods for high-producing mammalian cell lines. *Trends Biotechnol* **25**(9): 425-432.

Burger, W. and Burge, M. J. 2008. Digital Image Processing-An Algorithmic Introduction using Java. Verlag New York, Springer.

Burky, J. E., Wesson, M. C., Young, A., Farnsworth, S., Dionne, B., Zhu, Y., Hartman, T. E., Qu, L. M., Zhou, W. C. and Saner, P. W. 2007. Protein-free fed-batch culture of non-GS NS0 cell lines for production of recombinant antibodies. *Biotechnology and Bioengineering* **96**(2): 281-293.

Butler, M. 2005. Animal cell cultures: recent achievements and perspectives in the production of biopharmaceuticals. *Appl Microbiol Biotechnol* **68**(3): 283-291.

Caramihai, M., Severin, I., Chirvase, A. A., Onu, A., Tanase, C. and Ungureanu, C. 2010. Therapeutic Product Preparation Bioprocess Modeling. *World Academy of Science, Engineering and Technology* **66**: 955-958.

Chadd, H. E. and Chamow, S. M. 2001. Therapeutic antibody expression technology. *Curr Opin Biotechnol* **12**(2): 188-194.

Chib, S. and Greenberg, E. 1995. Understanding the Metropolis-Hastings Algorithm. *American Statistician* **49**(4): 327-335.

Chong, W. P., Yusufi, F. N., Lee, D. Y., Reddy, S. G., Wong, N. S., Heng, C. K., Yap, M. G. and Ho, Y. S. 2011. Metabolomics-based identification of apoptosis-inducing metabolites in recombinant fed-batch CHO culture media. *J Biotechnol* **151**(2): 218-224.

Chu, L. and Robinson, D. K. 2001. Industrial choices for protein production by large-scale cell culture. *Curr Opin Biotechnol* **12**(2): 180-187.

Cipollaro, M., Corsale, G., Esposito, A., Ragucci, E., Staiano, N., Giordano, G. G. and Pagano, G. 1986. Sublethal pH decrease may cause genetic damage to eukaryotic cell: a study on sea urchins and Salmonella typhimurium. *Teratog Carcinog Mutagen* **6**(4): 275-287.

Dinnis, D. M. and James, D. C. 2005. Engineering mammalian cell factories for improved recombinant monoclonal antibody production: lessons from nature? *Biotechnology and Bioengineering* **91**(2): 180-189.

Dochain, D. 2008. Dynamic Models of Biochemical Processes: Properties of Models. *Bioprocess Control*. O. Bernard and I. Quelinnec. Hoboken, New York, Wiley Interscience Publishing**:** 17-47.

Dorai, H., Kyung, Y. S., Ellis, D., Kinney, C., Lin, C., Jan, D., Moore, G. and Betenbaugh, M. J. 2009. Expression of anti-apoptosis genes alters lactate metabolism of Chinese Hamster Ovary cells in culture. *Biotechnology and Bioengineering* **103**(3): 592-608.

Dorka, P., Fischer, C., Budman, H. and Scharer, J. M. 2009. Metabolic flux-based modeling of mAb production during batch and fed-batch operations. *Bioprocess Biosyst Eng* **32**(2): 183-196.

Dutton, R. L., Scharer, J. M. and Moo-Young, M. 1998. Descriptive parameter evaluation in mammalian cell culture. *Cytotechnology* **26**(2): 139-152.

Even, M. S., Sandusky, C. B. and Barnard, N. D. 2006. Serum-free hybridoma culture: ethical, scientific and safety considerations. *Trends Biotechnol* **24**(3): 105-108.

Farid, S. S. 2007. Process economics of industrial monoclonal antibody manufacture. *Journal of Chromatography B-Analytical Technologies in the Biomedical and Life Sciences* **848**(1): 8-18.

Fuchs, B. C. and Bode, B. P. 2006. Stressing out over survival: glutamine as an apoptotic modulator. *J Surg Res* **131**(1): 26-40.

Fussenegger, M., Bailey, J. E. and Varner, J. 2000. A mathematical model of caspase function in apoptosis. *Nat Biotechnol* **18**(7): 768-774.

Gambhir, A., Korke, R., Lee, J. C., Fu, P. C., Europa, A. and Hu, W. S. 2003. Analysis of cellular metabolism of hybridoma cells at distinct physiological states. *Journal of Bioscience and Bioengineering* **95**(4): 317-327.

Gao, J., Gorenflo, V. M., Scharer, J. M. and Budman, H. M. 2007. Dynamic metabolic modeling for a MAB bioprocess. *Biotechnol Prog* **23**(1): 168-181.

Gao, J. Y., Gorenflo, V. M., Scharer, J. M. and Budman, H. M. 2007. Dynamic metabolic modeling for a MAB bioprocess. *Biotechnology Progress* **23**(1): 168-181.

Gheshlaghi, R., Scharer, J. M., Moo-Young, M. and Douglas, P. L. 2008. Application of statistical design for the optimization of amino acid separation by reverse-phase HPLC. *Anal Biochem* **383**(1): 93-102.

Goswami, J., Sinskey, A. J., Steller, H., Stephanopoulos, G. N. and Wang, D. I. 1999. Apoptosis in batch cultures of Chinese hamster ovary cells. *Biotechnology and Bioengineering* **62**(6): 632-640.

Goudar, C., Biener, R., Boisart, C., Heidemann, R., Piret, J., de Graaf, A. and Konstantinov, K. 2010. Metabolic flux analysis of CHO cells in perfusion culture by metabolite balancing and 2D [13C, 1H] COSY NMR spectroscopy. *Metab Eng* **12**(2): 138-149.

Goudar, C. T., Joeris, K., Konstantinov, K. B. and Piret, J. M. 2005. Logistic equations effectively model Mammalian cell batch and fed-batch kinetics by logically constraining the fit. *Biotechnol Prog* **21**(4): 1109-1118.

Grosfils, A., Wouwer, A. V. and Bogaerts, P. 2007. On a general model structure for macroscopic biological reaction rates. *Journal of Biotechnology* **130**(3): 253-264.

Hacker, D. L., De Jesus, M. and Wurm, F. M. 2009. 25 years of recombinant proteins from reactor-grown cells - where do we go from here? *Biotechnol Adv* **27**(6): 1023-1027.

Han, Y. K., Kim, Y. G., Kim, J. Y. and Lee, G. M. 2010. Hyperosmotic stress induces autophagy and apoptosis in recombinant Chinese hamster ovary cell culture. *Biotechnology and Bioengineering* **105**(6): 1187-1192.

Harding, C. L., Lloyd, D. R., McFarlane, C. M. and Al-Rubeai, M. 2000. Using the microcyte flow cytometer to monitor cell number, viability, and apoptosis in mammalian cell culture. *Biotechnology Progress* **16**(5): 800-802.

Hardy, K. and Stark, J. 2002. Mathematical models of the balance between apoptosis and proliferation. *Apoptosis* **7**(4): 373-381.

Hodge, G. 2005. Media development for mammalian cell culture. *Biopharm International* **18**(5): 54-+.

Houdebine, L. M. 2002. Antibody manufacture in transgenic animals and comparisons with other systems. *Curr Opin Biotechnol* **13**(6): 625-629.

Huang, Y. M., Hu, W., Rustandi, E., Chang, K., Yusuf-Makagiansar, H. and Ryll, T. 2010. Maximizing productivity of CHO cell-based fed-batch culture using chemically defined media conditions and typical manufacturing equipment. *Biotechnol Prog* **26**(5): 1400-1410.

Hudson, P. J. and Souriau, C. 2003. Engineered antibodies. *Nat Med* **9**(1): 129-134.

Huerta, S., Heinzerling, J. H., Anguiano-Hernandez, Y. M., Huerta-Yepez, S., Lin, J., Chen, D., Bonavida, B. and Livingston, E. H. 2007. Modification of gene products involved in resistance to apoptosis in metastatic colon cancer cells: Roles of Fas, Apaf-1, NF kappa B, IAPs, Smac/DIABLO, and AIF. *Journal of Surgical Research* **142**(1): 184-194.

Hwang, S. O. and Lee, G. M. 2008. Nutrient deprivation induces autophagy as well as apoptosis in Chinese hamster ovary cell culture. *Biotechnology and Bioengineering* **99**(3): 678-685.

Invitrogen (2006). Tools for increasing performance of Mammalian Expression platforms**:** 1-5.

Jayapal, K. R., Wlaschin, K. F., Hu, W. S. and Yap, M. G. S. 2007. Recombinant protein therapeutics from CHO cells - 20 years and counting. *Chemical Engineering Progress* **103**(10): 40-47.

Jitjareonchai, J. J., Reilly, P. M., Duever, T. A. and Chambers, D. B. 2006. Parameter estimation in the Error-in-Variables models using the Gibbs Sampler. *Canadian Journal of Chemical Engineering* **84**(1): 125-138.

Johnston, S. and Siegel, C. 1990. Comparison of a serum replacement (Omni Serum) and fetal bovine serum in cell cultures used to isolate herpes simplex virus from clinical specimens. *J Clin Microbiol* **28**(4): 643-645.

Kaufmann, H. and Fussenegger, M. 2004. Caspase regulation at the molecular level. *Cell Engineering* M. Al- Rubeai and M. Fussenegger. Netherlands, Kluwer Academic. **4:** 1-23.

Khavarpour, M., Najafpour, G. D., Ghoreyshi, A. A., Jahanshahi, M. and Bambai, B. 2011. Biodesulfurization of Natural Gas: Growth Kinetic Evaluation. *Middle-East Journal of Scientific Research* **7**(1): 22-29.

Kim, Y. G., Kim, J. Y., Mohan, C. and Lee, G. M. 2009. Effect of Bcl-xL overexpression on apoptosis and autophagy in recombinant Chinese hamster ovary cells under nutrient-deprived condition. *Biotechnology and Bioengineering* **103**(4): 757-766.

Knight, R. A. 2006. The archaeology of apoptosis. *Parasitology* **132 Suppl**: S3-5.

Kontoravdi, C., Wong, D., Lam, C., Lee, Y. Y., Yap, M. G., Pistikopoulos, E. N. and Mantalaris, A. 2007. Modeling amino acid metabolism in mammalian cells-toward the development of a model library. *Biotechnol Prog* **23**(6): 1261-1269.

Kumar, S., Wittmann, C. and Heinzle, E. 2004. Minibioreactors. *Biotechnol Lett* **26**(1): 1-10.

Laken, H. A. and Leonard, M. W. 2001. Understanding and modulating apoptosis in industrial cell culture. *Curr Opin Biotechnol* **12**(2): 175-179.

Lee, E. Y. 2002. Kinetic Analysis of the Effect of Cell Density on Hybridoma Cell Growth in Batch Culture. *Biotechnol. Bioprocess Eng* **7**: 117-120.

Lewis, D. (2008). Automated CHO cell classification using Matlab. Waterloo, Ontario, University of Waterloo**:** 22.

Link, T., Backstrom, M., Graham, R., Essers, R., Zorner, K., Gatgens, J., Burchell, J., Taylor-Papadimitriou, J., Hansson, G. C. and Noll, T. 2004. Bioprocess development for the production of a recombinant MUC1 fusion protein expressed by CHO-K1 cells in protein-free medium. *Journal of Biotechnology* **110**(1): 51-62.

Lucas, B. K., Giere, L. M., DeMarco, R. A., Shen, A., Chisholm, V. and Crowley, C. W. 1996. High-level production of recombinant proteins in CHO cells using a dicistronic DHFR intron expression vector. *Nucleic Acids Res* **24**(9): 1774-1779.

Macey, M. G. 2007. Flow Cytometry: Principles and Applications Totowa, New Jersey, Humana Press Inc.

Majors, B. S., Betenbaugh, M. J., Pederson, N. E. and Chiang, G. G. 2009. Mcl-1 overexpression leads to higher viabilities and increased production of humanized monoclonal antibody in Chinese hamster ovary cells. *Biotechnol Prog* **25**(4): 1161-1168.

Matasci, M., Hacker, D. L., Baldi, L. and Wurm, F. M. 2008. Recombinant therapeutic protein production in cultivated mammalian cells: current status and future prospects. *Drug Discovery Today: Technologies* **5**: e37-e42.

Mendonca, R. Z., Arrozio, S. J. and Antoniazzi, M. M. 2009. Morphological Characterization of Vero Cell Death Induced by Nutrient Depletion. *Acta Microscopica* **18**(3): 204-219.

Mercille, S. and Massie, B. 1994. Induction of apoptosis in nutrient-deprived cultures of hybridoma and myeloma cells. *Biotechnology and Bioengineering* **44**(9): 1140-1154.

Meshram, M., Naderi, S., Wie, C., Scharer, J., Budman, H., McConkey, B. and Ingalls, B. 2009. Toward an understanding of the role of apoptosis. *FOSBE Conference on Systems Biology*, Denver.

Meuwly, F., Weber, U., Ziegler, T., Gervais, A., Mastrangeli, R., Crisci, C., Rossi, M., Bernard, A., von Stockar, U. and Kadouri, A. 2006. Conversion of a CHO cell culture process from perfusion to fed-batch technology without altering product quality. *J Biotechnol* **123**(1): 106-116.

Min Lee, G., Koo , J. and Flickinger, M. C. 2009. Osmolarity Effects, Chinese Hamster Ovary Cell Culture. New York, N, Wiley.

Mulvey, C. S., Curtis, A. L., Singh, S. K. and Bigio, I. J. 2007. Elastic scattering spectroscopy as a diagnostic tool for apoptosis in cell cultures. *Ieee Journal of Selected Topics in Quantum Electronics* **13**(6): 1663-1670.

Naderi, S., Meshram, M., Wei, C., McConkey, B., Ingalls, B., Budman, H. and Scharer, J. 2011. Development of a mathematical model for evaluating the dynamics of normal and apoptotic Chinese hamster ovary cells. *Biotechnol Prog*.

Naderi, S., Meshram, M., Wie, C., Scharer, J., Budman, H., McConkey, B. and Ingalls, B. 2010. Metabolic flux and nutrient uptake modeling of normal and apoptotic CHO cells. *11th Computer Applications in Biotechnology Conference (CAB)*, Leuven, Belgium.

Nolan, R. P. and Lee, K. 2011. Dynamic model of CHO cell metabolism. *Metab Eng* **13**(1): 108-124.

NRC (1999). Monoclonal Antibody Production. Washington DC.

Nyberg, G. B., Balcarcel, R. R., Follstad, B. D., Stephanopoulos, G. and Wang, D. I. 1999. Metabolism of peptide amino acids by Chinese hamster ovary cells grown in a complex medium. *Biotechnology and Bioengineering* **62**(3): 324-335.

Oliveira, J. E., Damiani, R., Vorauer-Uhl, K., Bartolini, P. and Ribela, M. T. 2008. Influence of a reduced CO2 environment on the secretion yield, potency and N-glycan structures of recombinant thyrotropin from CHO cells. *Mol Biotechnol* **39**(2): 159-166.

Paredes, C., Sanfeliu, A., Cardenas, F., Cairo, J. J. and Godia, F. 1998. Estimation of the intracellular fluxes for a hybridoma cell line by material balances. *Enzyme and Microbial Technology* **23**(3-4): 187-198.

Pattison, R. N., Swamy, J., Mendenhall, B., Hwang, C. and Frohlich, B. T. 2000. Measurement and control of dissolved carbon dioxide in mammalian cell culture processes using an in situ fiber optic chemical sensor. *Biotechnol Prog* **16**(5): 769-774.

Portner, R. and Schafer, T. 1996. Modelling hybridoma cell growth and metabolism a comparison of selected models and data. *Journal of Biotechnology* **49**(1-3): 119-135.

Provost, A. and Bastin, G. 2004. Dynamic metabolic modelling under the balanced growth condition. *Journal of Process Control* **14**(7): 717-728.

Provost, A. and Bastin, G. 2006. Metabolic flux analysis: An approach for solving non-stationary underdetermined systems. *Proceedings 5th MATHMOD*, Vienna, Austria.

Provost, A., Bastin, G., Agathos, S. N. and Schneider, Y. J. 2006. Metabolic design of macroscopic bioreaction models: application to Chinese hamster ovary cells. *Bioprocess Biosyst Eng* **29**(5-6): 349-366.

Qualitz, J. 2005. High Throughput Bioprocessing Systems *Laboratory Focus* **9**(2): 6-16.

Quek, L. E., Dietmair, S., Kromer, J. O. and Nielsen, L. K. 2010. Metabolic flux analysis in mammalian cell culture. *Metab Eng* **12**(2): 161-171.

Reitzer, L. J., Wice, B. M. and Kennell, D. 1979. Evidence That Glutamine, Not Sugar, Is the Major Energy-Source for Cultured Hela-Cells. *Journal of Biological Chemistry* **254**(8): 2669-2676.

Renard, J. M., Spagnoli, R., Mazier, C., Salles, M. F. and Mandine, E. 1988. Evidence That Monoclonal-Antibody Production Kinetics Is Related to the Integral of the Viable Cells Curve in Batch Systems. *Biotechnology Letters* **10**(2): 91-96.

Rincheval, V., Renaud, F., Lemaire, C., Godefroy, N., Trotot, P., Boulo, V., Mignotte, B. and Vayssiere, J. L. 2002. Bcl-2 can promote p53-dependent senescence versus apoptosis without affecting the G1/S transition. *Biochemical and Biophysical Research Communications* **298**(2): 282-288.

Rodrigues, M. E., Costa, A. R., Henriques, M., Azeredo, J. and Oliveira, R. 2010. Technological progresses in monoclonal antibody production systems. *Biotechnol Prog* **26**(2): 332-351.

Ruaan, R. C., Tsai, G. J. and Tsao, G. T. 1993. Monitoring and modeling density-dependent growth of anchorage-dependent cells. *Biotechnology and Bioengineering* **41**(3): 380-389.

Ruiz, L., Traskine, M., Ferrer, I., Castro, E., Leal, J. F., Kaufman, M. and Carnero, A. 2008. Characterization of the p53 response to oncogene-induced senescence. *PLoS One* **3**(9): e3230.

Sandadi, S., Ensari, S. and Kearns, B. 2005. Heuristic optimization of antibody production by Chinese hamster ovary cells. *Biotechnol Prog* **21**(5): 1537-1542.
Sanderson, C. S., Jang, J. D., Barford, J. P. and Barton, G. W. 1999. A structured, dynamic model for animal cell culture systems: application to murine hybridoma. *Biochemical Engineering Journal* **3**(3): 213-218.
Sanfeliu, A. and Stephanopoulos, G. 1999. Effect of glutamine limitation on the death of attached Chinese hamster ovary cells. *Biotechnology and Bioengineering* **64**(1): 46-53.
Sanna, P. P. and Burton, D. R. 2000. Role of antibodies in controlling viral disease: lessons from experiments of nature and gene knockouts. *J Virol* **74**(21): 9813-9817.
Sauerwald, T. M., Oyler, G. A. and Betenbaugh, M. J. 2003. Study of caspase inhibitors for limiting death in mammalian cell culture. *Biotechnology and Bioengineering* **81**(3): 329-340.
Sekhon, B. S. 2010. Biopharmaceuticals: an overview. *Thai J. Pharm. Sci.* **34**: 1-19.
Sidoli, F. R., Mantalaris, A. and Asprey, S. P. 2004. Modelling of mammalian cells and cell culture processes. *Cytotechnology* **44**(1-2): 27-46.
Simon, L. and Karim, M. N. 2002. Control of starvation-induced apoptosis in Chinese hamster ovary cell cultures. *Biotechnology and Bioengineering* **78**(6): 645-657.
Simpson, N. H., Singh, R. P., Perani, A., Goldenzon, C. and Al-Rubeai, M. 1998. In hybridoma cultures, deprivation of any single amino acid leads to apoptotic death, which is suppressed by the expression of the bcl-2 gene. *Biotechnology and Bioengineering* **59**(1): 90-98.
Sinacore, M. S., Drapeau, D. and Adamson , S. R. 1999. Adaptation of Mammalian Cells to Growth in Serum-Free Media. *Animal Cell Biotechnology*. N. Jenkins. Totowa, NJ, Humana Press Inc. **8:** 11-22.
Singh, R. P., Al-Rubeai, M., Gregory, C. D. and Emery, A. N. 1994. Cell death in bioreactors: a role for apoptosis. *Biotechnology and Bioengineering* **44**(6): 720-726.
Stephanopoulos, G. 1998. Metabolic engineering. *Biotechnology and Bioengineering* **58**(2-3): 119-120.
Sucosky, P., Osorio, D. F., Brown, J. B. and Neitzel, G. P. 2004. Fluid mechanics of a spinner-flask bioreactor. *Biotechnology and Bioengineering* **85**(1): 34-46.
SUN , X. and ZHANG, Y. 2002. Effects of lactate on growth, metabolism and EPO expression of recombinant CHO cells. *Journal fo Chemical Industry and Engineering* **53**: 1034-1039.
Sun, X. M. and Zhang, Y. X. 2004. Glutamine cannot support recombinant CHO cell growth and maintenance inthe absence of glucose. *Process Biochemistry* **39**(6): 717-720.
Sunley, K. and Butler, M. 2010. Strategies for the enhancement of recombinant protein production from mammalian cells by growth arrest. *Biotechnol Adv* **28**(3): 385-394.
Thombre, S. and Gadgil, M. 2011. Increase in efficiency of media utilization for recombinant protein production in Chinese hamster ovary culture through dilution. *Biotechnol Appl Biochem* **58**(1): 25-31.
Trummer, E., Fauland, K., Seidinger, S., Schriebl, K., Lattenmayer, C., Kunert, R., Vorauer-Uhl, K., Weik, R., Borth, N., Katinger, H. and Muller, D. 2006. Process parameter shifting: Part I. Effect of DOT, pH, and temperature on the performance of Epo-Fc expressing CHO cells cultivated in controlled batch bioreactors. *Biotechnology and Bioengineering* **94**(6): 1033-1044.
Tsoularis, A. and Wallace, J. 2002. Analysis of logistic growth models. *Math Biosci* **179**(1): 21-55.
Walsh, G. 2010. Biopharmaceutical benchmarks 2010. *Nat Biotechnol* **28**(9): 917-924.
Wiersma, E. (2000). Expression and characterization of human IgG specific for the RhD antigen. *Final Project Report*. Toronto, Cangene Corporation**:** 23.

Wong, D. C. F., Heng , C. K., Wong , K. T. K., Nissom, P. M. and Yap, M. G. S. 2006. Elucidating apoptotic cell death in CHO cell batch & fed-batch cultures. *Animal cell technology: Basic & Applied Aspects*. S. Iijima and K. Nishijima New York, NY, Springer**:** 61-66.

Wong, D. C. F., Wong, K. T. K., Goh, L. T., Heng, C. K. and Yap, M. G. S. 2005. Impact of dynamic online fed-batch strategies on metabolism, productivity and N-glycosylation quality in CHO cell cultures. *Biotechnology and Bioengineering* **89**(2): 164-177.

Wong, J. H., Irie, R. F. and Morton, D. L. 1989. Human monoclonal antibodies: prospects for the therapy of cancer. *Semin Surg Oncol* **5**(6): 448-452.

Wurm, F. M. 2004. Production of recombinant protein therapeutics in cultivated mammalian cells. *Nat Biotechnol* **22**(11): 1393-1398.

Xie, L. and Wang, D. I. 1996. Material balance studies on animal cell metabolism using a stoichiometrically based reaction network. *Biotechnology and Bioengineering* **52**(5): 579-590.

Xie, L., Zhou, W. and Robinson, D. 2003. Protein production by large-scale mammalian cell culture *New Comprehensive Biochemistry*. Makrides. Amsterdam, Elsevier**:** 605-623.

Xing, Z. Z., Bishop, N., Leister, K. and Li, Z. J. 2010. Modeling Kinetics of a Large-Scale Fed-Batch CHO Cell Culture by Markov Chain Monte Carlo Method. *Biotechnology Progress* **26**(1): 208-219.

Xing, Z. Z., Li, Z. J., Chow, V. and Lee, S. S. 2008. Identifying inhibitory threshold values of repressing metabolites in CHO cell culture using multivariate analysis methods. *Biotechnology Progress* **24**(3): 675-683.

Yeo, J. H., Lo, J. C., Nissom, P. M. and Wong, V. V. 2006. Glutamine or glucose starvation in hybridoma cultures induces death receptor and mitochondrial apoptotic pathways. *Biotechnol Lett* **28**(18): 1445-1452.

Yoon, S. K., Choi, S. L., Song, J. Y. and Lee, G. M. 2005. Effect of culture pH on erythropoietin production by chinese hamster ovary cells grown in suspension at 32.5 and 37.0 degrees C. *Biotechnology and Bioengineering* **89**(3): 345-356.

Yun, C. Y., Liu, S., Lim, S. F., Wang, T., Chung, B. Y., Jiat Teo, J., Chuan, K. H., Soon, A. S., Goh, K. S. and Song, Z. 2007. Specific inhibition of caspase-8 and -9 in CHO cells enhances cell viability in batch and fed-batch cultures. *Metab Eng* **9**(5-6): 406-418.

Zhang, L., Shen, H. and Zhang, Y. X. 2004. Fed-batch culture of hybridoma cells in serum-free medium using an optimized feeding strategy. *Journal of Chemical Technology and Biotechnology* **79**(2): 171-181.

Zhou, H., Purdie, J., Wang, T. and Ouyang, A. 2010. pH measurement and a rational and practical pH control strategy for high throughput cell culture system. *Biotechnol Prog* **26**(3): 872-880.

Zhu, M. M., Goyal, A., Rank, D. L., Gupta, S. K., Vanden Boom, T. and Lee, S. S. 2005. Effects of elevated pCO2 and osmolality on growth of CHO cells and production of antibody-fusion protein B1: a case study. *Biotechnol Prog* **21**(1): 70-77.

Zupke, C. and Stephanopoulos, G. 1995. Intracellular flux analysis in hybridomas using mass balances and in vitro (13)C nmr. *Biotechnology and Bioengineering* **45**(4): 292-303.